VOT 75117

THE STUDY OF NORMAL INCIDENCE SOUND ABSORPTION COEFFICIENCE (SOUND ABSORPTION) OF WOOD CIRCULAR PERFORATED PANEL (CPP) USING NUMERICAL MODELLING TECHNIQUE

MOHAMAD NGASRI DIMON
MUNIRUL ULA
ABDUL WAHAB ISHARI MOHD HASHIM
SITI ZALEHA ABDUL HAMID
AMERUDDIN BAHAROM
ABDUL HAMID AHMAD

RESEARCH VOT NO:
75117

Department of Radio and Communication Engineering
Faculty of Electrical Engineering
Universiti Teknologi Malaysia

2006

DEDICATION

Thank to the government of Malaysia through Research Management Center (RMC) for providing research grant Vot #75117. This has allowed the research work successfully conducted. This paved the way for further in-depth and more challenging research work ahead.

ABSTRACT

(Keywords: normal incidence sound absorption, sound intensity, numerical simulation, direct piercing carved panel.)

Wood Circular Perforated Panel (WCPP) is the simple form of direct piercing carved wood panel (DPCWP) which has been widely used in traditional and modern mosques as part of wall partition. This DPCWP can act as sound absorption material. Normal incidence sound absorption coefficient (α_n) of WCPP can not be tested using conventional sound absorption measurement techniques. Nowadays, numerical modeling is a powerful technique to solve these difficulties. Numerical modeling based on Boundary Element Method (BEM) has been widely used for engineering design and prediction. This thesis report on work that has been carried out to investigate normal incidence sound absorption coefficient, (α_n) characteristics of wood circular perforated panel (WCPP) using Boundary Element Method. The perforation ratios investigated are 20%, 30% and 40 %. The panel perforation ratio is ranging in number of apertures, diameter, and distance between apertures. Boundary Element Method simulation is done using Beasy Acoustics software. The simulation is done by creating WCPP geometric model, defining acoustics media properties and boundary conditions. Net sound intensity is simulated by creating point source 2 meter in front of the panel and 16 internal points 0.25λ in front of the panel. Incidence sound intensity is obtained by removing the panel. Comparison and analysis of α_n of WCPP modeled by BEM with α_n measured using sound intensity technique and theoretical prediction were conducted. It was found out that there is a close correlation of α_n modeled using BEM and α_n measured using sound intensity and theoretical prediction. Statistical regression model for simulation result is developed using SPSS. Third order polynomial is applied to fit the curves of WCPP simulation result and multiple regression model with stepwise method is applied to fit the curve of over all result with perforation ratio and frequency band as independent variables.

Key researchers:

Assoc. Prof. Dr. Mohamad Ngasri Dimon (Head)
Munirul Ula
Abdul Wahab Ishari Mohd Hashim
Siti Zaleha Abdul Hamid
Ameruddin Baharom
Abdul Hamid Ahmad

E-mail : ngasri@fke.utm.my
Tel. No. : 075535901
Vot. No. : 75117

ABSTRAK

(Kata kunci: penyerap bunyi sudut tuju normal, keamatan bunyi, simulasi berangka, panel bertebuk penembusan terus.)

Panel kayu berlubang bulat (WCPP) adalah bentuk yang mudah daripada panel bertebuk penembusan terus (DPCWP) yang sudah dipakai secara luas pada masjid-masjid traditional dan masjid-masjid moden sebagai sebahagian daripada dinding. DPCWP ini boleh bertindak sebagai bahan penyerap bunyi. Angkali penyerap bunyi sudut tuju normal (α_n) WCPP tidak boleh diuji dengan teknik pengujian penyerapan bunyi yang konvensional. Sekarang ini, permodelan berangka adalah suatu teknik yang sangat baik untuk menyelesaikan masalah tersebut. Permodelan secara berangka berasaskan kaedah elemen sempadan (BEM) sudah dipakai secara luas untuk perancangan kejuruteraan dan ramalan. Thesis ini melaporkan tentang penyelidikan yg telah dilakukan untuk mengkaji kelakuan α_n daripada WCPP dengan menggunakan BEM. Simulasi BEM dilakukan dengan menggunakan perisian Beasy Acoustics. Simulasi dilakukan dengan membuat model geometri WCPP, mendefinasikan sifat media akustik dan keadaan-keadan sempadan. Kadar tebukan yang dikaji adalah 20%, 30% dan 40%. Kadar tebukan panel diubah-ubah pada jumlah lubang tebukan, garispusat dan jarak antara lubang tebukan. Jumlah keamatan bunyi disimulasi dengan membuat sumber titik 2 meter di depan panel and 16 titik pengukuran pada jarak 0.25λ di depan panel. Keamatan bunyi tuju di dapatkan dengan meniadakan panel. Perbandingan dan analisis α_n WCPP yang dimodelkan dengan BEM dan α_n yg diukur dengan teknik keamatan bunyi dan dengan ramalan teori dilakukan. Pekali sekaitan yang tinggi antara α_n yang dimodelkan dengan α_n yang diukur dengan keamatan bunyi dan dengan ramalan teori telah diperolehi. Model regressi statistik untuk hasil simulasi dibuat dengan menggunakan perisian "Statistic Packet for Social Sciences" (SPSS). Polynomial tertip 3 dapat digunakan untuk mensesuaikan dengan lengkungan dari hasil simulasi WCPP dan regressi keseluruhan dengan kaedah berlangkah di gunakan untuk mensesuaikan dengan lengkung dari semua data dengan kadar tebukan dan frekuensi sebagai pembolehubah bebas.

Penyelidik :

Assoc. Prof. Dr. Mohamad Ngasri Dimon (Ketua)
Munirul Ula
Abdul Wahab Ishari Mohd Hashim
Siti Zaleha Abdul Hamid
Ameruddin Baharom
Abdul Hamid Ahmad

E-mail : ngasri@fke.utm.my
Tel. No. : 075535901
Vot. No. : 75117

TABLE OF CONTENTS

LIST OF FIGURES

LIST OF SIMBOL

E_i	-	Incidence energy
E_r	-	Reflected energy
E_a	-	Absorbed energy
E_t	-	Transmitted energy
I_i	-	Incident sound intensity
I_r	-	Reflected sound intensity
I_a	-	Absorbed sound intensity
I_t	-	Transmitted sound intensity
I_n	-	Net sound intensity
α	-	Sound absorption coefficient
δ	-	Dissipation coefficient
τ	-	Transmission coefficient
f_{res}	-	Frequency resonance
V	-	Volume of the body
S	-	Closed surface
$n_{i:}$	-	Unit vector normal to the surface S
F	-	Vector field acting on the body
ϕ	-	Potential function in the domain V
G	-	Free space Green's function due to a time harmonic point source
X_i	-	Cartesian coordinate
$\int_s$	-	Surface integration
$\int_v$	-	Volume integration
∇	-	Del operator
ϕ	-	The velocity potential

c	-	The speed of sound
b	-	The noise source
x	-	The position
t	-	Time variables
e	-	Exponential
w	-	Angular frequency
B	-	Obstacle body
B'	-	Infinite acoustic medium
ρ_o	-	Fluid density
P	-	The point in acoustic medium B'
Q	-	The point on the boundary surface
r	-	The distant between P and Q
k	-	Wave number
j	-	Imaginer
α, β, γ	-	Specified complex constant
Z	-	Acoustics impedance of the obstacle
C(P)	-	A constant that depend on the geometry shape of S at P
ϕ_i	-	Incident velocity potential from the source
E_i	-	Incidence energy
E_r	-	Reflected energy
E_a	-	Absorbed energy
E_t	-	Transmitted energy
I_i	-	Incident sound intensity
I_r	-	Reflected sound intensity
I_a	-	Absorbed sound intensity

LIST OF ABBREVIATIONS

WCPP	Wood Circular Perforated Panel
DPCWP	Direct Piercing Carved Wood Panel
ISO	International Standard Organization
UTM	Universiti Teknologi Malaysia
SPL	Sound Pressure Level
CNC	Computer Numerical Control
BEM	Boundary Element Method
FEM	Finite Element Method
NRC	Noise Reduction Coefficient

LIST OF APPENDICES

CHAPTER 1

INTRODUCTION

1.1. Background of the Research Problem

Wood circular perforated panel (WCPP) is the simple form of direct piercing carved wood panel (DPCWP) which has been widely used as decoration element in Malay architecture especially in palaces, mosques, public building and some houses. In house and mosques, wood carving perforated panel has been used mainly as part of the wall panels and also on the upper part partition of the doors and windows. In tropical country like Malaysia, the wood carving perforated panels is also used to help in achieving thermal comfort and fresh air circulation in rooms. In addition, the use of wood carving is also for natural lighting during the day. But in early traditional houses, the wood carving especially in the guess areas serves not only as a decorative element but also reflects the social status of the owner (Lim Jee Yuan, 1987).

WCPP not only used as part of decoration in building, but also can act as sound absorption material. Its have high contribution to reduce sound reflection in the room, so that it can improve the reverberation time in the room and result in better speech intelligibility. Sound absorption coefficient (α) of WCPP can not be tested using conventional sound absorption measurement techniques such as Impedance Tube and Reverberation Chamber technique. In the previous research work, α_n experimental data derived from sound transmission coefficient (τ_n) were measured using sound intensity technique. It's very difficult to vary the material tested variables because of its complex process and very costly to produce a WCPP with good

uniform apertures dimension and perforation ratio. It's begin with panels design using CAD, then CAD designs were translated to Computer Numerical Control (CNC) model to fabricate the real panels. In addition, its need much extra cost for raw materials and good transportation. The wood moisture content is also affected the accuracy of measurement result (Mohamad Ngasri Dimon, 2003).

The boundary element method (BEM) is a numerical method that solves boundary value problems through the boundary integral equation (BIE) formulations. The applications of direct BIE formulations started in the early 1960's by Jaswon on a potential problem. This work was extended by Rizzo to solve the electrostatic problem. Since then, extensive research efforts have been made to develop BIE formulations for a variety of problems in applied mechanics. As the result, the BEM has become an attractive numerical tool useful in many engineering applications, such as acoustics, heat transfer, solid mechanics, structural mechanics, fluid mechanics, fracture mechanics, geomechanics, and electromagnetic.

Nowadays, numerical modeling techniques such as Finite Element Method (FEM) and Boundary Element Method (BEM) have been broadly used in engineering problem to minimize the complexity of research process and reduce the cost. BEM is becoming a popular numerical technique for acoustical modeling for research and development in industries. BEM has some advantages compare to FEM. The BEM approach requires only the boundary condition of complex geometry. The real disadvantages of BEMs are that the method is prone to human error in meshing the surface, it takes quite long computer calculation time for high frequencies and large surfaces, because it is needed four elements per λ to obtain an accurate simulation result (Cox and Antonio, 2004a)

In addition, the application of BEM to predict the α_n of stand alone WCPP never been done yet by any researchers. Stand alone WCPP is barely used in modern country such as in Europe and United State because stand alone WCCP is not suitable to apply in sub tropical region with cool temperature. The common research publications can be found in the literatures are mostly discussing about perforated panel with air cavity and hard backing and perforated panel with porous absorber backing and modification of Helmholtz resonator.

1.2. Research Objective

The objectives of the research work are:

i. To investigate normal incidence sound absorption coefficient (α_n) characteristics of wood circular perforated panel (WCPP) using boundary element method.

ii. To conduct the comparison and analysis of α_n resulted from simulation with α_n experimental and theoretical data to further understand the α_n of WCPP obtained through BEM modeling technique.

iii. To develop a statistical regression models for simulated α_n in correlation with frequencies and perforation ratio as the variables.

1.3 Research Scope

The research work involved boundary element method simulation of WCPP using Beasy Acoustics software. The samples and models created are based on the conditions of the experimental work conducted in previous research by Mohamad Ngasri Dimon in Acoustic research Laboratory, UTM. The WCPP samples thickness is 20 mm, panel dimension is 1.2 m x 1.2 m. The perforation ratio of the panel is varied with 20 %, 30 % and 40 % by varying apertures dimension and the apertures distance. α_n from simulation result is validated by comparing with experimental data and theoretical prediction result. Statistical regression model is conducted for further understand the correlation of perforation ratio and frequency analysis with α_n from simulation result.

CHAPTER 2

SOUND ABSORPTION

2.1 Introduction

In this chapter, the principle of sound absorption is elaborated. This followed by various types of sound absorption material, which include porous absorber, Helmholtz resonator, membrane absorber and perforated panel absorber. The sound absorption measurement principles based on random sound incidence, normal sound incidence and sound intensity technique are discussed. The theoretical prediction of normal incidence sound absorption coefficient of perforated panel is also discussed.

2.2 Sound Absorption

When a sound wave impinges on an acoustic material, there would occur an absorbed and reflected energy depending on the material sound absorption performance. If 45% of the incidence energy is absorbed and 55% of the incidence energy is reflected, then sound absorption coefficient (α) is 0.45. An open window is an example of perfect absorber where all incidence energy would be transferred to the other side of the window which results in $\alpha = 1.0$. The one square meter of an open window would give 1 Sabine of absorption. Whenever the material impedance is equal to the characteristic impedance of the air (medium), the maximum sound absorption would occur. Therefore, the amount of the energy absorbed by the

acoustic material depends on its material impedance (Z_c). The sound absorption of an acoustic material varies with frequency and angle of incidence of the sound waves impinge upon the material (Everest, 1994).

The opposite of sound absorption is sound reflection. For a geometrical or specular reflection to occur, it is required that the reflecting surface is large compared to the wavelength of the incidence energy. However, from the work conducted by Leonard et al (1964), it was calculated that for a specular reflection to occur, minimum panel dimension required is 30 x λ. When the panel dimension is about 10 x λ some diffraction occurs and when the panel dimension is less than 5 x λ, the incident energy is diffracted.

When a sound wave hits a wall, its energy is divided into three parts. If the sound incident on a wall has energy wave E_i, part of the sound energy E_r is reflected back while part of energy E_a is absorbed in a wall. The rest of the energy E_t is transmitted to the other side of the wall as shown in Figure 2.1. These phenomena can be written as (Maekawa and Lord, 1994a)

$$\boldsymbol{E_i = E_r + E_a + E_t} \tag{2.1}$$

Then the sound absorption coefficient, α is defined as follow:

$$\alpha = \frac{E_i - E_r}{E_i} = \frac{E_a + E_t}{E_i} \tag{2.2}$$

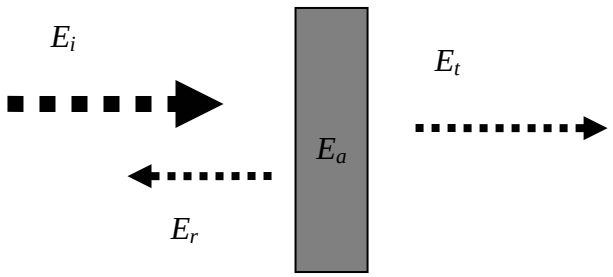

Figure 2.1 Reflection, absorption, and transmission

The above equation shows that all portion of the sound energy which is not reflected is considered to be absorbed.

2.3 Coefficients of Absorption

Suppose the boundary plane between two media is infinitely large and a plane sound wave travelling in medium 1 is normally incident on the plane, as shown in Figure. 2.2. Then, the relationship between the magnitude of the reflected and the transmitted sound is derived as follows (Maekawa and Lord, 1994b)

$$P_i + P_r = P_t \tag{2.3}$$

$$V_i + V_r = V_t \tag{2.4}$$

$$\frac{p_i}{Z_1} = \frac{p_r}{Z_1} = \frac{p_t}{Z_2} \tag{2.5}$$

where, P_i is incidence sound pressure, P_r is reflected sound pressure, $V = P/Z$, $Z_1 = \rho_1 c_1$, and $Z_2 = \rho_2 c_2$

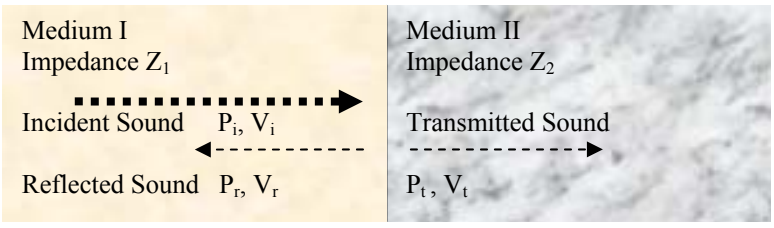

Figure 2.2 Reflection and transmission at boundary between two media

The relationship between the absorption coefficient and sound pressure reflection coefficient between two media is given as follow

$$\alpha = 1 - \frac{\mathrm{Er}}{\mathrm{Ei}} = \frac{|P_r|}{|P_i|} = \frac{(Z_2 - Z_1)^2}{(Z_2 + Z_1)^2} \tag{2.6}$$

Therefore,

$$\alpha = 1 - \frac{\mathrm{Er}}{\mathrm{Ei}} = 1 - |r_p|^2 = 1 - \frac{(Z_2 - Z_1)^2}{(Z_2 + Z_1)^2} \tag{2.7}$$

Considering the media of Z_2 is an open window, then $Z_1 = Z_2$, in this case α = 1.0 as in confirmation to the α of open window defined by Sabine. As defined by Sabine, sound absorption coefficient is the ratio between the non-reflected sound intensity and the incident sound intensity. Sabine (α) consist of two components, namely dissipation coefficient (δ) and transmission coefficient (τ) (Cremer and Muller, 1982a).

$$\alpha = \delta + \tau \tag{2.8}$$

It is stressed that, the concept of Sabine sound absorption is not confined only to the transformation of sound energy into heat energy (dissipation). The sound absorption goes beyond the dissipation process where the transmitted energy to other side of the material also constitutes as part of sound absorption. From the equation 2.8 above, there are two extreme cases of sound absorption that could occur, either due to dissipation process only or transmission process only; $\alpha = \delta$ as in thick porous material placed on the wall, and $\alpha = \tau$ as in open window (Cremer and Muller, 1982a)

2.4 Types of Sound Absorption Materials

The main aim of using sound absorption material is to reduce Sound Pressure Level (SPL) within the spaces to an acceptable level. High SPL could create listening discomfort inside the spaces. Further, sound absorption material is able to prevent undesirable reflection from surfaces. Undesirable reflections are particularly detrimental to speech intelligibility. Undesirable reflections, which are delayed in the region of 30 ms to 50 ms as compare to direct sound results in echo. The availability

of echo results in poor speech intelligibility (Maekawa and Lord, 1994c). Finally, the use of sound absorption material in an enclosed space is able to control reverberation level within the spaces. Suitable level of reverberation would result in good speech intelligibility (Yerges, 1978). There are mainly four types of sound absorption materials available that can be used to achieve the above as discussed below namely porous absorber, Helmholtz resonator, membrane absorber and perforated panel absorber.

2.4.1 Porous Absorber

Porous absorber is the most common material used in an enclosed room acoustic treatment. These materials which could be from mineral or cellulose fibre is a good sound absorber in the mid to high frequency range. Typical porous absorbers are carpets, acoustic tiles, acoustic (open cell) foams, curtains, cushions, cotton and mineral wool. The porosity created by the fibre interstices can trap and dissipates the sound energy. The frictional resistance change impinges sound energy into frictional heat and viscous losses within the pores due to small fibre vibrations. Energy conversion into heat is the most important mechanism of sound absorption for a porous material. The energy intensity would decrease over the distance travel through the material. The porous fibre sound absorption is affected by the density, the thickness, the airspace behind the material and the surface treatment (Everest, 1994b).

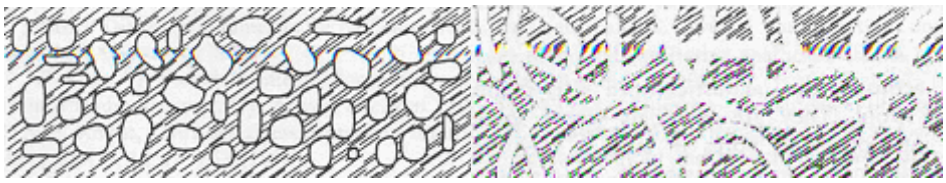

Figure 2.3 Illustration of porous absorber (Cox and Antonio, 2004a)

Density changes are known to have little effect on porous material sound absorption performance. The thicker the porous absorbers, the higher the sound

absorption at lower frequencies, particularly at below 500 Hz. The material thickness of λ/4 should results in higher sound absorption performance at the respected frequency (Maekawa and Lord, 1994d). This explains why porous material has low sound absorption at lower frequency range and become higher at higher frequency range.

Additional sound absorption for a porous material can be achieved whenever the porous material is position with an air-gap distance where the particle velocity of the sound waves is maximum, such as at λ/4. Acoustically transparent surface treatment such as acoustic fabric, tissue lamination or water based paint should be able to preserve the sound absorption of the porous fibre.

2.4.2 Helmholtz Resonator

Sound absorption at lower frequency range could be achieved particularly using Helmholtz resonator. The quality of this resonator is indicated by its quality factor (Q). This indicates the bandwidth of its tuning which is –3dB from its resonance frequency (Everest, 1994c). The quality factor of the Helmholtz resonator is formulated as

$$Q = \frac{f_{res}}{\Delta f} \qquad (2.9)$$

where Q is quality factor, f_{res} is resonance frequency and Δf is bandwidth

Helmholtz resonator consists of a volume of air contained in a cavity where there is a neck of small opening. When there is no porous fibre in the cavity, the Helmholtz resonator is considered undamped. The undamped resonance frequency of a Helmholtz resonator could be estimated using the following equation (Lawrence, 1970a).

$$f_{res} = \frac{1}{2\pi\sqrt{MC}} \qquad \text{(No porous fibre)} \qquad (2.10)$$

where M is inertance and C is acoustical capacitance

$$M = \frac{\rho(L + 1.7R)}{\pi R^2} \qquad (2.11)$$

where

ρ = Density of the air, kg/m^3

(L+1.7R) = Effective length of the neck, m

πR^2 = Area of the opening, m^2

R = Radius of the hole

$$C = \frac{V}{\rho c^2} \qquad (2.12)$$

where

C = Acoustical capacitance

V = Volume of the chamber, m^3.

c = Speed of sound in air, m/sec.

ρ = Density of air, kg/m^2

Alternatively, the approximate resonance frequency (no porous fibre) could be calculated using the following equation (Lawrence, 1970a).

$$f_{res} \frac{cA}{2\pi\sqrt{vV}} \quad (2.13)$$

where

c = Speed of sound, m/s

A = Area of the neck, m^2

v = A (L + 1.7R) Effective volume of the neck, m^3

V = Volume of the chamber, m^3

The sound absorption performance of the Helmholtz resonator at its resonance frequency can be estimated using the following equation

$$A = 0.159\left(\frac{c}{f_{res}}\right)^2 \quad (2.14)$$

where

A = Sound absorption, m^2 Sabine

c = Speed of sound in air, m/sec

2.4.3 Membrane Absorber

A Membrane absorber or diaphragmatic absorber is used to absorb low frequencies sound energy. It works by vibrating at these low frequencies and turning the sound energy into heat conversion to heat takes place through the resistance of the membrane to rapid flexing and due to the resistance of the enclosed air to compression. Practically, a membrane absorber is constructed by flexible sheets made

from plywood or rubber is stretched over supports or rigid panels mounted at some distance from the front of a solid wall as showed in Figure 2.4 below.

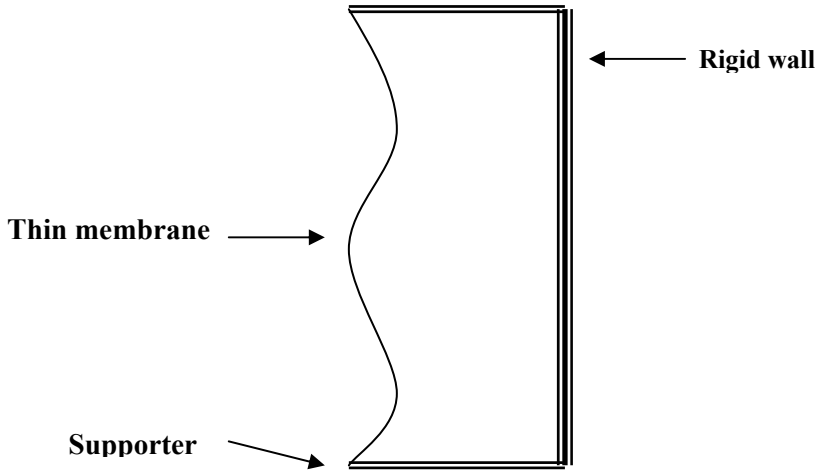

Figure 2.4 Membrane absorber

In practice, the method of fixing and the stiffness of the panels will also have some effect as the panel itself will tend to vibrate (Marsh, 1999).

2.4.4 Perforated Panel Absorber

Perforated panel is typically made from rigid thin sheet of metal perforated with circular aperture. The perforated panel is normally mounted over some distance from the wall. There is an air cavity behind the wall and this air cavity could be filled with porous fibre to result in broader frequency range of sound absorption.

The resonance frequency of perforated panel can be estimated using the following equation (Lawrence, 1970b).

$$f_{res} = \frac{c}{2\pi}\left(\frac{\mathrm{P}}{\mathrm{d(L+1.7R)}}\right) \qquad (2.15)$$

where

c = Speed of sound in air, m/sec
P = Perforation ratio (hole area/plate area)

d = Distance of the perforated panel from the wall, m

L = Perforated panel thickness, m

(L + 1.7R) = Effective length of the neck

R = Radius of the hole, m.

To broaden the frequency range of sound absorption performance of the perforated panel, the air cavity behind the wall should be filled with porous fibre. An air-gap between the porous fibre and the wall should be maintained. Increasing the thickness of the perforated panel and also the depth of the air gap would lower its resonance frequency. Therefore, by varying the depth of the air space and the thickness of the perforated panel, broader frequency range of sound absorption performance could be achieved.

A perforation ratio of more than 20% with small aperture would not affect the sound absorption of porous fibre. However, a smaller perforation ratio would reduce higher frequency sound absorption performance of porous fibre (Maekawa and Lord, 1994e).

2.5 Principles of Sound Absorption Measurement

There are two standard measurement techniques that can be used to measure sound absorption coefficient of an acoustic material. The measurement technique is based on either random sound incidence or normal sound incidence principle.

The coefficient of sound absorption measured using the two techniques are denoted by different symbols. α_n denotes coefficient of sound absorption using normal incidence technique. α_r denotes coefficient of sound absorption using random incidence technique.

2.5.1 Normal Incidence Technique

This technique requires a tube where its diameter is smaller than the wavelength. In order for a normal sound incidence of a plane wave to occur in a tube, the measuring tube should satisfy the following requirement (Maekawa and Lord, 1994c).

$$D < 0.59\lambda \tag{2.16}$$

where

D = Diameter of the tube

λ = Wavelength of sound

These require two different tube diameters to measure α_n from 250 Hz to 4 kHz. The larger tube with the diameter of 100 mm is able to measure lower frequency range up to 1.6 kHz. The smaller tube with the diameter of 20 mm is able to measure from 1 kHz to 4 kHz.

2.5.1.1 Standing Wave Method

The advantage of the standing wave method is that it is very dependable, and relatively easy to proof. But by this method, it only can measure one frequency at one time, so only spot frequency information is available. The procedure to get phase

information by locating minima in the standing wave is rather slow and so measuring a large number of frequencies is tedious. The standing wave method system is described in Figure 2.5 below (Cox and Antonio, 2004b)

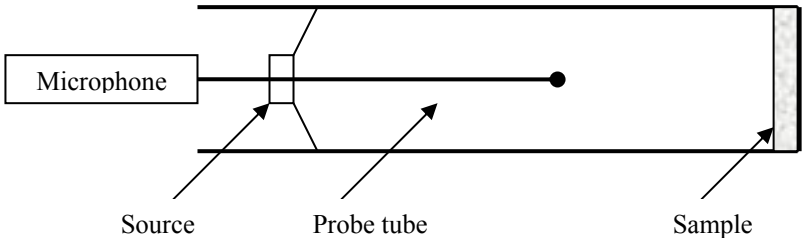

Figure 2.5 Standing wave method

The length of the measuring tube should be greater than $3/4\,\lambda$, so that more than two measurement positions could be located in order to determine its standing wave ratio.

The tested material is placed at one end of the tube and the sound source is positioned in the other end. The resultant of incidence and reflected sound wave is resulted in standing waves where the distance between every maximum position and minimum position is $\lambda/4$. This system can be formulated by equations below.

$$P_{max} = |A + B| \tag{2.17}$$

$$P_{min} = |A - B| \tag{2.18}$$

where

P_{max} = Maximum Sound Pressure Level

P_{min} = Minimum Sound Pressure level

A = Amplitude of the incidence wave

B = Amplitude of the reflected wave

The standing wave ratio (n) for this method is defined as (Cox and Antonio, 2004b)

$$n = \frac{P_{max}}{P_{min}} = \frac{|A + B|}{|A - B|} \tag{2.19}$$

Sound pressure reflection coefficient $|r_p|$ is defined as

$$|r_p| = \left|\frac{B}{A}\right| = \frac{n-1}{n+1} \tag{2.20}$$

Normal incidence sound absorption coefficient is as follow

$$\alpha_n = 1 - |r_p|^2 = 1 - \left(\frac{n-1}{n+1}\right)^2 \tag{2.21}$$

Therefore,

$$\alpha_n = \frac{4}{n + 1/n + 2} \tag{2.22}$$

Then, by knowing the standing wave ratio, normal incidence sound absorption coefficient of the material could be determined.

2.5.2 Random Incidence Technique

This technique requires a reverberation chamber. The α_r is calculated using the following formula (Cramer and Muller, 1982a; Maekawa and Lord, 1994f).

$$\alpha_r = \frac{0.16V}{S}\left[\frac{1}{RT60ws} - \frac{1}{RT60e}\right] + \bar{\alpha} \qquad (2.23)$$

where

V = Volume of reverberation chamber, m^3

S = Surface area of material tested, m^2

RT60ws = RT60 with tested material, sec.

RT60e = RT60 empty, sec

$\bar{\alpha}$ = Average sound absorption coefficient of reverberation chamber

The value of $\bar{\alpha}$ is normally very small to obtain high RT60e. Therefore, $\bar{\alpha}$ could normally be ignored.

The major requirements that must be satisfied to ensure reliable random incidence sound absorption measurement results are as follows:

1. The reverberation room volume should be at least of 180 m^3. This to enable measurement to go down to 125 Hz reliably.
2. The area of material used for testing should be of at least 10 m^2.
3. The sound field in the reverberation room should be completely diffused. There should be no parallel wall inside the room. Furthermore, the sound field should be diffused by using either diffuser or rotating panel.

The Noise Reduction Coefficient (NRC) is the single figure index, indicating the quality of the sound absorption material tested. NRC is calculated using the average of the tested sound absorption coefficient at 250 Hz, 500 Hz, 1000 Hz and 2000 Hz rounded to the nearest 0.05. (Cowan, 2000a).

Higher NRC value indicates better sound absorption material as opposed to low NRC value.

2.5.3 Sound Absorption Measurement Using Sound Intensity Technique

By using the principle of the conservation of energy where energy can neither be created nor destroyed but it can be changed from one form to another. Considering the situation as in Figure 2.6, where an incident energy (E_i) impinges on an acoustics material, there would be reflected energy (E_r), absorbed energy (E_a) and transmitted energy (E_t) (Cowan, 2000b ; Maekawa and Lord, 1994a).

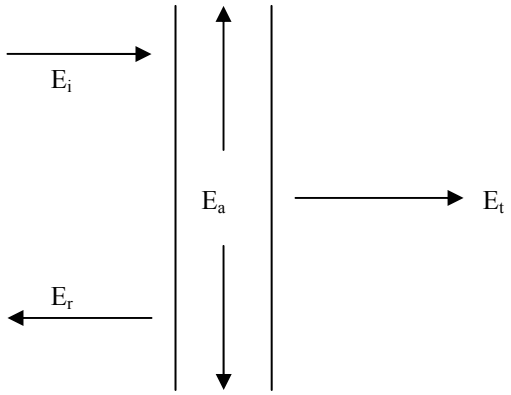

Figure 2.6 The phenomena of the principle of conservation energy

Using energy conservation rule,

$$E_i = E_r + E_a + E_t \tag{2.24}$$

Sound absorption coefficient of an acoustic material is defined as

$$\alpha = \frac{E_i - E_r}{E_i} = \frac{E_a + E_t}{E_i} \tag{2.25}$$

where

$E_i - E_r$ = Net energy in front of the sample

E_i = Incident energy, when the material is removed

Using the illustration as in Figure 2.6 and referring to figure 2.8, consider an acoustic material surface exposed to plane progressive sound wave with zero angle of incidence. Upon arrival at the acoustic material surface, the incident sound power (W_i) is partly reflected (W_r), partly absorbed (W_a) and partly transmitted (W_t) to the other side of the acoustics material. The normal incidence sound absorption coefficient is (Lai et al, 1991)

$$\alpha = \frac{Wi - Wr}{Wi} \tag{2.26}$$

where

α_n = Normal incidence sound absorption coefficient

W_n = Net sound power in front the material

$$W_n = W_i - W_r \tag{2.27}$$

$$\alpha_n = \frac{W_n}{W_i} \tag{2.28}$$

Sound Intensity is defined as

$$I = W/A \tag{2.29}$$

where

W = Sound power level (Watt/m^2)

A = Surface area (m^2)

Considering the surface area as in equation 2.28 is the common factor, equation 2.28 can be deduced to

$$\alpha_n = \frac{I_n}{I_1} \tag{2.30}$$

where

I_n = Net sound intensity in front of the acoustic material

I_1 = Incident sound intensity when the acoustic material is removed.

Therefore, based on the above discussion, it is possible to measure α_n of an acoustics material using sound intensity technique. To achieve sound free field environment, the sound intensity measurement should be conducted in an anechoic chamber.

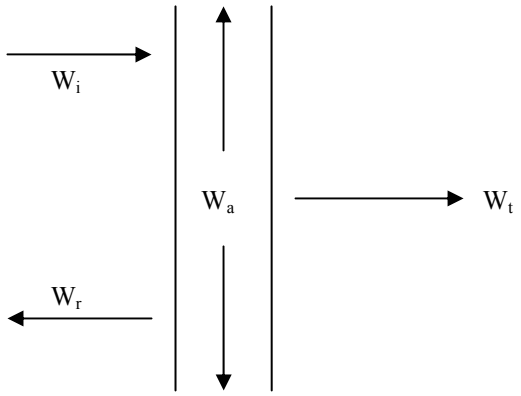

Figure 2.7 The phenomenon of reflection, absorption and transmission of sound power in an acoustic material

2.6 Kutruff Prediction Formulas for the α_n of a Perforated Panel

The α_n Kutruff prediction formula of the stand alone circular perforated panel could be obtained using the following equation (Kutruff, 1979).

$$\alpha_n = \left[1 + (\omega m / 2\rho_O c)^2\right]^{-1} \quad (2.31)$$

$$\approx \quad (2\rho_O c / \omega m)^2 \quad (2.32)$$

where

ρ_o = Density of the air = 1.2 kg/m^3

c = Speed of sound, in air = 340 m/s

$\rho_o c$ = Characteristic impedance of the medium (air) = 408 kg/m^{2}s

m = Mass of the air

$$m = \rho_o b' / б \quad (2.33)$$

б = Perforation ratio of the plate

$$б = S_1/S_2 \quad (2.34)$$

S_1 = Area of the hole

S_2 = Plate area per hole

The correction factor for the thickness of the perforated panel, b'

$$b' = b + 2\,\delta b \qquad (2.35)$$

where

b = Thickness of the perforated panel

$2\delta b$ = End correction

$\delta b = 0.8a$

a = Circular apertures with radius 'a' and with relatively large mutual distances.

Based on the above α_n theoretical prediction formula, there are three possibilities that may cause normal incidence sound absorption performance of perforated panel. These are (Cremer and Muller, 1982b).

1. The effect of the mass of the air (m) only. For this to occur, the perforated panel mounting must be very rigid, where there is no perforated panel vibration when sound waves impinge upon the perforated panel.

2. The effect of the mass of the perforated panel (M) only. Under this condition, there is a substantial perforated panel vibration when sound waves impinge upon the perforated panel.

3. The effect of the resultant mass (M_{res}). This occurs due to the combination effect of (1) and (2) above.

The resultant mass (M_{res}) can be calculated using the following formula

$$M_{res} = \frac{(m \times M)}{(m + M)} \qquad (2.36)$$

where

M_{res} = Resultant mass

m = Mass of the air only

M = Mass of the perforated panel only

Based on the α_n Kutruff prediction formula, for a certain thickness of the perforated panel, the α_n is higher for low frequency and reduces as the frequency increases. As the thickness of the perforated panel increases with the perforation ratio remains the same, the predicted α_n would reduce over its frequency range. As the thickness of the perforated panel remains the same, increasing the perforation ratio would increase the predicted α_n over its frequency range.

2.7 Applications of Absorbers

2.7.1. Reverberation Control

One of the main applications of sound absorber material is to reduce reflected sound energy in the room and to reduce the reverberance and sound level. The amount of reverberation in a space depends on the size of the room and the amount of sound absorption. This kind of absorber is commonly used in restaurants or railway stations to improve the speech intelligibility by reducing the noise.

2.7.2 Noise Control in Factories and Large Rooms

The other application of sound absorber is to control the noise level in working environment or factory to protect the hearing lost of the workers. The treatment method to solve this problem is to reduce the reverberance sound level within the space. By adding sound absorption materials on the wall, the noise exposure is decrease to save level for human ear.

2.7.3 Modal Control in Critical Listening Space

Bass trap or bins absorption is commonly apply for controlling low frequency problem in recording studio, home theatre and conference rooms. Resonant and Helmholtz absorber are usually used for mass spring system with damping to provide absorption at the resonant frequency of the system.

2.7.4 Echo Control in Auditorium and Lecture Theatres

Sound absorption material are commonly used to absorb the late arriving reflected sound in large auditorium, a late arriving reflection appears as an echo if its level is significantly above the general reverberation level. By adding sound absorption material at rear wall, it can optimally reduce the echo in audience areas near to the stage.

2.7.5 Absorption in Sound Insulation

The other applications of porous absorbers materials are in sound insulation building system, to protect the noise entering the room. The porous absorber is commonly used to prevent a resonance of air cavity of light weight construction based on leaf partition with an air gap

2.8 Summary

Some theoretical reviews related to sound absorption coefficient has been discussed and elaborated. Sound absorption coefficient definitions by using energy conservation and then combine with Sabine definition are elaborated. Various types of sound absorber material are also discussed such as porous absorber, Helmholtz

resonator, membrane absorber and perforated panel absorber. There are several techniques to measured sound absorption coefficient, which are sound intensity technique, random sound incidence, normal sound incidence such as standing wave method and transfer function method. Kutruff prediction formulas and mass transfer to predict the sound absorption coefficient of stand alone perforated panel and the common application of sound absorber materials are also highlighted.

CHAPTER 3

BOUNDARY ELEMENT METHOD IN ACOUSTICS

3.1 Introduction

The boundary element method (BEM) is a numerical method that solves boundary value problems through the boundary integral equation (BIE) formulations. The applications of direct BIE formulations started in the early 1960‘s by Jaswon on a potential problem. This work was extended by Rizzo to solve the electrostatic problem. Since then, extensive research efforts have been made to develop BIE formulations for a variety of problems in applied mechanics. As the result, the BEM has become an attractive numerical tool useful in many engineering applications, such as acoustics, heat transfer, solid mechanics, structural mechanics, fluid mechanics, fracture mechanics, geomechanics, and electromagnetic.

Nowadays, The BEM is becoming a popular numerical technique for acoustical modeling for research and development in industries. The major advantage of this numerical method is that only boundary surface of the body need to be modeled with it mesh of elements. Boundary element has become a powerful alternative to finite element method particularly in cases where better accuracy is required due to problems where the domain is extends to infinity (Seybert and Wu, 1997a). The only real disadvantages of BEMs are that the method is prone to human error in meshing the surface, and the other real problem

is it takes very long calculation time for high frequencies and large surfaces, requiring super computer or a considerable amount of patience while waiting for results.

The purpose of this chapter is to give and overall reviews of the BEM in acoustic scattering and radiation problems useful to predict the sound absorption coefficient of Wood Circular Perforated Panel (WCPP).

3.2 Acoustics Problems

Generally, there are three types of acoustic problems that can be solved using Boundary Element Method, which are interior, exterior and combined interior/exterior problems as showed in Figure 3.1. For interior problems, the acoustic domain is finite and enclosed by boundaries, such as calculating transmission loss of silencer, prediction of sound field inside the cabin of a car, or problems involved with noise generated by industrial machinery in a factory enclosure.

In contras to interior problems, the acoustic domain for exterior problems is infinite and outside the boundaries of object. Typical exterior problems include sound wave propagation in free field, noise radiated from an engine or machinery within an open environment, or those of sound barriers in open space.

The combined interior/exterior problems have two types of acoustics domain, one is infinite and the other is finite. It can be analogize by referring to as interior problems with openings surfaces, such as an enclosed room with open door, car cabins with sunroofs or noise generated from industrial machinery within a partial enclosure.

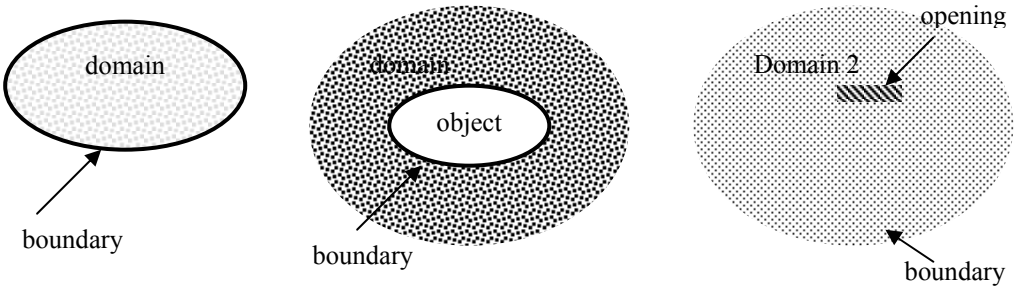

(a) Interior Problem (b) Exterior Problem (C) Interior/Exterior Problem

Figure 3.1 Acoustics problems

3.3 Basic Concepts

The basic concepts of potential theory in BEM direct formulation is started from Green's identities and uses the potential function and it derivative as main variable.

3.3.1 Green's Identities

Green's Identities is also known as Divergence Theorem or Gauss' Theorem. Let consider an arbitrary body with volume V bounded with closed surface S and F be a vector field acting on the body. Based on Gauss' theorem established that "the total flux of the vector field F across the closed surface S must be equal to the volume integral of the divergence of this vector" (Wrobel, 2002a)

$$\oint_S F_i n_i dS = \oint_v \frac{\partial F_i}{\partial x_i} dV \tag{3.1}$$

where n_i are the outward direction component of unit vector normal to the surface

S. Based on flux conservation for potential flow, the relation of potential function ϕ in the domain V with any closed surface S in V is given below. The equation is obtained by substituting $\partial\phi/\partial x_i$ for F_i and $\nabla^2\phi = 0$

$$\int_s \frac{\partial \phi}{\partial x_i} n_i dS = \int_s \frac{\partial \phi}{\partial n} dS = \int_v \frac{\partial^2 \phi}{\partial x_i \partial x_i} dV = \int_v \nabla^2 \phi dV = 0 \tag{3.2}$$

This equation means that, in potential problems without internal sources, all flux across the surface must be eliminated.
By substituting $F_i = \phi \partial G/\partial x$ into Gauss' theorem gives

$$\int_s \phi \frac{\partial G}{\partial x_i} n_i dS = \int_v \frac{\partial}{\partial x_i}\left(\phi \frac{\partial G}{\partial x_i}\right) dV \tag{3.3}$$

By using the chain rule, it result in

$$\frac{\partial}{\partial x_i}\left(\phi \frac{\partial G}{\partial x_i}\right) = \frac{\partial \phi}{\partial x_i}\frac{\partial G}{\partial x_i} + \phi \nabla^2 G \tag{3.4}$$

Substituting the above result into right-hand side of equation 3.3, Green's first identity is obtained:

$$\int_s \phi \frac{\partial G}{\partial n} dS = \int_v \frac{\partial \phi}{\partial x_i}\frac{\partial G}{\partial x_i} dV + \int_v \phi \nabla^2 G dV \tag{3.5}$$

The Green's first identity is also valid when interchanging ϕ and G

$$\int_s G \frac{\partial \phi}{\partial n} dS = \int_v \frac{\partial \phi}{\partial x_i}\frac{\partial G}{\partial x_i} dV + \int_v G \nabla^2 \phi dV \tag{3.6}$$

Green's second identity as in Equation 3.7 is obtained by subtracting Green's first

identity (3.5) with equation 3.6 above

$$\int_s \left(\phi \frac{\partial G}{\partial n} - G \frac{\partial \phi}{\partial n} \right) dS = \int_v \left(\phi \nabla^2 G - G \nabla^2 \phi \right) dV \tag{3.7}$$

3.4 Governing Equation for Acoustic Problems

3.4.1 Basic Equation

The governing equation for acoustic wave propagation through a linear elastic medium can be expressed by the linear wave equation (JSilva, 1994)

$$\nabla^2 = \frac{1}{c^2} \frac{\partial^2 \phi}{\partial t^2} + b \tag{3.8}$$

where ϕ (x,t) is the velocity potential, c is the speed of sound, b(x,t) is the noise source and x is the position and t is time variables. By assuming the motion is time harmonic, the function ϕ can be expanded as

$$\phi(x,t) = \phi(x_i) e^{iwt} \tag{3.9}$$

i= 1, 2, 3

3.4.2 Boundary Integral Formulation

In the BIE formulation, the domain-based governing equation for a given boundary value problem, the Helmholtz equation for acoustics is reformulated into an integral equation that involves only integrals on the boundary of the

domain. A known solution of the fundamental problem, the free space response to a point source and the Green's second identity are utilized in this process. All field variables at any point in the domain can be evaluated using this integral equation provided the boundary variable (e.g. the acoustics surface impedance) and its spatial gradient are known. In order to solve the BIE numerically, the boundary of the domain is discretized into many small patches called boundary elements. A linear system of equations is then formed by evaluating the BIE with the prescribed boundary conditions for every node in the discretization. The solution of the linear system of equations together with the boundary conditions provide all the information needed for evaluating the field variables at any point in the domain.

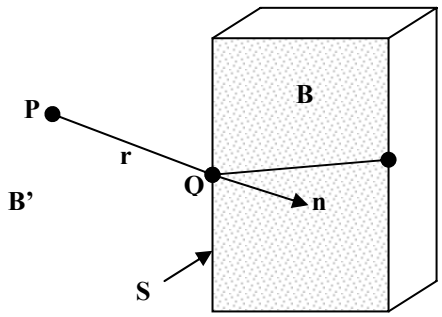

Figure 3.2 Boundary integral problems formulation

In the Figure 3.2 show that, an obstacle body B of boundary surface S mounting in an infinite acoustic medium B' with density ρ_o and speed of sound c. P is the point in acoustic medium B', Q is the point on the surface S. r is the distant between P and Q, and n is the unit normal vector of S directed away from acoustic domain.

The governing differential equation in steady state linear acoustics is the well-known Helmholtz equation (Kirkup, 1998a),

$$\nabla^2\phi + k^2\phi = 0 \tag{3.10}$$

where:

ϕ : Velocity potential

k : Wave number, k = ω/c

ω : Angular frequency in radian

The above equation must be satisfied in acoustic medium B'. The acoustic medium is assumed not moving so that the flow velocity is to be zero and the acoustic particle velocity can be prescribed as follow,

$$V = -\nabla\phi \tag{3.11}$$

The sound pressure can be evaluated by

$$P = j\,\rho_o\,\omega\,\phi \tag{3.12}$$

where :

$j^2 = -1$

The general forms of boundary condition on the boundary surface S is:

$$\alpha\phi + \beta\frac{\partial\phi}{\partial n} = \gamma \tag{3.13}$$

where α, β, γ are specified complex constant, the above equation can be use to specify acoustics impedance of the obstacle (Kirkup, 1998b) by setting α = 1, β = -z and γ = 0

To obtain the accurate result in acoustic problems, the scattered potential ϕ_s must also satisfy The Sommerfeld radiation condition at infinity, which is

$$\lim_{r \to \infty} \left[r \left(\frac{\partial \phi}{\partial r} + ik\phi \right) \right] = 0 \tag{3.14}$$

The Helmholtz equation for the problem can be reformulated by starting from Green's second identity and The Sommerfeld radiation condition. The boundary integral equation defined on the surface S which sometime called as Helmholtz integral equation can be written as follow:

$$C(p)\phi(P) = \oint_s \left[G(Q,P) \frac{\partial \phi}{\partial n}(Q) - \frac{\partial G}{\partial n}(Q,P) \phi(Q) \right] dS(Q) + 4\pi\phi_i(P) \tag{3.15}$$

where:

ϕ (P) = Velocity potential at P

ϕ (Q) = Velocity potential at point Q

C(P) = A constant that depend on the geometry shape of S at P

G(Q,P)= Free space Green's function for a time harmonic point source at P,

$\phi_i(P)$ = Incident velocity potential from the source

In the boundary integral equation above, the explicit expression of free space Green's function is:

$$G = \frac{e^{-ikr}}{r} \tag{3.16}$$

It derivative with respect to the normal is given by

$$\frac{\partial G}{\partial n} = -\frac{e^{-ikr}}{r} (ik + \frac{1}{r}) \frac{\partial r}{\partial n} \tag{3.17}$$

where r = | Q - P |

For the equation (3.17),

C(P) = 4π for P in acoustic medium B'

C(P) = 0 for P in the body B

For P at any location at the boundary surface S, C(P) is given by the following equation:

$$C(P) = 4\pi - \oint_S \frac{\partial}{\partial n}\frac{1}{r} dS \tag{3.18}$$

3.5 Numerical Solution

"The Boundary Element Method is a numerical method of solution of Boundary Integral Equation, based on a discretization procedure". (Wrobel, 2002b).

A numerical solution for Helmholtz integral equation above is achieved by discretizing the boundary surface into a number of elements and nodes. The elements are usually classified in two types (Seybert and T. W. Wu, 1997b), triangular and quadrilateral and both can be linear or quadratic (curved). For linear element, acoustic variables are represented by a linear or first order approximation. Quadratic elements represent the acoustic variables in second order or curved approximation. Therefore it can accurately follow the geometry shape of the body and resulting in higher result accuracy. Nowadays, boundary element technology has been developed to agree with isoparametric element in which the surface shape and acoustic variables are approximated by using the same polynomials (shape function).

3.5.1 Computational Implementation

By assuming that the surface S is discretized into a series of N boundary elements, Boundary Integral equation (3.15) can be written as

$$C(p)\phi(P) = \sum_{j=1}^{N} \oint_{S_j} \left[G(Q,P)\frac{\partial \phi}{\partial n}(Q) - \frac{\partial G}{\partial n}(Q,P)\phi(Q) \right] dS(Q) + 4\pi\phi_i(P) \qquad (3.19)$$

The shape and size of elements are determined by geometry of the body and acoustic frequency. At least 4 elements per wave length are required for linear element and minimum 2 elements per wave length for quadratic element (Seybert and Wu, 1997b).

For each elements, a singular point P is placed at each node for generating a set of linearly independent boundary integral equations. The nodes arrangement for quadratic and isoparametric elements can be described in Figure 3.3 below. Quadratic element, have 8 nodes for quadrilateral and 6 nodes for triangular, it has a node at each vertex and one node at each side. By this side point, the elements can be assumed as a curved shape.

For each position of P the Helmholtz integral equation can be represented by a sum of integrals over the elements (denoted by S_j, where j = 1, M). The number of nodes and number of element is denoted by N and M. The Cartesian coordinate used in this approach is X_i (i= 1, 2, 3). To study quadratic element, it is defined the way to pass from the X_i global Cartesian system to ξ_1, ξ_2, n system defined locally over the element, where ξ_1, ξ_2 are oblique coordinates and n is the normal direction of the element (Brebbia and Domoniquez, 1992).

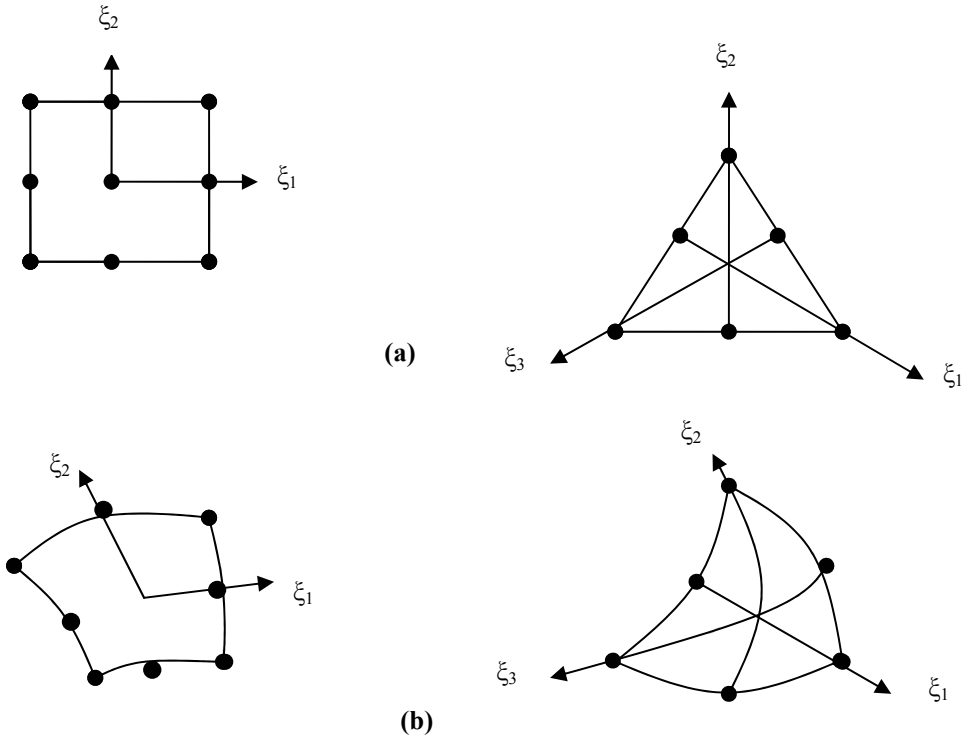

Figure 3.3 Isoparametric element (a) linear (b) quadratic

Every point on each element is assumed to be formulated to nodal coordinates $X_i\alpha$ given by (Seybert *et al*, 1985):

$$X_i(\xi) = \sum_M N_m{}^m(\xi) X_m{}^m \qquad \text{M = 1, 2, 3, …, 6 or 8,} \qquad (3.20)$$

where M is the number of points necessary to define geometry of elements, and $N_m(\xi)$ is the shape function of the local coordinates $(\xi) = (\xi_1, \xi_2)$.

For three-dimensional boundary elements, the transformation from the global Cartesian system x_1, x_2, x_3 to a local system ξ_1, ξ_2, n defined over the surface of the body is given by a Jacobian, similar to two-dimensional problems, which now take the form

$$dS = |J| d\xi_1 d\xi_2 \tag{3.21}$$

The Jacobian is calculated by

$$|J| = \sqrt{J_1^2 + J_2^2 + J_3^2} \tag{3.22}$$

where:

$$J_1 = \frac{dx_2}{d\xi_1}\frac{dx_3}{d\xi_2} - \frac{dx_3}{d\xi_2}\frac{dx_2}{d\xi_1} \tag{3.23}$$

$$J_2 = \frac{dx_3}{d\xi_1}\frac{dx_1}{d\xi_2} - \frac{dx_1}{d\xi_2}\frac{dx_3}{d\xi_1} \tag{3.24}$$

$$J_3 = \frac{dx_1}{d\xi_1}\frac{dx_2}{d\xi_2} - \frac{dx_2}{d\xi_2}\frac{dx_1}{d\xi_1} \tag{3.25}$$

The components of the unit normal vector are given by $n_i = J_i / |J|$ (i = 1, 2, 3.)

Interpolation functions for three-dimensional boundary elements are analogous to those of two-dimensional finite elements. The most common geometrical forms are triangular and quadrilateral.

The simplest triangular element has three nodes, and its geometry is generally defined with oblique coordinates ξ_1, ξ_2, ξ_3 varying from 0 to 1 over two sides (Figure 3.3). The coordinates of each point are given in the form

$$x_i = \xi_1 x_i^1 + \xi_2 x_i^2 + \xi_3 x_i^3 \tag{3.26}$$

with x_i^1, x_i^2, x_i^3 the coordinates of the nodal points, and ξ_3 a dependent coordinate such that $\xi_3 = (1 - \xi_1 - \xi_2)$. The relationship between the natural, oblique

coordinates and the Cartesian ones is given by

$$\xi_1 = \frac{1}{2A}(2A_1^0 + b_1 x_1 + a_1 x_2) \tag{3.27a}$$

$$\xi_2 = \frac{1}{2A}(2A_2^0 + b_2 x_1 + a_2 x_2) \tag{3.7b}$$

$$\xi_3 = \frac{1}{2A}(2A_3^0 + b_3 x_1 + a_3 x_2) \tag{3.27c}$$

where

$$a_i = x_1^k - x_1^j$$

$$b_i = x_2^k - x_2^j$$

$$2A_i^0 = x_1^j x_2^k - x_1^k x_2^j$$

With i = 1, 2, 3 for j = 2, 3, 1 and k = 3, 1, 2

$$A = \frac{1}{2}(b_1 a_2 - b_2 a_1) \tag{3.28}$$

3.5.2 Interpolation Function

The interpolation functions for quadrilateral elements are the same used in finite element analysis. The quadratic quadrilateral element uses Lagrangian polynomials.

1. Linear quadrilateral elements:

$$N_1(\xi)=\frac{1}{4}(1-\xi_1)(1-\xi_2) \tag{3.29a}$$

$$N_2(\xi)=\frac{1}{4}(1+\xi_1)(1-\xi_2) \tag{3.29b}$$

$$N_3(\xi)=\frac{1}{4}(1+\xi_1)(1+\xi_2) \tag{3.29c}$$

$$N_4(\xi)=\frac{1}{4}(1-\xi_1)(1+\xi_2) \tag{3.29d}$$

2. Quadratic quadrilateral elements:

$$N_1(\xi)=\frac{1}{4}(\xi_1+1)(\xi_2+1)(\xi_1+\xi_2-1), \tag{3.29e}$$

$$N_2(\xi)=\frac{1}{4}(\xi_1-1)(\xi_2+1)(\xi_1-\xi_2+1), \tag{3.29f}$$

$$N_3(\xi)=\frac{1}{4}(1-\xi_1)(\xi_2-1)(\xi_1+\xi_2+1), \tag{3.29g}$$

$$N_4(\xi)=\frac{1}{4}(\xi_1+1)(\xi_2-1)(\xi_1-\xi_2+1), \tag{3.29h}$$

$$N_5(\xi)=\frac{1}{2}(\xi_1+1)(1-\xi_2^2), \tag{3.29i}$$

$$N_6(\xi)=\frac{1}{2}(\xi_1+1)(1-\xi_1^2), \tag{3.29j}$$

$$N_7(\xi) = \frac{1}{2}(\xi_1 - 1)(\xi_2^2 - 1), \tag{3.29k}$$

$$N_8(\xi) = \frac{1}{2}(1 - \xi_2)(1 - \xi_1^2), \tag{3.29l}$$

The shape functions for triangular elements are written in terms of triangular area coordinates $(\xi_1 + \xi_2 + \xi_3 = 1)$:

1. Linear triangular elements

$$N_1(\xi) = \xi_1 \tag{3.30a}$$

$$N_2(\xi) = \xi_2 \tag{3.30b}$$

$$N_3(\xi) = \xi_3 \tag{3.30c}$$

2. Quadratic triangular elements

$$N_1(\xi) = \xi_1(2\xi_1 - 1), \tag{3.31a}$$

$$N_2(\xi) = \xi_2(2\xi_2 - 1), \tag{3.31b}$$

$$N_3(\xi) = \xi_3(2\xi_3 - 1), \tag{3.31c}$$

$$N_4(\xi) = 4(\xi_1 \xi_3), \tag{3.31d}$$

$$N_5(\xi) = 4(\xi_1 \xi_2), \tag{3.31e}$$

$$N_6(\xi) = 4(\xi_2 \xi_3), \tag{3.31f}$$

For acoustic problems, the velocity potential $\phi(\xi)$ and the particle velocity $\frac{\partial\phi(\xi)}{\partial n}$ are approximated over each element through interpolation function $N(\xi)$ and their nodal values, in the form

$$\phi(\xi) = \sum_{n=1}^{N} N(\xi)^n \phi_\alpha{}^n \tag{3.32}$$

and

$$\frac{\partial\phi(\xi)}{\partial n} = \sum_{n=1}^{N} N(\xi)^n \frac{\partial\phi_\alpha{}^n}{\partial n} \tag{3.33}$$

where ϕ_α is a nodal value of ϕ and $\frac{\partial\phi_\alpha}{\partial n}$ is a nodal value of $\frac{\partial\phi}{\partial n}$.

After the boundary discretization and approximation of the values of ϕ and $\frac{\partial\phi}{\partial n}$ within each element through interpolation functions and nodal values, the following integrals have to be computed over each element

$$h^n = \int_s \frac{\partial G}{\partial n} N^n dS \tag{3.34}$$

and

$$g^n = \int_s G N^n dS \tag{3.35}$$

The vector of interpolation functions N^n are usually expressed in terms of a homogeneous coordinate system (ξ_1, ξ_2) considering a quadrilateral integration domain, i.e $|\xi_1|, |\xi_2| \leq 1$. Taking into account this coordinate transformation, expressions (3.27) and (3.28) become

$$h^n = \int_{-1}^{1}\int_{-1}^{1} \frac{\partial G}{\partial n} N^n(\xi) J(\xi) d\xi_1 \xi_2 \tag{3.36}$$

$$g^n = \int_{-1}^{1} \int_{-1}^{1} GN^n(\xi) J(\xi) d\xi_1 \xi_2 \tag{3.37}$$

where $J(\xi) = J(\xi_1, \xi_2)$ is the Jacobian of the transformation, possibly non-linear.

The application of Boundary integral equation (3.15) to all nodal points, corresponding to a collocation technique, produces a system of algebraic equation of the form

$$H\phi = G\frac{\partial \phi}{\partial n} \tag{3.38}$$

in matrix notation, it can be written as follow

$$\begin{bmatrix} H_{11} H_{12} \text{ K } H_{1N} \end{bmatrix} \begin{bmatrix} \phi_1 \\ \phi_2 \\ \text{M} \\ \phi_N \end{bmatrix} = \begin{bmatrix} G_{11} G_{12} \text{ K } G_{1N} \end{bmatrix} \begin{bmatrix} \frac{\partial \phi_1}{\partial n} \\ \frac{\partial \phi_2}{\partial n} \\ \text{M} \\ \frac{\partial \phi_N}{\partial n} \end{bmatrix} \tag{3.39}$$

by collocating the load point on the nodes 2 to N, the missing equations are obtained by assembling to form the system

$$\begin{bmatrix} H_{11} H_{12} \text{ K } H_{1N} \\ H_{21} H_{22} \text{ K } H_{2N} \\ \text{M M O M} \\ H_{N1} H_{N2} \text{ K } H_{NN} \end{bmatrix} \begin{bmatrix} \phi_1 \\ \phi_2 \\ \text{M} \\ \phi_N \end{bmatrix} = \begin{bmatrix} G_{11} G_{12} \text{ K } G_{1N} \\ G_{21} G_{22} \text{ K } G_{2N} \\ \text{M M O M} \\ G_{N1} G_{N2} \text{ K } G_{NN} \end{bmatrix} \begin{bmatrix} \frac{\partial \phi_1}{\partial n} \\ \frac{\partial \phi_2}{\partial n} \\ \text{M} \\ \frac{\partial \phi_N}{\partial n} \end{bmatrix} \tag{3.40}$$

After boundary condition values are applied to the system (3.37), the matrices can

be recorded in form

$$AX = F \tag{3.41}$$

where X containing the unknown values of ϕ and $\frac{\partial \phi}{\partial n}$, the known boundary values are multiplied with the corresponding matrix entries to yield the vector F. The above system (3.41) can be solved by standard Gauss elimination algorithms. All variables are in complex form.

3.6 Problem Formulation for Scattering

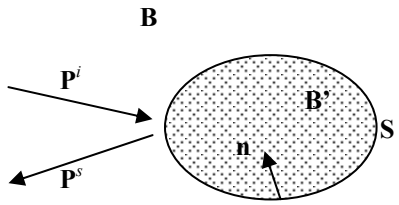

Figure 3.4 Scattering problem

Consider the scattering sound wave by a thin body in a compressible fluid medium, the incidence wave potential from the source is represented by

$$\phi^i = e^{\pm iKx} \tag{3.42}$$

where k is wave number and B is a constant related to the strength of point source. The total exterior potential is obtained as the sum of incident and scattered wave

$$\phi(x) = \phi^i(x) + \phi^s(x) \tag{3.43}$$

The Helmholtz integral equation formulates the potential at the point, as combination of the potential direct from the source and a surface integral of the potential and it derivative over the reflecting surfaces.

$$\phi(x) = \phi^i(x) + \int_s G(x,y)\frac{\partial \phi}{\partial n}(y)dS - \int \frac{\partial G}{\partial n}(x,y)\phi(y)dS \tag{3.44}$$

The equation is valid for x point in unbounded domain exterior to the scattering body. If the surface is assumed to be rigid, the Neuman boundary condition is applied to entire surface, where $\frac{\partial \phi}{\partial n} = 0$, so that the above equation can be reduced to

$$\phi(x) = \phi^i(x) + \int_s \frac{\partial G}{\partial n}(x,y)\phi(y)dS\ ] \tag{3.45}$$

In acoustic scattering problem, both incident wave and reflected wave satisfy Helmhotz equation, but only scattered wave has to satisfy Sommerfeld radiation condition. In most acoustic applications, the incident wave may be either a plane wave or a spherical wave. Incident pressure for plane wave as follow

$$P^i = Ae^{-iK(\alpha x+\beta y+\gamma z)} \tag{3.46}$$

where A is the amplitude of the incident plane wave, α,β, and γ are the direction cosines along the incident direction. For an incident spherical wave,

$$P^i = B\frac{e^{-iKR}}{R} \tag{3.47}$$

where the constant B is related to the strength of the point source. R is the measurement distance from the position of the point source. To derive the integral equation for scattering problem, first, applying the exterior Helmholtz integral equation to scattered pressure in the exterior domain B in Figure 3.4. This give

$$C(p)P^s(p) = -\int_s (j\rho\omega v_n^s G + P^s \frac{\partial G}{\partial n})dS \tag{3.48}$$

Then, interior Helmholt integral equation is applied to the incident wave P^i in the interior domain B' in Figure 3.4. The Sommerfeld radiation condition is not required for this equation. Helmholtz integral equation in the interior domain in the same normal direction with equation (3.48) (in the absence of the obstacle) become

$$C^0(p)P^i(p) = \int_s (j\rho\omega v_n^i G + P^i \frac{\partial G}{\partial n})dS \tag{3.49}$$

Subtracting Equation 3.41 from Equation 3.40 produce

$$C(p)\left[P(p) - P^i(p)\right] - C^0(p)P^i(p) = -\int_s (j\rho\omega v_n G + P\frac{\partial G}{\partial n})dS \tag{3.50}$$

because $C(p) + C^0(p) = 1$, Equation (3.49) can be rewritten as

$$C(p)P(p) = -\int_s (j\rho\omega v_n G + P\frac{\partial G}{\partial n})dS + P^i(p) \tag{3.51}$$

This is integral equation applied for scattering problems

3.7 Radiation Problems

For radiation problem in exterior domain, the objective is to solve the Helmholtz equation in an infinite domain B due to the acoustic radiation from a vibrating surface S. The normal direction n is pointed away from infinite domain and the boundary condition of the surface can be specified by general form as in Equation 3.13.

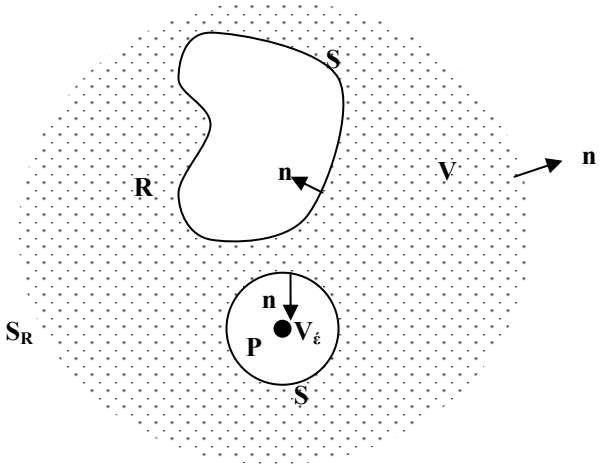

Figure 3.5 Radiation problems in infinite domain

Figure 3.5 show a tiny spherical volume V_ε enclosing the singular point P is excluded from acoustic domain B and a far field boundary surface S_R of radius R is temporarily constructed to bind the acoustic domain B. The Green's second identity can be written as

$$\int_{V-V_\varepsilon}(G\nabla^2 P - P\nabla^2 G)dV = \int_{S+S_\varepsilon+S_R}(G\frac{\partial P}{\partial n} - P\frac{\partial G}{\partial n})dS \tag{3.52}$$

Since the singular point P is exclude from the domain, the left hand side is simply zero due to cancellation of two terms, and it is shown that

$$\lim_{\varepsilon\to 0}\int_{S_\varepsilon} G\frac{\partial P}{\partial n}dS = 0 \tag{3.53}$$

$$\lim_{\varepsilon\to 0}\int_{S_\varepsilon} G\frac{\partial P}{\partial n}dS = p(P)\lim_{\varepsilon\to 0}\int_{S_\varepsilon}\frac{\partial G}{\partial n}dS = p(P) \tag{3.54}$$

By applying the Sommerfeld radiation condition, the solution p can be represented by

$$P \to A\frac{e^{-ikr}}{r} \quad \text{as r goes to infinity} \tag{3.55}$$

where A is a constant. Since P has the same form as G at infinity, it can be shown that

$$\lim_{R\to\infty}\int_{S_R}(G\frac{\partial P}{\partial n} - p\frac{\partial G}{\partial n})dS = 0 \tag{3.56}$$

Therefore, the boundary integral equation is

$$p(P) = \int_S (G\frac{\partial P}{\partial n} - p\frac{\partial G}{\partial n})dS = 0 \tag{3.57}$$

in the other form (for P in the domain) can be written as

$$p(P) = -\int_S (j\rho\omega V_n G + p\frac{\partial G}{\partial n})dS \tag{3.58}$$

For P on the boundary, P can be excluded from the acoustic domain as shown in Figure 3.6 below.

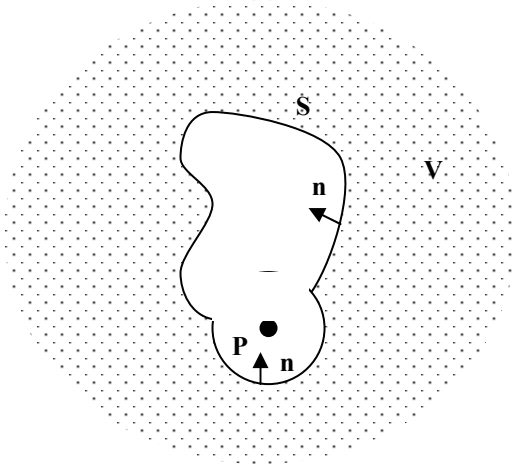

Figure 3.6 P excluded from an exterior domain on a smooth boundary

From the figure 3.6, then, the boundary equation becomes

$$C(P)p(P) = -\int_S (j\rho\omega V_n G + p\frac{\partial G}{\partial n})dS\,, \tag{3.59}$$

where C(P) is defined by

$$C(p) = \lim_{\varepsilon\to\infty}\int_{S_\varepsilon} \frac{\partial G}{\partial n})dS = \lim_{\varepsilon\to\infty}\int_{S_\varepsilon} \frac{\partial G_L}{\partial n})dS \tag{3.60}$$

It is then defined a complimentary surface S'$_\varepsilon$ on the interior side of S so that S_ε and $S_{\varepsilon'}$ form a full spherical surface of radius *l* centered at P, as shown in Figure 3.6. The normal on the sphere is pointing toward P. It is showed that

$$\int_{S_\varepsilon + S'_\varepsilon} \frac{\partial G_L}{\partial n})dS \tag{3.61}$$

$$C(P) = 1 - \int_S (\frac{\partial G_L}{\partial n})dS \tag{3.62}$$

Note that C(P) is equal to 1 for P in the acoustic domain, and it is equal to 1/2 for P on a smooth boundary. Under these two circumstances, there is no need to use Equation 3.53. Equation 3.61 is only used when P is on the boundary. It can also be shown that C(P)=0 for P outside the acoustic domain.

3.8 Summary

The boundary element method applications to acoustical problem are elaborated. Common acoustics problem such as interior, exterior and combine interior exterior problems are highlighted. Governing equation and boundary integral formulation for acoustics problems is derived based on Helmholtz integral

equation and Green second identity function. Numerical solution and computational implementation and types of element used in simulation are discussed. Boundary integral formulation for scattering and radiation problem is governed by applying Sommerfeld radiation condition.

CHAPTER 4

WOOD CIRCULAR PERFORATED PANEL SIMULATION PROCESS USING BEASY ACOUSTIC SOFTWARE

4.1 Introduction

This chapter discusses the detail of Wood Circular Perforated Panel (WCPP) simulation process based on Boundary Element Method using Beasy Acoustics software. The simulation process was started by creating the geometrical model of the panel and anechoic room followed by checking patch orientation and geometrical error, meshing, defining zone, defining fluid properties, creating internal points, creating sound source, defining boundary condition and frequency response, calculating sound intensity, and viewing simulation result data .

4.2 BEASY Modeling Fundamentals

4.2.1 Patch

Patch in Beasy is a surface created by several lines connections. Patch orientation is very important to describe the zone and domain that discussed later in section 4.2.3. Patches that have normal direction points out the acoustics domain or normal direction away from the center of the domain are called *outward patches*. Outward patch is described in Figure 4.1a. The other way, patches that have normal

direction toward the centre of the domain is called *inward patches* as described in Figure 4.1b.

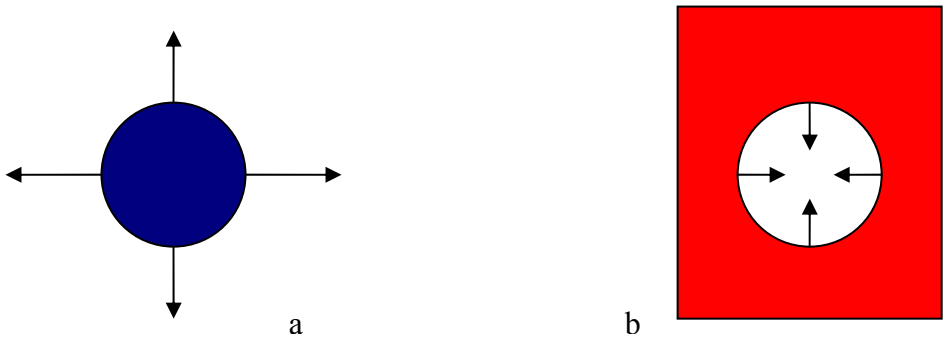

a b

Figure 4.1: (a) Outward Patch, (b) Inward Patch

4.2.2 Elements

For acoustics problems, boundary elements are in surfaces form, it can be quadrilateral or triangular in shape. Each element is used to represent the acoustic behavior of a small section of the surface area being analyzed. All quadrilateral elements have nine mesh points, arranged in a regular 3x3 grid as showed in Figure 3.3. As there are 9 mesh points, the geometry is quadratic and so may be curved to follow the shape of the model. Similarly, triangular elements have six mesh points, with one at each vertex and one on each mid-side; triangular elements do not have a central mesh point. Every element also has a number of nodes. These are the positions where the values of the problem variables are calculated. The order of the element may be constant, linear, reduced quadratic or quadratic. In normal circumstances, by default, BEASY creates reduced quadratic elements for 3D model.

The accuracy of the boundary element model will be dependent upon the size and the order of the elements. Therefore where conditions are changing rapidly smaller elements or higher order elements should be used. But if small elements are used in one part of a model, it would be uneconomic in terms of computer run-time. So it is necessary to increase the size of elements gradually, fanning out to larger elements on less sensitive parts of the model.

BEASY offers a variety of elements with different *orders*. There are; constant, linear and quadratic elements.

- Constant elements run fastest, use little disk space but many elements may be required to produce an accurate solution.
- Quadratic elements runs the slowest and use the most disk space of the three element types, but produce the most accurate results
- Linear elements provide an option in between these two extremes.

4.2.3 Zones

Zones are groups of elements which can be considered as substructures of the component. All problems will consist of at least one zone. Zones are separated by interface elements. These are created in exactly the same way as boundary elements, but are inside the material. The definition of the zones in a model is taken care of in the preprocessing stage of building the model. Each zone is treated as a boundary element model in its own right for the first part of the analysis. For each zone, a set of equations is generated which fully describes the behavior of the zone. These separate sets of equations are coupled together before being solved in order to enforce the coupling between zones. The coupling can take a variety of forms, depending on the interface conditions which have been applied.

4.2.4 Material Properties

Material properties in Beasy are to define the environment of the model, to define the acoustic media where the acoustic parameter will be measured; commonly it is define as air or water.

4.2.5 Internal points

Internal points are points which lie inside the domain being analyzed, and at which BEASY finds the acoustics pressure or intensity at the end of the analysis run. They are zone entities as they belong to the zone in which they are physically located. The use of internal points allows users to investigate internal behavior of components without being overwhelmed with information from all parts of the model. It is important that internal points should not be placed on the boundary. Its may not be placed on interface elements either. Note that internal points should be concentrated near important features, in regions where the solution is varying rapidly.

4.2.6 Boundary Conditions

There are two kinds of boundary condition applied in Beasy, it's classified as active or passive. Active boundary conditions are those in which either the motion or sound pressure on the boundary or part of the boundary is known. A passive boundary condition occurs when sound reflects from a passive surface (such as an absorbing material) in contact with the medium. When this occurs, the amplitude and phase of the reflected wave relative to the incident wave depends on the acoustic impedance of the surface or boundary. The acoustic impedance is a property of the material (e.g., glass fiber) covering the surface and can be measured in an impedance tube.

4.3 Simulation Process

The simulation flow chart for creating WCPP models in this research work is shown in Figure 4.2 below.

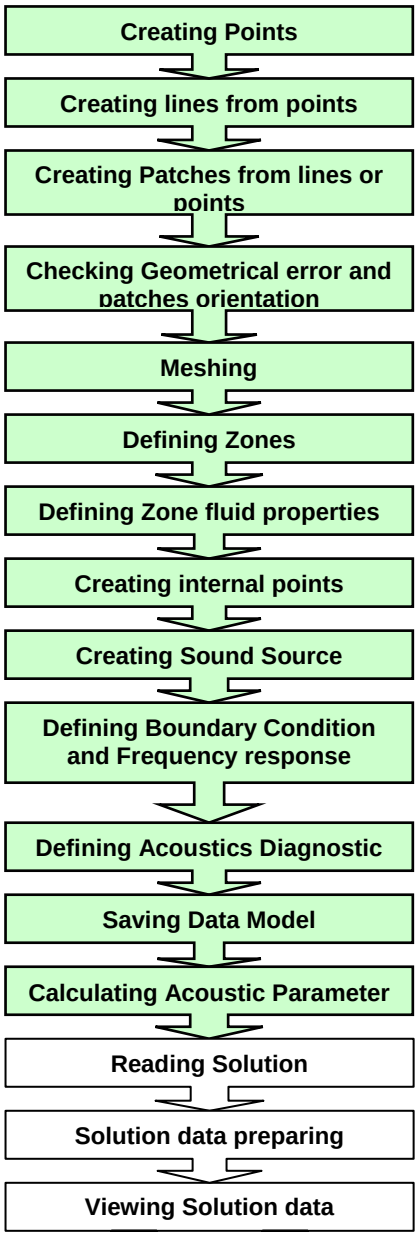

Figure 4.2 WCPP simulation flow chart

4.3.1 S1 Model

This section is to describe the detail of S1 WCPP modeling process in BEASY Acoustics software. S1 is a WCPP with physical properties; The centre to centre aperture distance (d) are 60 mm while the radius of the aperture 16 mm, perforation ratio of 20% and thickness is 20 mm. In Beasy model, S1 WCPP would

content 400 apertures, 20 rows and 20 columns. This model is started by forming the first aperture; begin with creating its points, lines, and patches. After the first aperture is completely created, then the first row is formed by copying the first aperture to the right and left side. The rest of the panel was created by copying and transforming the first row to upper and lower side.

a) Creating Point

The first step of S1 WCPP geometrical modeling in Beasy is creating the first aperture. The modeling begins with creating the first points as the base of all modeling sequence. Points may be created by entering its co-ordinates directly in Beasy sub-menu POINT-POSITION. Table 4.1 below shows the points and its 3D coordinates of the first aperture of S1 WCPP. The point position in 3D coordinate is showed in Figure 4.3 below.

Table 4.1 S1 first aperture points coordinate

Points No.	X (meter)	Y (meter)	Z (meter)
1	0.000	0.000	0.000
2	0.000	0.030	0.000
3	0.000	0.030	0.014
4	0.000	0.030	0.030
5	0.000	0.014	0.030
6	0.000	0.000	0.030
7	0.000	0.060	0.000
8	0.000	0.060	0.030
9	0.000	0.060	0.060
10	0.000	0.030	0.060
11	0.000	0.000	0.060
12	0.000	0.046	0.030
13	0.000	0.030	0.046
14	0.020	0.000	0.030
15	0.020	0.000	0.000
16	0.020	0.014	0.030
17	0.020	0.030	0.014
18	0.020	0.030	0.030
19	0.020	0.030	0.000
20	0.020	0.046	0.030
21	0.020	0.060	0.030
22	0.020	0.060	0.000

23	0.020	0.030	0.046
24	0.020	0.030	0.060
25	0.020	0.060	0.060
26	0.020	0.000	0.060

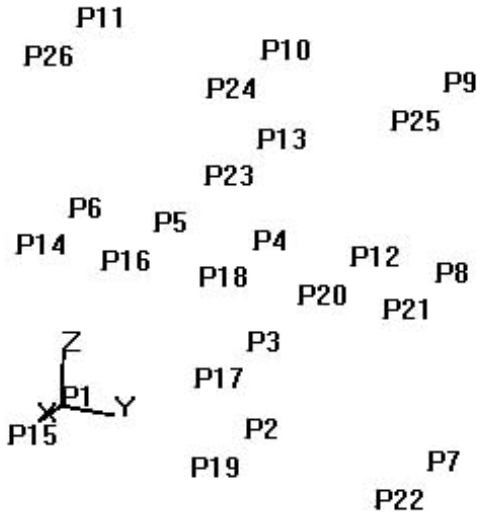

Figure 4.3 S1 First Aperture Points Position

b) Creating Lines

The next process of modeling is creating lines to form a WCPP aperture. Line was created by connected two points. Creating straight lines from two points were done by sub-menu, LINE – END_PTS and circular lines was creating by connecting two points with another point as center of the arc, its were done by sub-menu LINE-CIRCULAR_ARC.

Table 4.2 S1 first aperture lines creating from points

Lines	No	Start Point	End Point	Center point
Straight line	1	1	2	
Straight line	2	2	3	
Straight line	4	5	6	
Straight line	5	6	1	
Straight line	6	2	7	
Straight line	7	7	8	
Straight line	8	8	9	

Straight line	9	9	10	
Straight line	13	8	12	
Straight line	14	13	10	
Straight line	15	10	11	
Straight line	16	11	6	
Straight line	17	14	15	
Straight line	18	16	14	
Straight line	20	19	17	
Straight line	21	15	19	
Straight line	23	21	20	
Straight line	24	22	21	
Straight line	25	19	22	
Straight line	27	23	24	
Straight line	28	25	24	
Straight line	29	21	25	
Straight line	30	26	14	
Straight line	31	24	26	
Straight line	33	12	20	
Straight line	34	3	17	
Straight line	35	5	16	
Straight line	36	13	23	
Circular Line	3	3	5	4
Circular Line	10	3	12	4
Circular Line	11	12	13	4
Circular Line	12	13	5	4
Circular Line	19	17	16	18
Circular Line	22	17	20	18
Circular Line	26	20	23	18
Circular Line	32	23	16	18

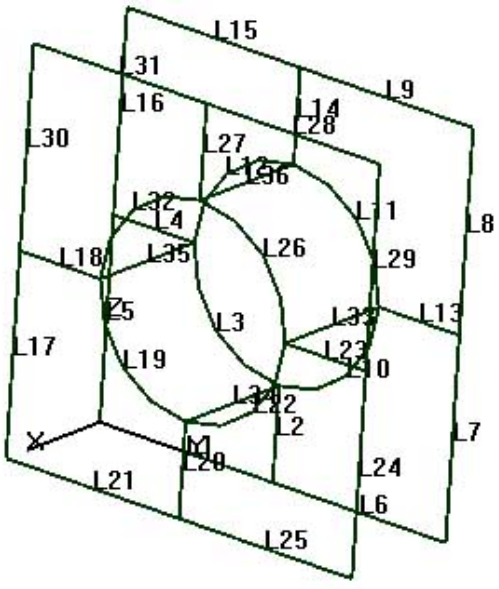

Figure 4.4 S1 first aperture lines position

c) Creating Patches

In WCPP model, patches were created with four corners and five corners with arc line in one side. Simple patches with four corners were created by four lines and are bounded by these lines. In Beasy sub-menu, it was used PACTH – BY_EDGE to create four lines patches and PACTH – MULTI_EDGES to create five line patches. The detail of patches creation is showed in Table 4.3 below.

Table 4.3 S1 First Aperture Patches Creating from Lines

Patches Creation	Patch No.	Line 1	Line 2	Line 3	Line 4	Line 5
By five lines	1	5	4	3	2	1
By five lines	2	10	13	7	6	2
By five lines	3	11	14	9	8	13
By five lines	4	16	15	14	12	4
By five lines	5	21	20	19	18	17
By five lines	6	20	25	24	23	22
By five lines	7	23	29	28	27	26
By five lines	8	18	32	27	31	30
By four lines	9	10	34	22	33	
By four lines	10	34	3	35	19	
By four lines	11	35	12	36	32	
By four lines	12	33	26	36	11	

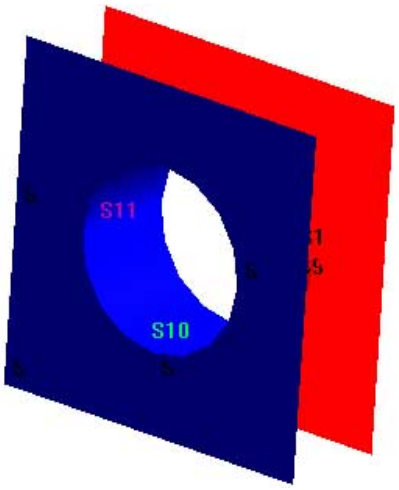

Figure 4.5 S1 first aperture patches

After the first aperture was completely created, the second aperture was created by copying and transforming the first aperture to the right side. In Beasy, this process was done by PACTH – COPYTRANSFORM sub-menu. The first aperture was copied and transformed to 0.06 m its right side or 0 0.06 0 in x y z coordinate transformation position. The result of those processes is showed in Figure 4.6 below.

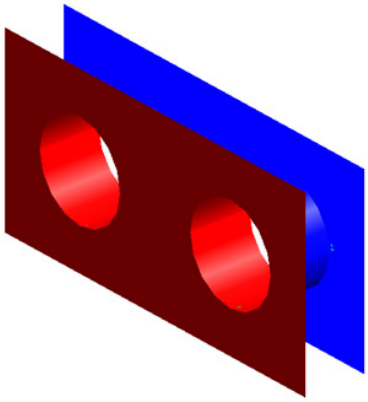

Figure 4.6 S1 second apertures

The same approach was applied to create the third and the fourth apertures to construct the first row of S1 WCPP with 1.2 m x 1.2 m dimension. The first and second apertures formed before was copied and transformed to right side with transformation coordinate 0 0.12 0. The result of those processes is showed in Figure 4.7 below.

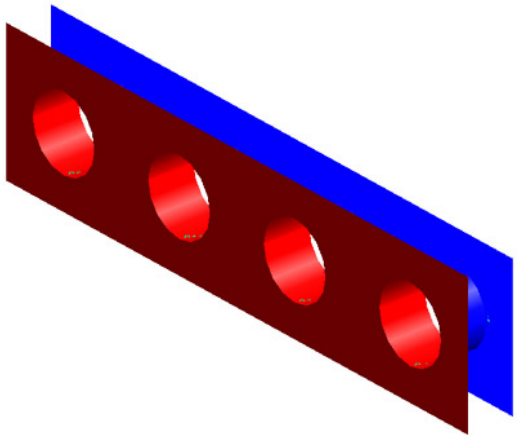

Figure 4.7 4 apertures of WCPP model

Then the process was continued to form the fifth to the eighth apertures. All of apertures created before was copied and transformed to coordinate 0 0.24 0. The

result of those processes is showed in Figure 4.8. Now there are 8 apertures had already formed.

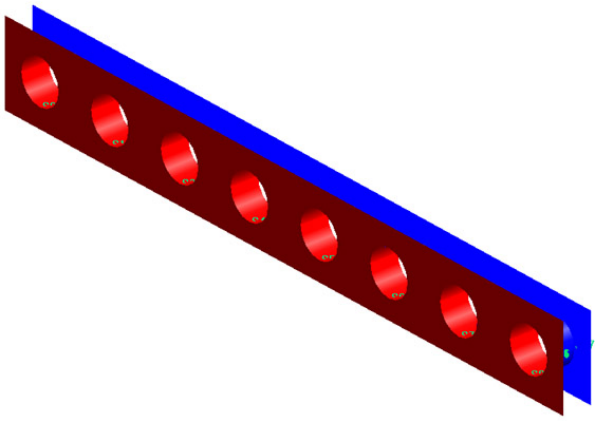

Figure 4.8 8 apertures of WCPP model

After that the first and the second aperture was copied and transformed to coordinate 0 0.48 0 to create the two latest apertures of the first row. Now the right part of the first row is already complete. The process is showed in Figure 4.9 below.

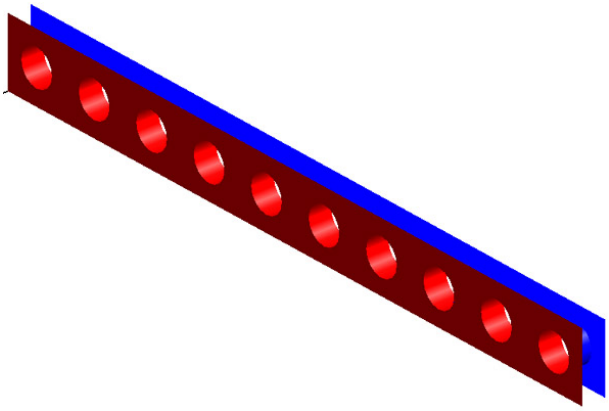

Figure 4.9 The first row of WCPP model

To form the second row, the entire apertures in the first row were copied and transformed to the upper side with coordinate 0 0 0.06. The new row formed is showed in Figure 4.10 below. To form the third and fourth rows, the first and second row formed before was copied and transformed to upper side with transformation coordinate 0 0 0.12 The result of those processes is showed in Figure 4.11 below

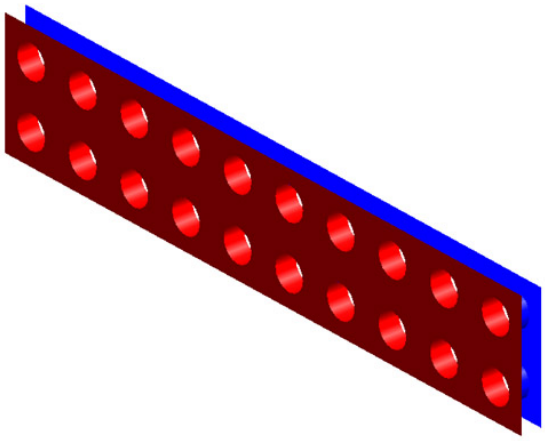

Figure 4.10 2 rows of WCPP model

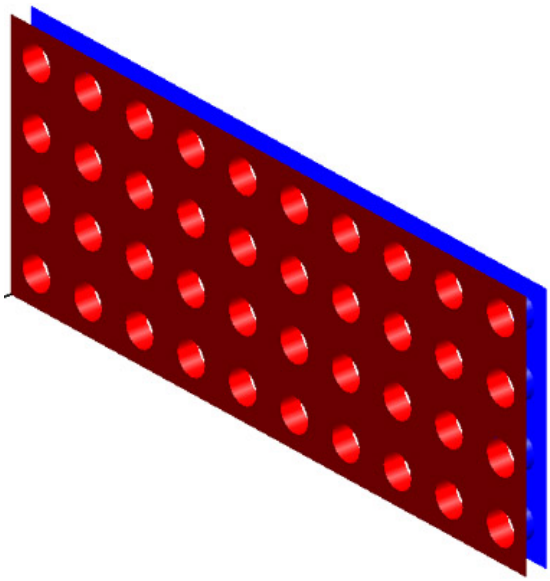

Figure 4.11 4 rows of WCPP model

Then the process is continued to form the fifth to eighth rows. All of row created before was copied and transformed to coordinate 0 0 0.24. The new rows formed are showed in Figure 4.12. Now there are 8 rows had already formed. After that the first and the second rows was copied and transformed to coordinate 0 0 0.48 to create the two latest rows of the right part of the WCPP. The result of the process is showed in Figure 4.13 below.

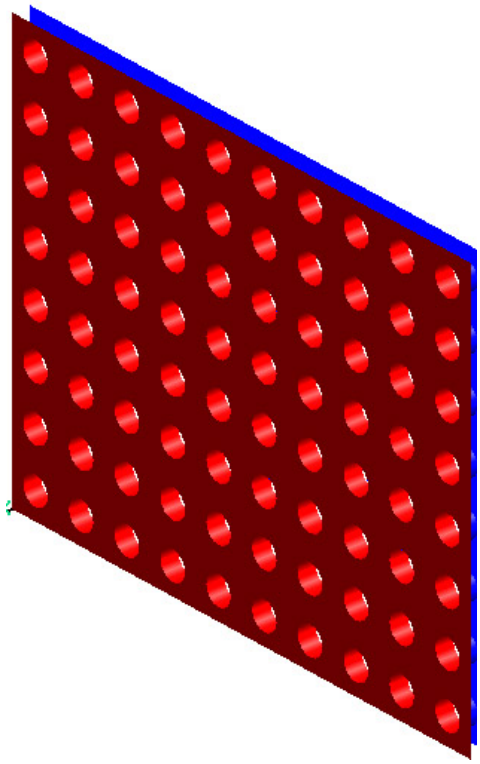

Figure 4.12 rows of WCPP model

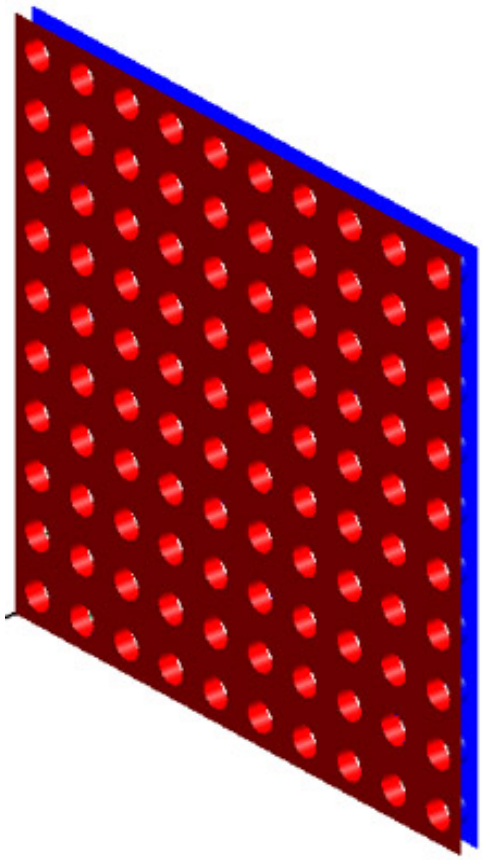

Figure 4.13 Right upper side of WCPP model

After the right upper part of the WCPP had been created, the modeling process was moved to create the other parts of the panel. The lower right part of WCPP was created by copying and transforming the upper right part with transformation coordinate 0 0 -0.6. And then the left part of the WCPP could easily created by copying and transforming the right part with transformation coordinate 0 -0.6 0. The WCPP model had been entirely created. The result of the entire process is showed in Figure 4.14 below.

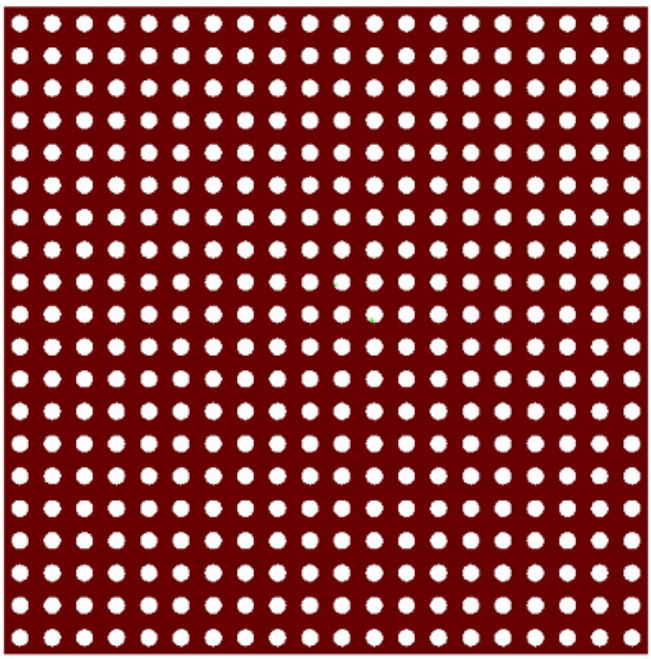

Figure 4.14 Full panel of WCPP model

d) Creating Anechoic Room

After the entire WCPP had been created, the modeling process was moved to model the anechoic room. There are two anechoic rooms, in front of the WCPP and behind the WCPP. For Anechoic room in front of the panel, modeling was started by creating a line as a based to form the room surfaces, this line was created by vectoring point 1 to 2.2 m to the front of WCPP (x axis) with vector coordinate 2.2 0 0, this procedure was done by LINE, POINT_VECTOR in Beasy sub-menu. The

next step was creating the bottom surface, this surface was created by vectoring this line to Y axis along the WCPP border with coordinate 0 1.2 0 using PATCH-LINE_VECTOR in Beasy sub menu. The result is showed in Figure 4.15 below.

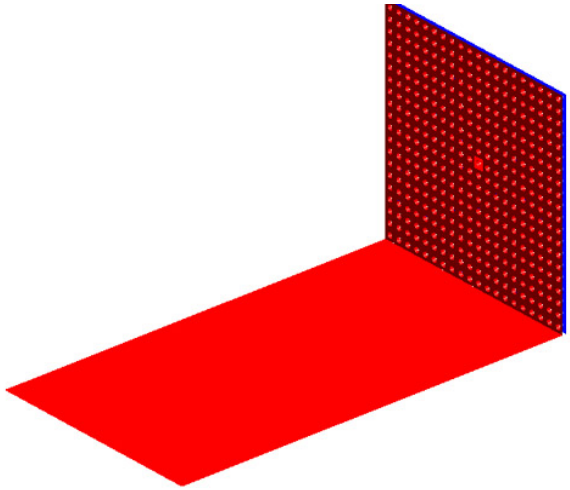

Figure 4.15 S1 anechoic front surfaces 1

Then the right side surface was formed in the same way with bottom one, it was done by vectoring bottom surface right border line to Z axis with coordinate 0 0 1.2. The result is showed in Figure 4.16 below

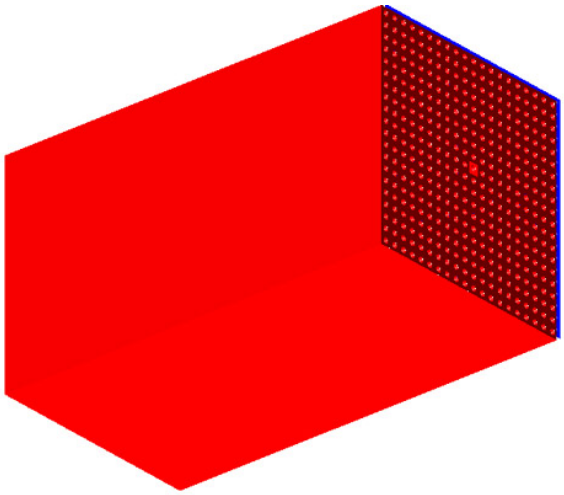

Figure 4.16 S1 anechoic front surfaces 2

The left side surface was formed by vectoring bottom surface left border line to Z axis with coordinate 0 0 1.2. The front side surface was formed by vectoring bottom surface front border line to Z axis with coordinate 0 0 1.2. Then the roof

surface was formed by vectoring upper border line of left surface to Y axis with coordinate 0 1.2 0. The result of the mentioned process above is showed in Figure 4.17, 4.18 and 4.19 below.

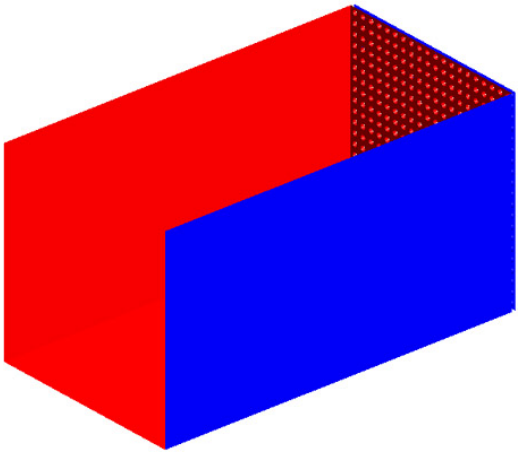

Figure 4.17 S1 anechoic front surfaces 3

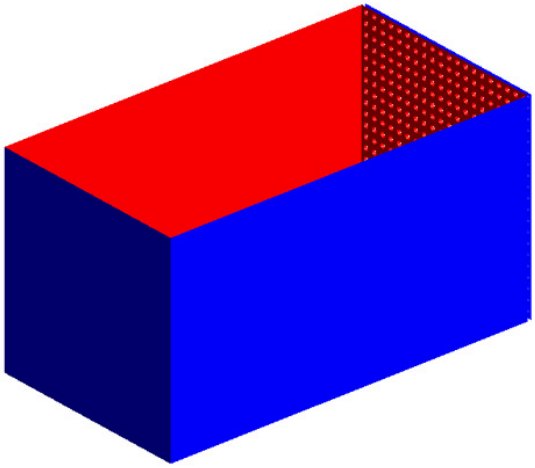

Figure 4.18 S1 anechoic front surfaces 4

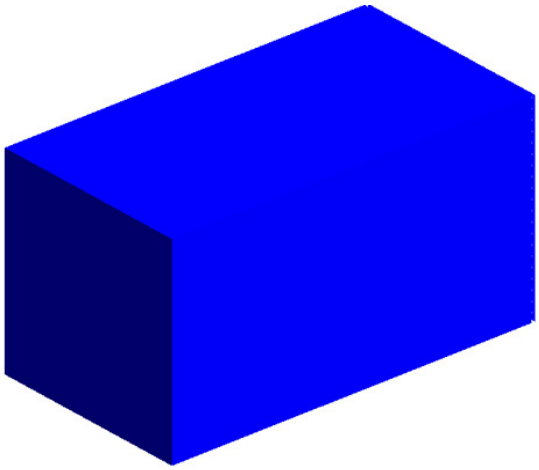

Figure 4.19 S1 anechoic front surfaces 5

For Anechoic room in behind of the panel, modeling was start by creating a line as the base to create the entire room surfaces. This line was created by vectoring point 1 (the back corner of the panel) to 0.75 m to the front of WCPP (x axis) with vector coordinate -0.75 0 0. The next step is creating the bottom surface, this surface was created by vectoring this line to Y axis along the WCPP dimension with coordinate 0 1.2 0. The process result is shown in Figure 4.20 below.

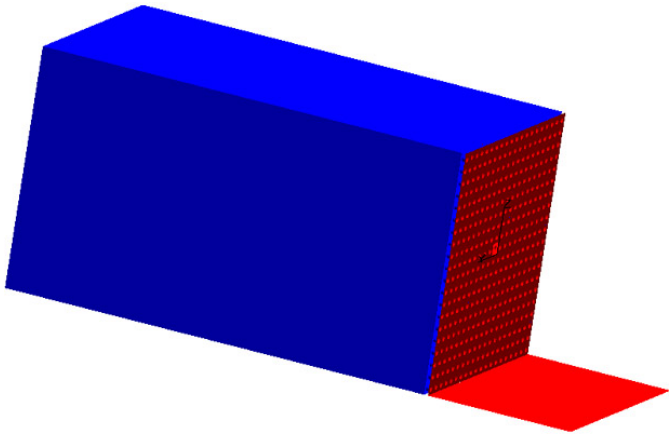

Figure 4.20 S1 anechoic front surfaces 6

Then the right side surface was formed in the same way with bottom one, it was done by vectoring bottom surface right border line to Z axis with coordinate 0 0 1.2. The left side surface was formed by vectoring bottom surface left border line to Z axis with coordinate 0 0 1.2. The process result is shown in Figure 4.21 and 4.22 below.

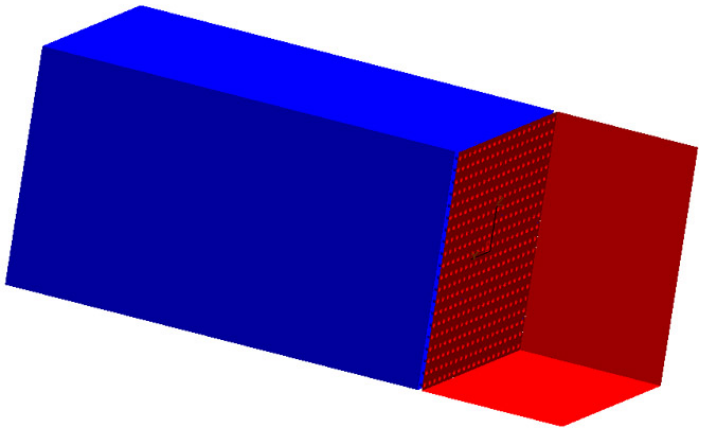

Figure 4.21 S1 anechoic front surfaces 7

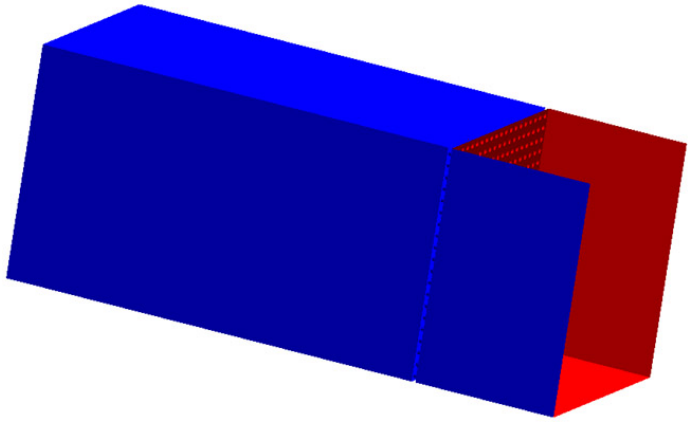

Figure 4.22 S1 anechoic front surfaces 8

The front side surface was formed by vectoring bottom surface front border line to Z axis with coordinate 0 0 1.2. Then the roof surface was formed by vectoring upper border line of left surface to Y axis with coordinate 0 1.2 0. The process result is shown in Figure 4.23 and 4.24 below.

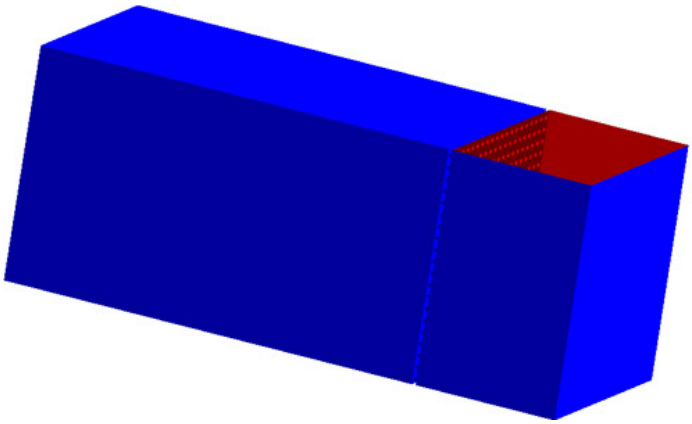

Figure 4.23 S1 anechoic front surfaces 9

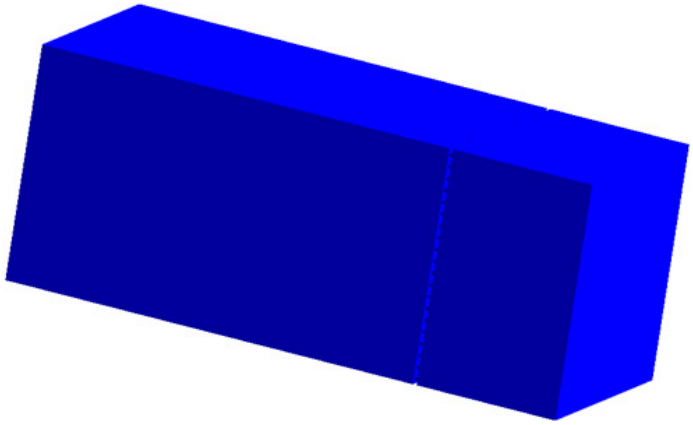

Figure 4.24 Complete geometrical models

At this stage, the geometrical model is completed. Then the modeling process is moved to check the patches orientation, all the patches in the zone were defining to have outward normal direction. All the patches which have inward direction were reversed. This process was done in Beasy sub menu PATCH-REVERSE. Outward patches would show blue color and inward patches would show red color in Beasy main display.

After all patches had been reversed to outward normal direction, the geometrical modeling error checking was performed. The geometrical model was checked for three kinds of properties to avoid the modeling errors. There are patches connectivity, patches overlapping, and patches direction.

Patches connectivity checking was performed to avoid the error in the model cause by patches discontinue or error cause by holes. This process was performed in Beasy sub menu CHECK_GEOM - CONNECTIVITY. Patches overlapping checking was performed to avoid an error caused by patches overlapping. This process was performed in Beasy sub menu CHECK_GEOM - OVERLAPS. Then patches direction was also checked, this process is to avoid an error cause by patches wrong normal direction. This process was performed in Beasy sub menu CHECK_GEOM – DIRECTION. At this stage, all the geometrical modeling process was completed.

e) Meshing

After geometrical modeling was done, the simulation process was moved to define meshing for the model previously created. For WCPP meshing, it used quadratic elements with sizes were defined automatically by Beasy to match with geometrical shapes. For frequency 250 Hz, the biggest element size defined was $\lambda/4$; 0.34 m and the smallest size was 0.02 m which is the smallest panel shape dimension. For frequency 500 Hz, the biggest element size was 0.17 m and the smallest was 0.02 m. For frequency 1 kHz, the biggest element size was 0.085 m and the smallest was 0.02 m. For frequency 2 kHz, the biggest element size was 0.0425

m and the smallest was 0.02 m and for frequency 4 kHz, the biggest element size was 0.02125 m and the smallest was 0.02 m. This process was performed in Beasy sub menu ELEMENT - AUTO_MESH.

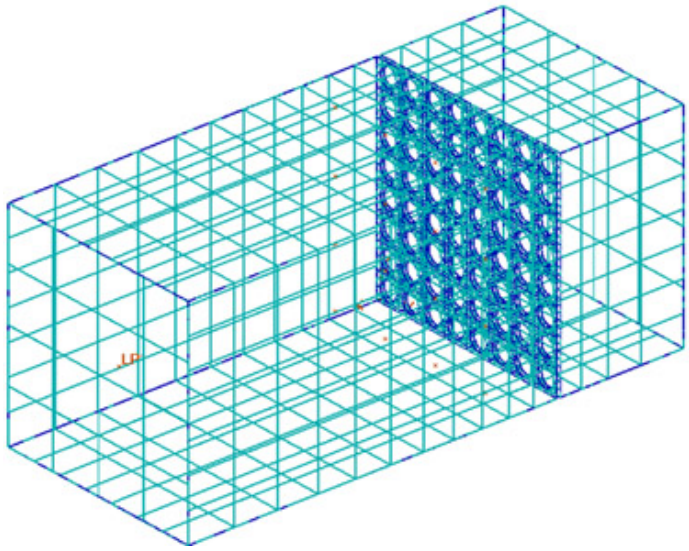

Figure 4.25 Transparent view of element meshing

f) Defining Zone

In this model, only one zone was defined which was called Zone 1. From Figure 4.24 above, Zone 1 is the space in the anechoic room, at the front and the back of the panel. Zone 1 was included all outward patches which zone type was fully bounded to describe that was only the space in the anechoic room would take into consideration in calculating acoustic parameter. This process was performed in Beasy sub menu ZONE - ID_NUMBER, OUTWARD_PATCH, and ZONE _TYPE.

g) Creating Internal Points

16 internal points to record net intensity values are defined 0.25λ of each frequency in front of WCPP in the acoustic domain. 0.25λ was chosen to agree with

measurement technique conducted in anechoic chamber [Mohamad Ngasri Dimon, 2003b]. The sound pressure level is lowest at 0.25λ so that it will minimize the error in obtaining sound intensity values. This process was performed in Beasy sub menu INTERNAL_PT – POINT – POSITION. The detail of x y z coordinate of the 16 internal points is given in Table 4.4 below and shown in Figure 4.26 below.

Table 4.4 Internal points coordinate

Internal points	x (meter)	y (meter)	z (meter)
1	0.25λ	0.100	0.100
2	0.25λ	0.433	0.100
3	0.25λ	0.767	0.100
4	0.25λ	1.100	0.100
5	0.25λ	0.100	0.430
6	0.25λ	0.433	0.430
7	0.25λ	0.767	0.430
8	0.25λ	1.100	0.430
9	0.25λ	0.100	0.760
10	0.25λ	0.433	0.760
11	0.25λ	0.767	0.760
12	0.25λ	1.100	0.760
13	0.25λ	0.100	1.100
14	0.25λ	0.433	1.100
15	0.25λ	0.767	1.100
16	0.25λ	1.100	1.100

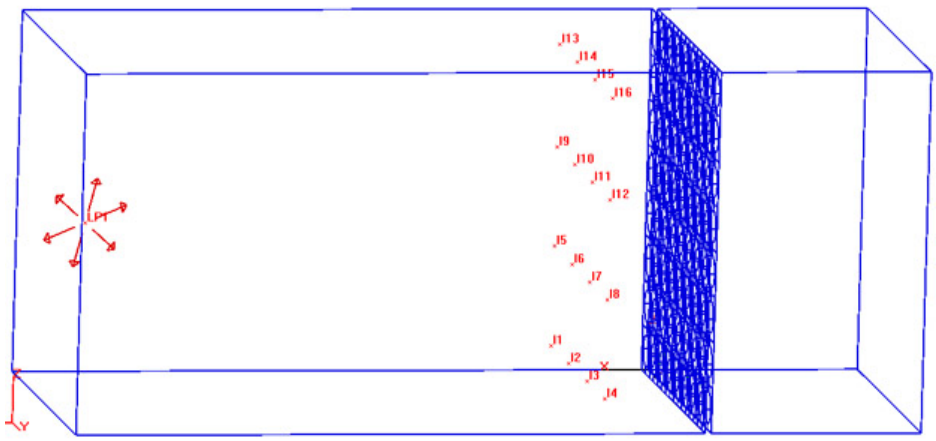

Figure 4.26 Internal points positions

h) Defining Acoustic Media Properties

The acoustic media defined in the zone was air. The material properties used are air density =1.21 Kg/m3, sound speed is 340 m/s, reference pressure is 2.0e-5 *Pa.* This process was performed in Beasy sub menu MAT_PROPS - DENSITY, SOUND_SPEED, and REF_PRESSURE.

i) Creating Point Source

In this model the sound source was represented by a point source of strength 0.1 Pa/m positioned at diagonal center, 2 m in front of the WCPP. This process was performed in Beasy sub menu LOAD_GEOMETRY – POINT – POSITION, followed by BOUNDARY_GEOMETRY - BODY LOAD - PT_SOURCE. The point source position is show as a point with arrows in Figure 4.27 below.

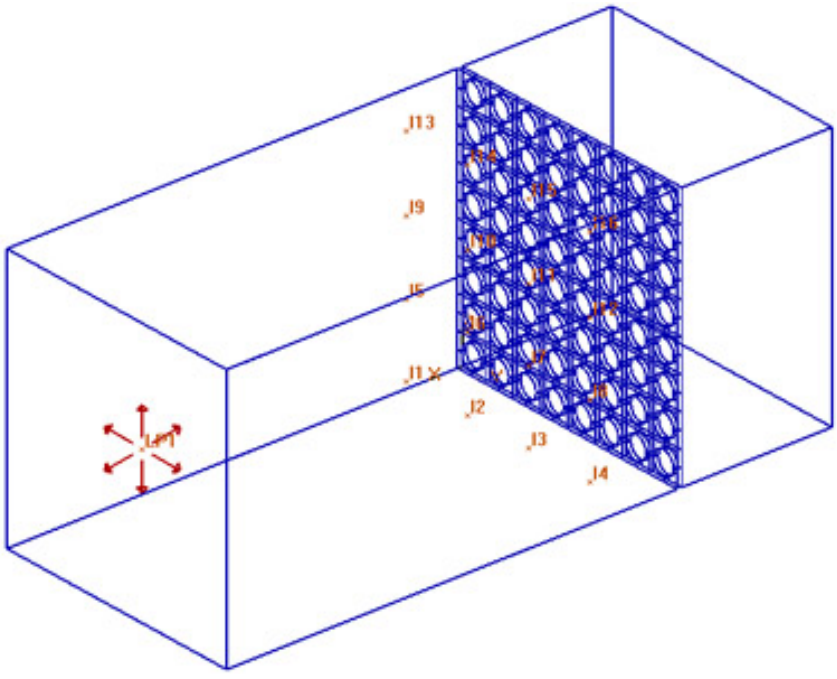

Figure 4.27 Point source position

j) Defining Boundary Condition and Frequency Analysis

Zero pressure was prescribed on all side of the cubic box and WCPP elements representing there is no vibration. Zero normal velocity was prescribed on all elements. The acoustic impedance of the WCPP is set 49800; this value was defined by measuring the real WCPP sample using Impedance Tube. The acoustic impedance for anechoic room is 415 to define that the room is totally absorber to create free field condition. Frequency analysis was set to 250 Hz, 500 Hz, 1 kHz, 2 kHz, and 4 kHz. This process was performed in Beasy sub menu LOAD+BCS – REAL_IMPEDANCE, and LOAD_BCS – FREQUENCY. The boundary condition applied to the model is shown in Figure 4.28 below.

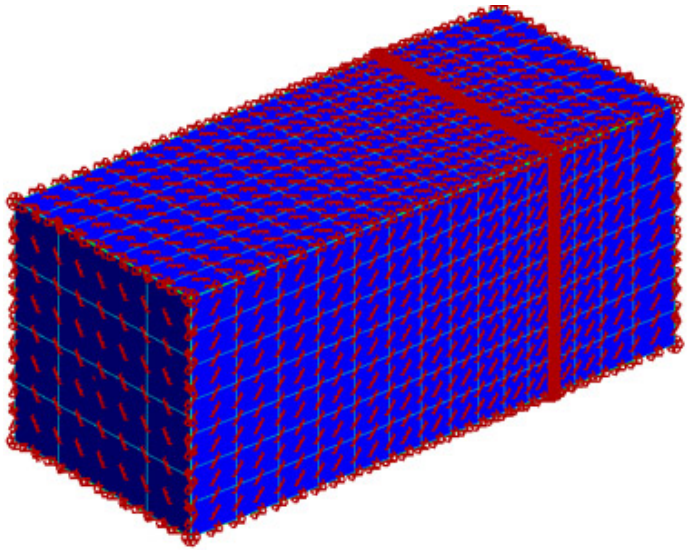

Figure 4.28 Boundary Condition

k) Saving Model Data

At this stage, all modeling process had been completely done. All the change had been made to the model was saved to Beasy model directory. This process was performed in Beasy sub menu WRITE_DATA.

l) Calculating Acoustics Parameter

After the data model was saved, acoustic parameter was ready to calculate. Beasy would solve the acoustic problem in the model based on Boundary Element Method by Beasy Solver software. The result of this process is that sound intensity value can be predicted at all internal point positions and elements. This process was performed in Beasy sub menu SOLVE.

m) Reading Calculated Result

After solving process was completely done, the simulation result was uploaded to Beasy main software. This process was performed in Beasy sub menu READ_SOLUTION.

n) Viewing Sound Intensity Result

Viewing sound intensity result was performed in Beasy sub menu LIST_RESULT – INT_POINT, and 3 was chosen in QUANTITIES sub menu to defined that only intensity values at internal points would be viewed. After all data had been viewed, it was transferred to Microsoft Excel to be averaged to be used in α_n calculation.

4.3.2 S2 Model

S2 is a WCPP with physical properties; The centre to centre aperture distance (d) are 60 mm while the radius of the aperture 20 mm, perforation ratio of 30% and thickness is 20 mm. S2 WCPP model would content 400 apertures, 20 rows and

20 columns. Simulation process for S2 model has exactly the same steps with S1 one, the only difference is in some points coordinate. It‘s because S2 has different size of apertures but the distance between the aperture is the same. The detail of S2 model points coordinate is given in Table 4.5 below

Table 4.5 S2 first aperture points

Points No	X (meter)	Y (meter)	Z (meter)
1	0.000	0.000	0.000
2	0.000	0.030	0.010
3	0.000	0.030	0.030
4	0.000	0.050	0.030
5	0.000	0.010	0.030
6	0.000	0.030	0.050
7	0.020	0.030	0.050
8	0.020	0.030	0.000
9	0.020	0.030	0.010
10	0.020	0.010	0.030
11	0.020	0.030	0.030
12	0.020	0.000	0.030
13	0.020	0.060	0.000
14	0.020	0.060	0.030
15	0.020	0.050	0.030
16	0.020	0.060	0.060
17	0.020	0.030	0.060
18	0.020	0.000	0.060
19	0.000	0.090	0.010
20	0.000	0.070	0.030
21	0.000	0.090	0.030
22	0.000	0.060	0.030
23	0.000	0.110	0.030
24	0.000	0.090	0.050
25	0.020	0.090	0.010
26	0.020	0.070	0.030

4.3.3 S3 Model

S3 is a WCPP with physical properties; The centre to centre aperture distance (d) are 60 mm while the radius of the aperture 23 mm, perforation ratio of 40% and thickness is 20 mm. S3 WCPP model would contain 400 apertures, 20 rows and

20 columns. Simulation process for S3 model has exactly the same steps with S1 one, the only difference is in some points coordinate. It‘s because S3 has different size of apertures but the distance between the aperture is the same. The detail of S3 model points coordinate is given in Table 4.6 below

Table 4.6 S3 first aperture points

Points No	X (meter)	Y (meter)	Z (meter)
1	0.000	0.000	0.000
2	0.000	0.030	0.030
3	0.000	0.030	0.007
4	0.000	0.053	0.030
5	0.000	0.030	0.053
6	0.000	0.007	0.030
7	0.020	0.030	0.053
8	0.020	0.030	0.000
9	0.020	0.030	0.007
10	0.020	0.007	0.030
11	0.020	0.030	0.030
12	0.020	0.000	0.030
13	0.020	0.060	0.000
14	0.020	0.060	0.030
15	0.020	0.053	0.030
16	0.020	0.060	0.060
17	0.020	0.030	0.060
18	0.020	0.000	0.060
19	0.000	0.090	0.007
20	0.000	0.067	0.030
21	0.000	0.090	0.030
22	0.000	0.060	0.030
23	0.000	0.113	0.030
24	0.000	0.090	0.053
25	0.020	0.113	0.030
26	0.020	0.090	0.007

4.3.4 S4 Model

S4 is a WCPP with physical properties; The centre to centre aperture distance (d) are 75 mm while the radius of the aperture 20 mm, perforation ratio of 20% and thickness is 20 mm. S4 WCPP model would content 256 apertures, 16 rows and 16 columns. Simulation process for S4 model has exactly the same steps with S1

one, the differences are in some points coordinate and the number of patches to copy and to transform to form a 1.2 m x 1.2 m WCPP. It‘s because S4 has larger size of apertures and longer center to center aperture distance. The detail of S4 model points coordinate is given in Table 4.7 below. After forming the first aperture, it was needed to be copied and transformed to form 16 rows and 16 columns by the same manner with previously describe in S1 model.

Table 4.7 S4 first aperture points

Points No.	x (meter)	y (meter)	z (meter)
1	0.000	0.000	0.000
2	0.000	0.038	0.038
3	0.000	0.038	0.018
4	0.000	0.058	0.038
5	0.000	0.038	0.058
6	0.000	0.018	0.038
7	0.020	0.038	0.058
8	0.020	0.038	0.000
9	0.020	0.038	0.018
10	0.020	0.018	0.038
11	0.020	0.038	0.038
12	0.020	0.000	0.038
13	0.020	0.075	0.000
14	0.020	0.075	0.038
15	0.020	0.058	0.038
16	0.020	0.075	0.075
17	0.020	0.038	0.075
18	0.020	0.000	0.075
19	0.000	0.113	0.018
20	0.000	0.093	0.038
21	0.000	0.113	0.038
22	0.000	0.075	0.038
23	0.000	0.133	0.038
24	0.000	0.113	0.058
25	0.020	0.133	0.038
26	0.020	0.113	0.018

4.3.5 S6 Model

S6 is a WCPP with physical properties; The centre to centre aperture distance (d) are 75 mm while the radius of the aperture 20 mm, perforation ratio of 20% and thickness is 20 mm. S6 WCPP model would content 256 apertures, 16 rows and 16 columns. Simulation process for S6 model has exactly the same steps with S1, the differences are in some points coordinate and the number of patches to copy and to transform to form a 1.2 m x 1.2 m WCPP. It‘s because S6 has larger size of apertures and longer center to center aperture distance. The detail of S6 model points coordinate is given in Table 4.8 below. After forming the first aperture, it was needed to be copied and transformed to form 16 rows and 16 columns by the same manner with previously describe in S1 model.

Table 4.8 S6 first aperture points

Points No.	X (meter)	Y (meter)	Z (meter)
1	0.000	0.000	0.000
2	0.000	0.026	0.000
3	0.000	0.000	0.026
4	0.000	0.026	0.006
5	0.000	0.046	0.026
6	0.000	0.026	0.046
7	0.000	0.006	0.026
8	0.000	0.026	0.026
9	0.020	0.026	0.046
10	0.020	0.000	0.000
11	0.020	0.026	0.000
12	0.020	0.026	0.006
13	0.020	0.006	0.026
14	0.020	0.026	0.026
15	0.020	0.000	0.026
16	0.020	0.052	0.000
17	0.020	0.052	0.026
18	0.020	0.046	0.026
19	0.020	0.052	0.052
20	0.020	0.026	0.052
21	0.020	0.000	0.052
22	0.000	0.052	0.026
23	0.000	0.052	0.000
24	0.000	0.000	0.052
25	0.000	0.026	0.052
26	0.000	0.052	0.052

4.3.6 S8 Model

S8 is a WCPP with physical properties; The centre to centre aperture distance (d) are 150 mm while the radius of the aperture 44 mm, perforation ratio of 20% and thickness is 20 mm. S8 WCPP model would contain 64 apertures, 8 rows and 8 columns. Simulation process for S8 model has exactly the same steps with S1, the differences are in some points coordinate and the number of patches to copy and to transform to form a 1.2 m x 1.2 m WCPP. It‘s because S8 has larger size of apertures and longer center to center aperture distance. The detail of S8 model points coordinate is given in Table 4.9 below. After forming the first aperture, it was needed to be copied and transformed to form 8 rows and 8 columns by the same manner with previously describe in S1 model.

Table 4.9 S8 first aperture points

Points No	x(meter)	y(meter)	z(meter)
1	0.000	0.000	0.000
2	0.000	0.075	0.000
3	0.000	0.150	0.000
4	0.000	0.150	0.075
5	0.000	0.150	0.150
6	0.000	0.075	0.150
7	0.000	0.000	0.150
8	0.000	0.000	0.075
9	0.000	0.075	0.075
10	0.000	0.075	0.031
11	0.000	0.119	0.075
12	0.000	0.075	0.119
13	0.000	0.031	0.075
14	0.020	0.000	0.000
15	0.020	0.075	0.031
16	0.020	0.075	0.000
17	0.020	0.150	0.000
18	0.020	0.119	0.075
19	0.020	0.150	0.150
20	0.020	0.150	0.075
21	0.020	0.075	0.119
22	0.020	0.075	0.075
23	0.020	0.031	0.075
24	0.020	0.000	0.075
25	0.020	0.000	0.150
26	0.020	0.075	0.150

4.3.7 S10 Model

S10 is a WCPP with physical properties; The centre to centre aperture distance (d) are 150 mm while the radius of the aperture 54 mm, perforation ratio of 30% and thickness is 20 mm. S10 WCPP model would content 64 apertures, 8 rows and 8 columns. Simulation process for S10 model has exactly the same steps with S1, the differences are in some points coordinate and the number of patches to copy and to transform to form a 1.2 m x 1.2 m WCPP. It‘s because S10 has larger size of apertures and longer center to center aperture distance. The detail of S10 model points coordinate is given in Table 4.10 below. After forming the first aperture, it was needed to be copied and transformed to form 8 rows and 8 columns by the same manner with previously describe in S1 model.

Table 4.10 S10 first aperture points

Points No.	x(meter)	y(meter)	z(meter)
1	0.000	0.075	0.075
2	0.000	0.021	0.075
3	0.000	0.075	0.021
4	0.000	0.129	0.075
5	0.000	0.075	0.129
6	0.020	0.129	0.075
7	0.020	0.000	0.000
8	0.020	0.075	0.000
9	0.020	0.075	0.021
10	0.020	0.021	0.075
11	0.020	0.075	0.075
12	0.020	0.000	0.075
13	0.020	0.150	0.000
14	0.020	0.150	0.075
15	0.020	0.150	0.150
16	0.020	0.075	0.150
17	0.020	0.075	0.129
18	0.020	0.000	0.150
19	0.000	0.150	0.075
20	0.000	0.075	0.150
21	0.000	0.150	0.150
22	0.000	0.000	0.075
23	0.000	0.000	0.150
24	0.000	0.075	0.000
25	0.000	0.150	0.000
26	0.000	0.000	0.000

4.3.8 S12 Model

S12 is a WCPP with physical properties; The centre to centre aperture distance (d) are 150 mm while the radius of the aperture 62 mm, perforation ratio of 40% and thickness is 20 mm. S12 WCPP model would content 64 apertures, 8 rows and 8 columns. Simulation process for S12 model has exactly the same steps with S1, the differences are in some points coordinate and the number of patches to copy and to transform to form a 1.2 m x 1.2 m WCPP. It‘s because S12 has larger size of apertures and longer center to center aperture distance. The detail of S12 model points coordinate is given in Table 4.11 below. After forming the first aperture, it was needed to be copied and transformed to form 8 rows and 8 columns by the same manner with previously describe in S1 model.

Table 4.11 S12 first aperture points

Points No.	x(meter)	y(meter)	z(meter)
1	0.000	0.000	0.000
2	0.000	0.075	0.000
3	0.000	0.075	0.021
4	0.000	0.075	0.075
5	0.000	0.021	0.075
6	0.000	0.000	0.075
7	0.020	0.000	0.000
8	0.020	0.075	0.000
9	0.020	0.075	0.021
10	0.020	0.075	0.075
11	0.020	0.021	0.075
12	0.020	0.000	0.075
13	0.000	0.129	0.075
14	0.020	0.150	0.000
15	0.020	0.129	0.075
16	0.000	0.075	0.129
17	0.020	0.000	0.150
18	0.020	0.075	0.150
19	0.020	0.075	0.129
20	0.020	0.150	0.150
21	0.000	0.150	0.075
22	0.000	0.150	0.000
23	0.020	0.150	0.075
24	0.000	0.000	0.150
25	0.000	0.075	0.150
26	0.000	0.150	0.150

4.3.9 Anechoic Chamber Model

α_n of WCPP was calculated by dividing net sound intensity value in front of the panel with incident sound intensity as in equation 2.21. The incident sound intensity is obtained in anechoic chamber without any panel.

The anechoic chamber model was created in the same way with creating anechoic room with S1 panel; the only change is there is no panel. Anechoic chamber modeling was started by creating the first point at x y z coordinate 0 0 0. The first point is shown in Figure 4.29 below.

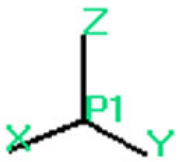

Figure 4.29 Anechoic room first point

Then it was followed by creating a line as a based to form the room surfaces, this line was created by vectoring point 1 to 2.2 m to the front of WCPP (x axis) with vector coordinate 2.2 0 0, this procedure was done by LINE, POINT_VECTOR in Beasy sub-menu. The first line created is shown in Figure 4.30 below.

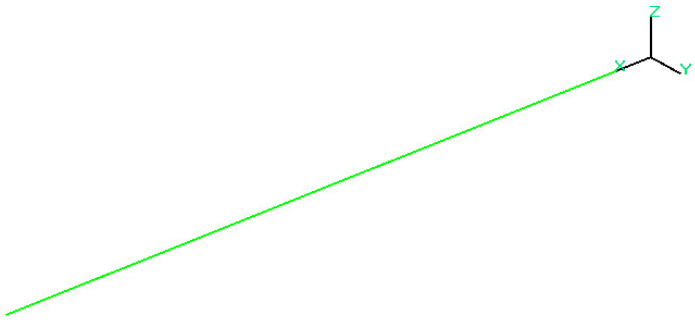

Figure 4.30 Anechoic room first line

The next step is creating the bottom surface, this surface was created by vectoring this line to Y axis along the WCPP with coordinate 0 1.2 0 using PATCH-LINE_VECTOR in Beasy sub menu. The result is shown in Figure 4.31 below.

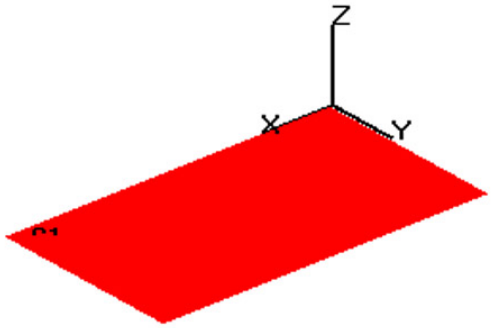

Figure 4.31 Anechoic room floor

Then the right side surface was formed in the same way with bottom one, it was done by vectoring bottom surface right border line to Z axis with coordinate 0 0 1.2. The result is shown in Figure 4.32 below.

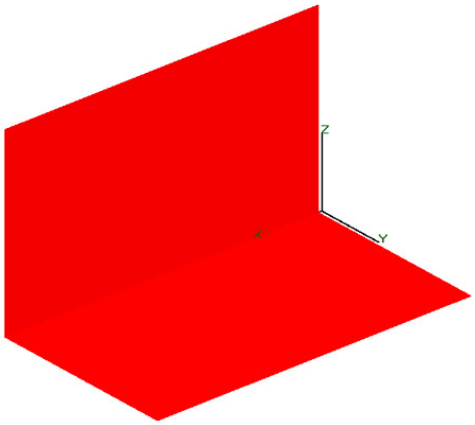

Figure 4.32 Anechoic room second surface

The left side surface was formed by vectoring bottom surface left border line to Z axis with coordinate 0 0 1.2. The process result is shown in Figure 4.33 below.

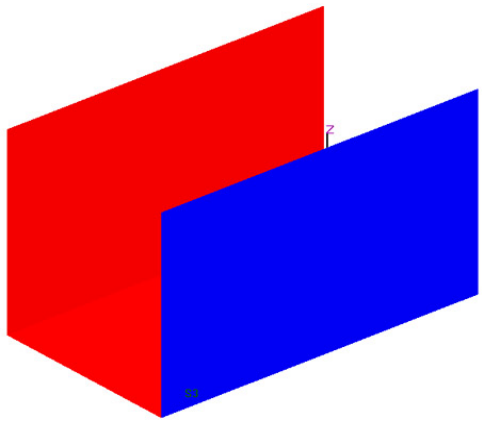

Figure 4.33 Anechoic room third surface

The front side surface was formed by vectoring bottom surface front border line to Z axis with coordinate 0 0 1.2. Then the roof surface was formed by vectoring upper border line of left surface to Y axis with coordinate 0 1.2 0. The process result is shown in Figure 4.34 and Figure 4.35 below.

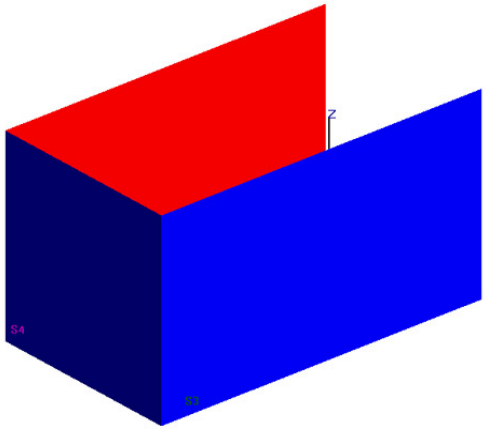

Figure 4.34 Anechoic room forth surface

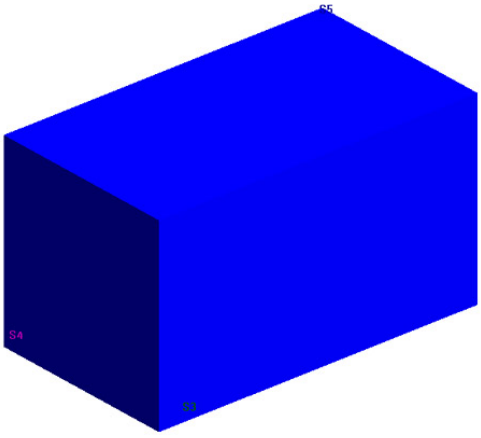

Figure 4.35 Anechoic room fifth surface

For anechoic room in behind of the panel, modeling was also start by creating a line as the base to create the entire room surfaces. This line was created by vectoring point 1 (the back corner of the panel) to 0.75 m to the front of WCPP (x axis) with vector coordinate -0.75 0 0. The process result is shown in Figure 4.36 below.

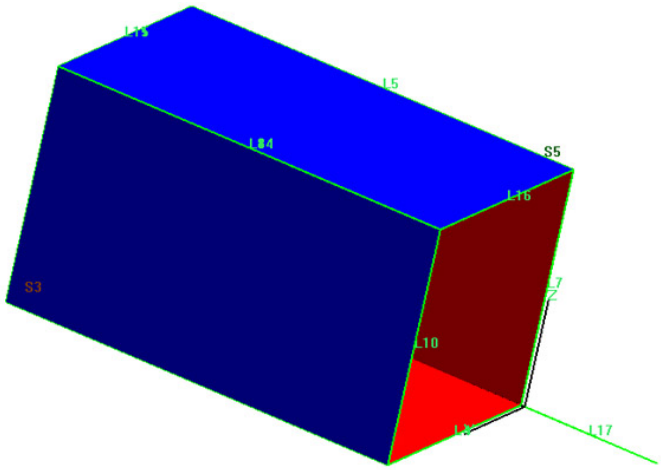

Figure 4.36 Anechoic room back side line

The next step is creating the bottom surface, this surface was created by vectoring this line to Y axis along the WCPP dimension with coordinate 0 1.2 0. The process result is shown in Figure 4.37 below

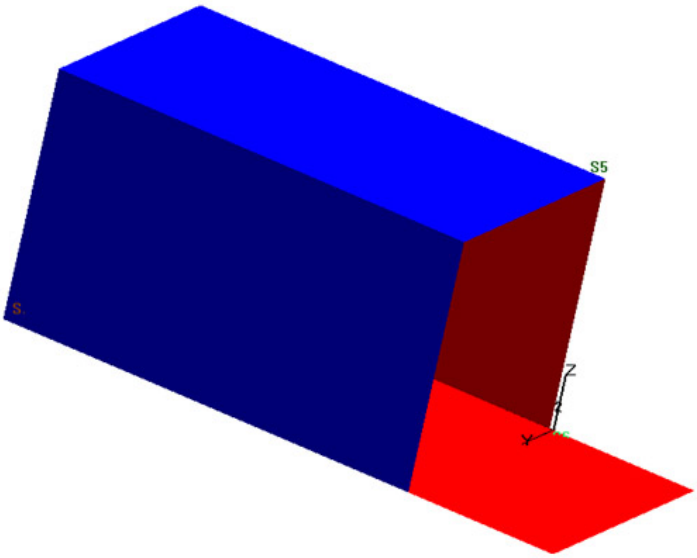

Figure 4.37 Anechoic room back floor

Then the right side surface was formed in the same way with bottom one, it was done by vectoring bottom surface right border line to Z axis with coordinate 0 0 1.2. The left side surface was formed by vectoring bottom surface left border line to Z axis with coordinate 0 0 1.2. The front side surface was formed by vectoring bottom surface front border line to Z axis with coordinate 0 0 1.2. The process result is shown in Figure 4.38, 4.39 and 4.40 below.

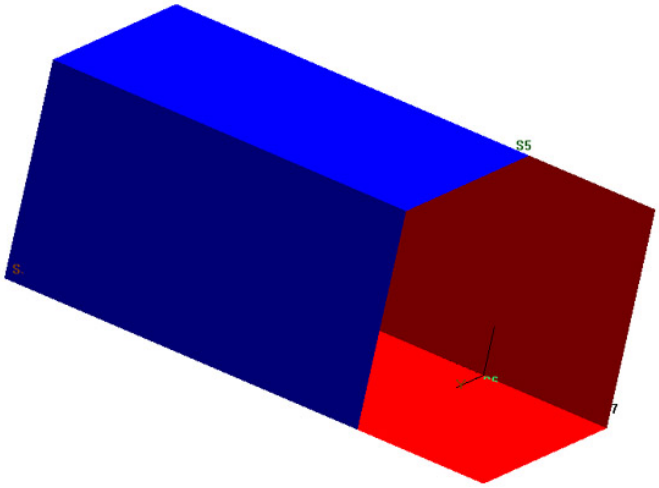

Figure 4.38 Anechoic room seventh surface

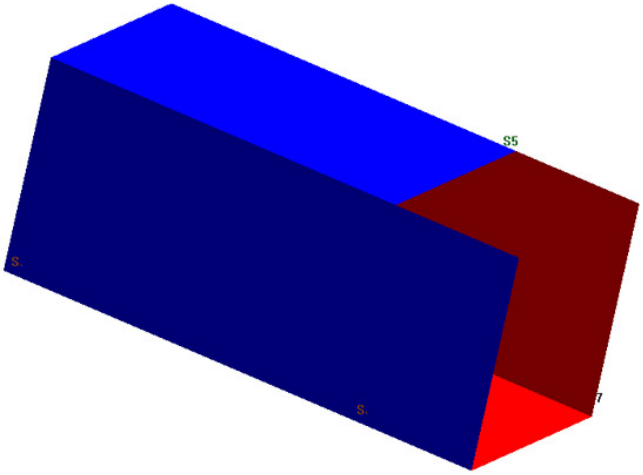

Figure 4.39 Anechoic room eighth surface

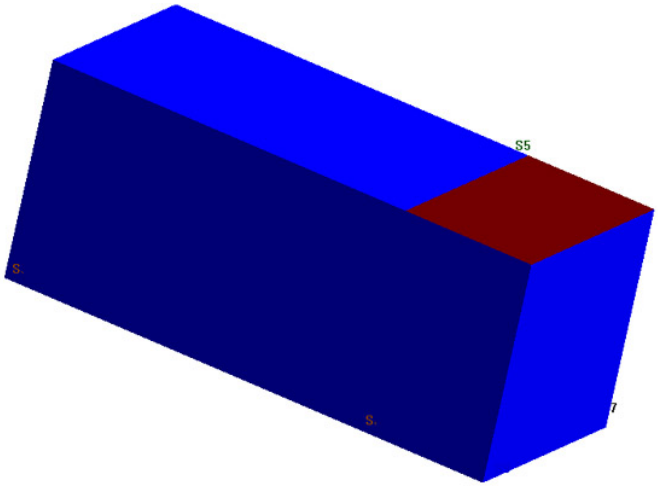

Figure 4.40 Anechoic room ninth surface

Then the roof surface was formed by vectoring upper border line of left surface to Y axis with coordinate 0 1.2 0. The process result is shown in Figure 4.41 below.

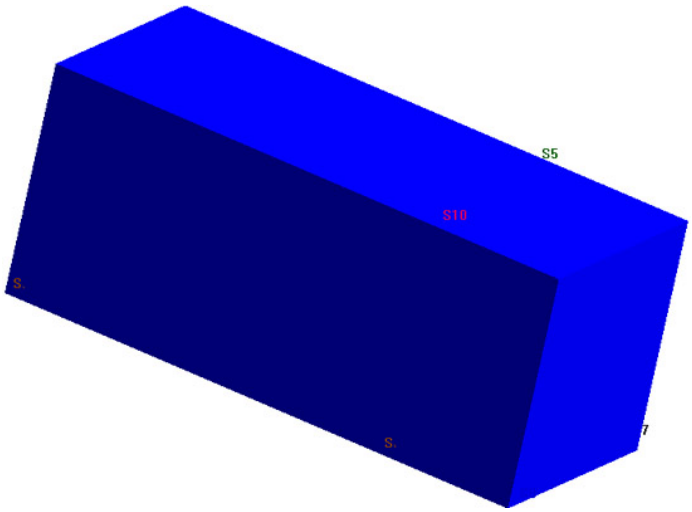

Figure 4.41 Anechoic room seventh surface

Then the entire simulation process was exactly the same with the simulation process of S1 explained in section 4.3.1 except for boundary condition definition. Acoustic impedance value 415 was applied to the all surfaces of the anechoic model to define that the surfaces was totally absorbed.

4.4 Sound Intensity Simulation

4.4.1 Net Sound Intensity

Net sound intensity is gathered in the anechoic room with a panel. The simulation setup to obtain the sound intensity is shown in the Figure 4.42 below. Sound source is placed 2 meters in front of the panel, and 16 internal points to record the intensity values are placed λ/4 in front of the panel.

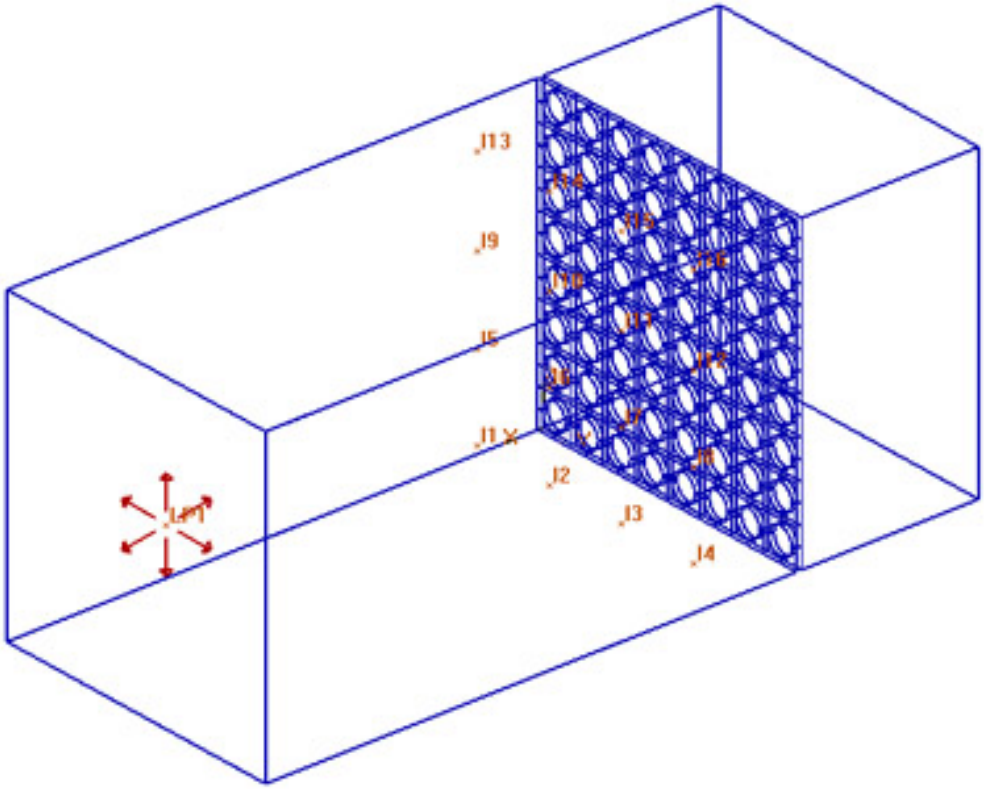

Figure 4.42 Net sound intensity simulations

4.4.2 Incidence Sound Intensity

Incidence sound intensity is gathered in an empty anechoic chamber without any panel. The simulation setup to obtain the incidence sound intensity is shown in

the Figure 4.43 below. Sound source is placed 2 meters in front of the origin point, and 16 internal points to record the intensity values are placed λ/4 in front of the panel stand placed (panel is removed).

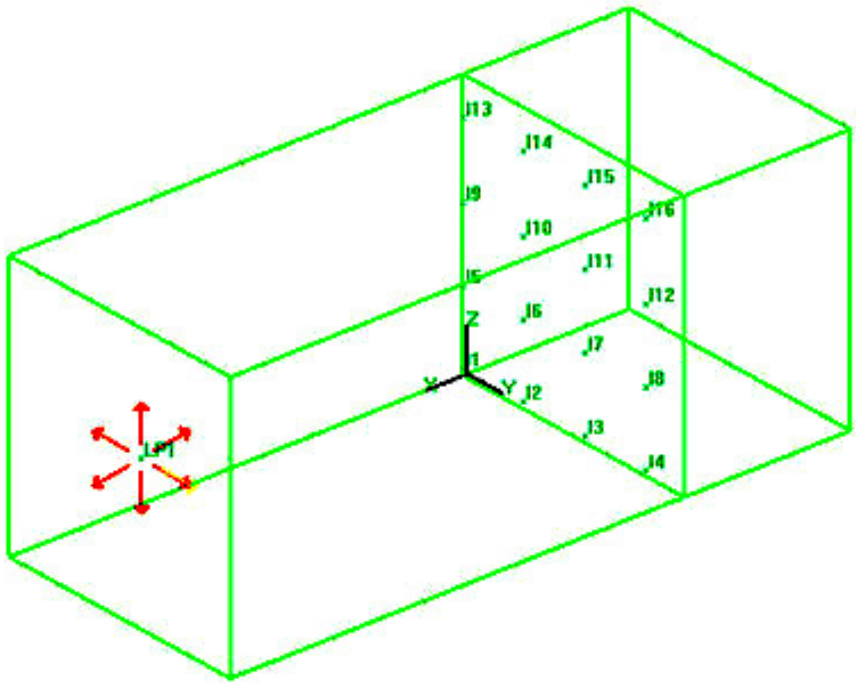

Figure 4.43 Incidence sound intensity simulation

The distances of the internal points for each frequency are showed in Table 4.12 below.

Table 4.12 Internal points distances for each frequency

Frequency (Hz)	250 Hz	500 Hz	1000 Hz	2000 Hz	4000 Hz
Internal points (0.25λ)	340 mm	170 mm	85 mm	42.5 mm	21.25 mm

The actual internal points distance coordinates defined in Beasy as shown in Table 4.13 below has been added by the thickness of the WCPP.

Table 4.13 Internal points distance in Beasy

Frequency (Hz)	250 Hz	500 Hz	1000 Hz	2000 Hz	4000 Hz
Internal points (0.25λ)	360 mm	190 mm	105 mm	62.5 mm	41.25 mm

4.5 Summary

The WCPP simulation process is done using Beasy Acoustic software. Beasy modeling fundamental for acoustic problem and WCPP simulation flow chart is elaborated to show the clear view of the modeling steps. Modeling process for WCPP panels is started by creating geometrical model follow by meshing, zone defining and boundary condition defining. A point source and 16 internal points are created to simulate the net sound intensity values inside the anechoic chamber. Incidence sound intensity value is simulated by creating anechoic room without any panel.

CHAPTER 5

RESULT AND DATA ANALYSIS

5.1 Introduction

This chapter discusses the simulation result of WCPP for 20 %, 30 % and 40 % perforation ratio obtained from simulation process discussed in Chapter 4. α_n data from simulation result would be compared with measured data obtained in previous research work conducted by Mohamad Ngasri Dimon and prediction data from theoretical modeling. The simulation result obtained by Boundary element method would be verified it accuracy by comparing with measured data and theoretical calculation.

5.2 Simulation Result for WCPP with 20% Perforation Ratio

The samples characteristic of WCPP with 20 % perforation ratio is described in Table 5.1 below

Table 5.1: WCPP with 20 % perforation ratio

Ref. No.	Radius (mm)	Aperture distance (mm)	% Perforation
S1	16	60	20
S4	20	75	20
S8	44	150	20

The simulation result for WCPP with 20 % perforation ratio show in Table 5.2 and Figure 5.1 below. The detail of sound intensity simulated, net sound intensity and incident intensity of α_n is as in Appendix A.

Table 5.2: α_n simulated result for 20 % perforation ratio

Samples	Frequencies (Hz)				
	250	500	1000	2000	4000
S1	0.83	0.92	0.75	0.43	0.46
S4	0.83	0.92	0.77	0.43	0.61
S8	0.99	1.00	0.90	0.35	0.56

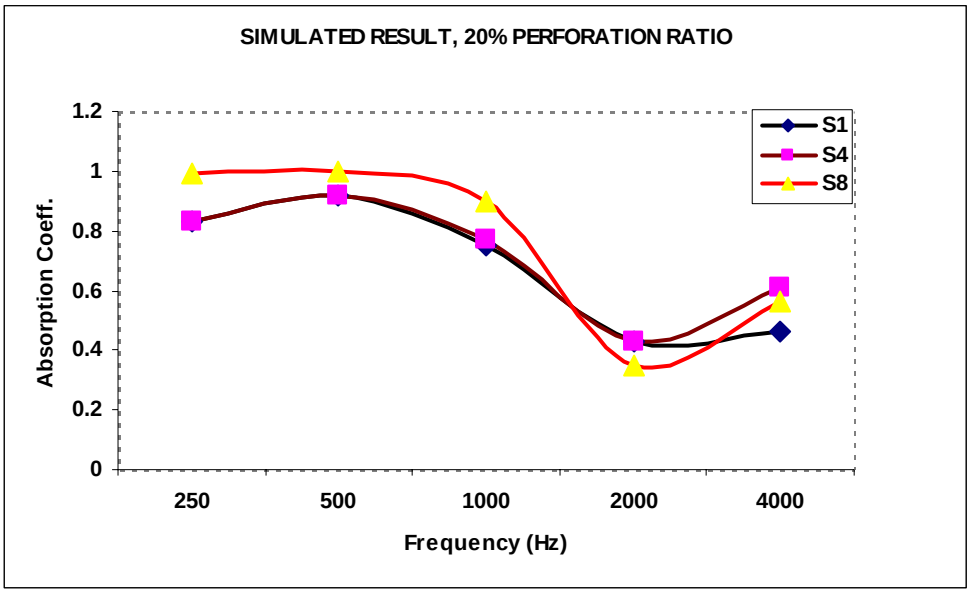

Figure 5.1 α_n simulated for 20 % perforation ratio

The simulated α_n in Table 5.2 and Figure 5.1 above show that α_n for S1 exhibit a small increment from 250 Hz to 500 Hz, then followed by steeper decay trend from 500 Hz to 2 kHz and a increment from 2 kHz to 4 kHz. S4 exhibit a smooth increment from 250 Hz to 500 Hz, followed by drastic decay from 500 Hz to 2 kHz and a stepper increment from 2 kHz to 4 kHz. S8 shows a small increment trend from 250 Hz to 500 Hz, followed by a drastic decay from 500 Hz to 2 kHz, and then followed by a drastic increment from 2 kHz to 4 kHz. It's observed that for WCPP with 20 % perforation ratio, α_n values are very high and shows that a small increment trend from 250 Hz to 1 kHz. From 1 kHz to 2 kHz α_n would significantly reduce and followed by small increment trend from 2 kHz to 4 kHz. It is foreseen that an α_n increment trend from 2 kHz to 4

kHz was caused by resonance frequencies effect, but it need deeper investigation to understand the contribution of resonance frequencies toward α_n simulated.

5.3 Result Comparison for WCPP with 20% Perforation Ratio

The α_n simulated result compared with measured data and theoretical result of WCPP with 20 % perforation ratio is described in Table 5.3 and Figure 5.2, 5.3 and 5.4 below

Table 5.3: α_n comparison for 20 % perforation ratio

		Frequencies (Hz)				
		250	**500**	**1000**	**2000**	**4000**
S1	**SIMULATED**	**0.83**	**0.92**	**0.75**	**0.43**	**0.46**
	MEASURED	1.00	0.82	0.67	0.33	0.31
S4	**SIMULATED**	**0.83**	**0.92**	**0.77**	**0.43**	**0.61**
	MEASURED	0.97	0.83	0.60	0.30	0.33
S8	**SIMULATED**	**0.99**	**1.00**	**0.90**	**0.35**	**0.56**
	MEASURED	0.93	0.80	0.60	0.26	0.49
	THEORY	0.95	0.82	0.54	0.23	0.07

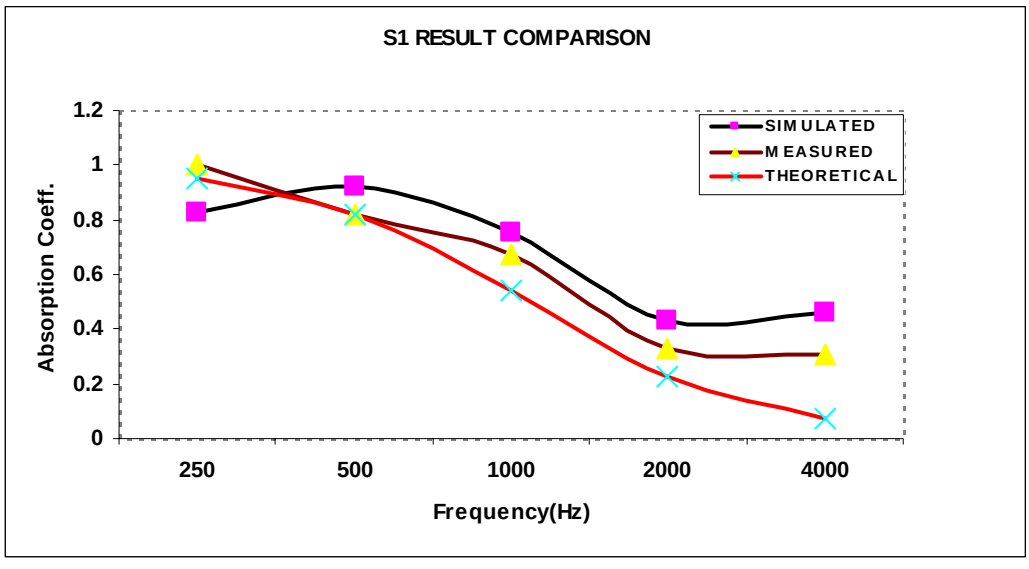

Figure 5.2 S1 α_n simulation result comparison

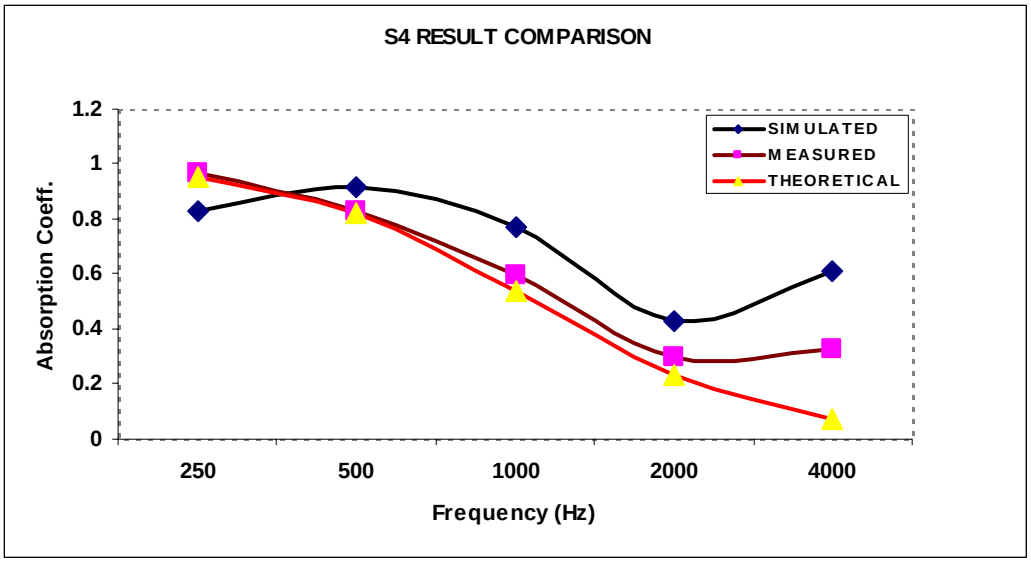

Figure 5.3 S4 α_n simulation result comparison

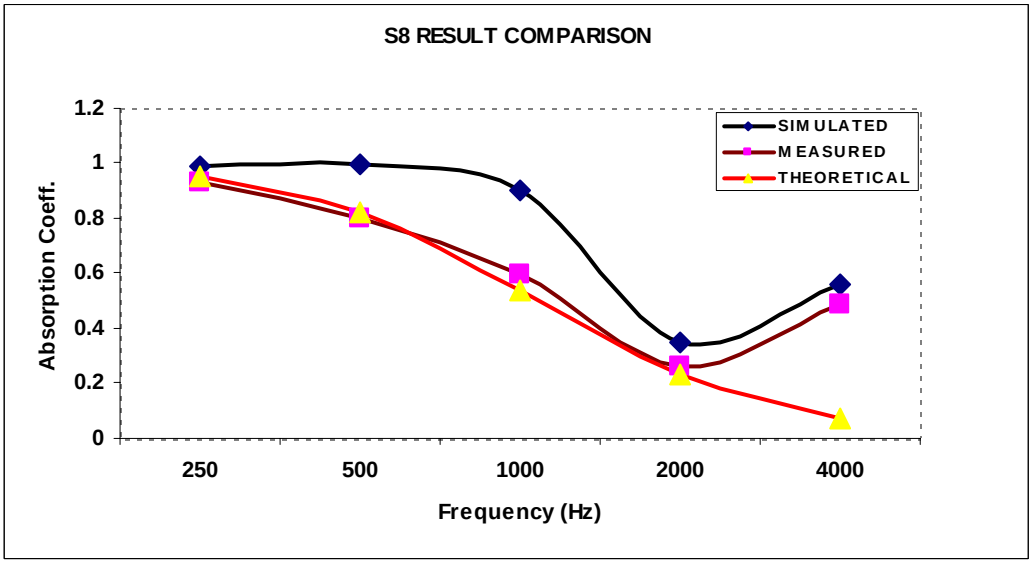

Figure 5.4 S8 α_n simulation result comparison

The α_n simulated compared with α_n measured which is derived from τ_n (Mohamad Ngasri bin Dimon, 2003d) and α_n calculated by theoretical prediction are showed in Table 5.3 and Figure 5.2, 5.3 and 5.4. It's suggested that over all S1 simulated data has slightly higher than measured data and theoretical result. From 500 Hz to 4 kHz, S1 simulated has almost the same trend with measured data and calculated result, but from 2 kHz to 4 kHz, the simulated data and measured data are slightly increase while theoretical result show decrease trend.

Over all S4 simulated data is higher than measured data and theoretical result. A small trend differences from 250 Hz to 500 Hz, simulated data is slightly increase while measured and theoretical data is slightly decrease but the α_n values are still very close. For 500 Hz to 4 kHz simulated data have the same trend, but theoretical data only show decay trend from 500 Hz to 4 kHz.

S8 simulated still has quite similar trend with measured data but simulated data is higher compare to measured data and theoretical result. While measured data and theoretical result show very close correlation for frequency 250 Hz to 2 kHz but its have different trend for frequency 2 kHz to 4 kHz.

5.4 Simulation Result for WCPP with 30% Perforation Ratio

The samples characteristic of WCPP with 30 % perforation ratio is described in Table 5.4 below

Table 5.4: WCPP with 30 % perforation ratio

Ref. No.	r (mm)	d (mm)	% Perforation
S2	20	60	30
S10	54	150	30

The simulation result of WCPP with 30 % perforation ratio is described in Table 5.5 and Figure 5.5 below

Table 5.5: α_n simulated for 30 % perforation ratio

Samples	Frequencies (Hz)				
	250	500	1000	2000	4000
S2	0.83	0.92	0.76	0.45	0.48
S10	1.00	1.00	0.98	0.36	0.44

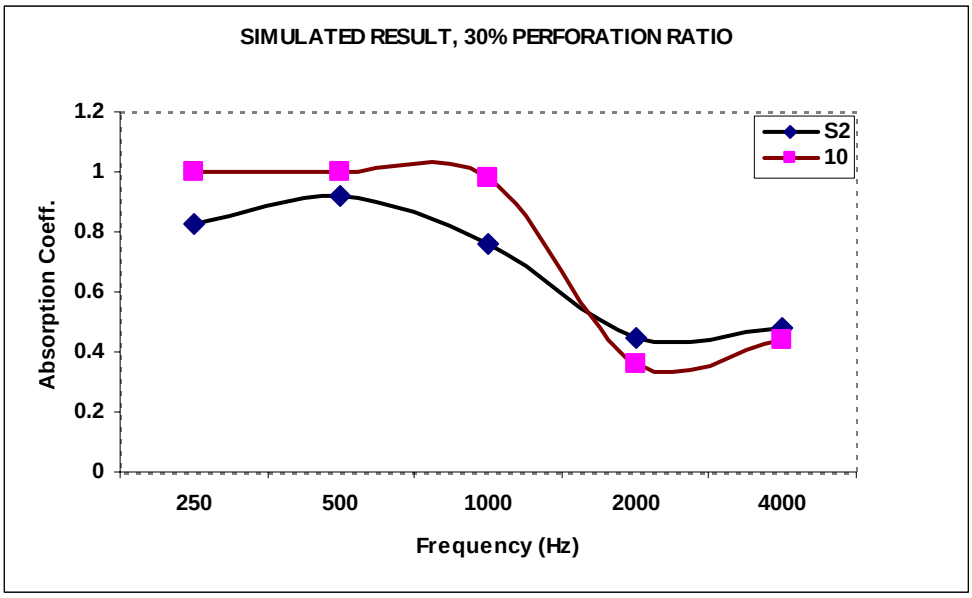

Figure 5.5 α_n simulated for 30 % perforation ratio

The simulated α_n in Table 5.5 and Figure 5.5 above show that α_n for S2 exhibit a small increment from 250 Hz to 500 Hz, then followed by steeper decay trend from 500 Hz to 2 kHz and a small increment from 2 kHz to 4 kHz. α_n for S10 is quite stable from 250 Hz to 1 kHz, followed by a very drastic decay from 1 kHz to 2 kHz and stepper increment from 2 kHz to 4 kHz. It's observed that for WCPP with 30 % perforation ratio, α_n values are very high at low frequencies. From 1 kHz to 2 kHz α_n would significantly reduce and followed by small increment trend from 2 kHz to 4 kHz.

5.5 Result Comparison for WCPP with 30% Perforation Ratio

The simulated result compared with measured data and theoretical result of WCPP with 30 % perforation ratio is described in Table 5.6 and Figure 5.6, 5.7 and 5.8 below

Table 5.6: α_n comparison for 30 % perforation ratio

		Frequencies (Hz)				
		250	**500**	**1000**	**2000**	**4000**
S2	**SIMULATED**	**0.83**	**0.92**	**0.76**	**0.45**	**0.48**
	MEASURED	0.97	0.96	0.83	0.50	0.53
S10	**SIMULATED**	**1.00**	**1.00**	**0.98**	**0.36**	**0.44**
	MEASURED	0.94	0.87	0.79	0.36	0.59
	THEORY	0.97	0.91	0.73	0.40	0.14

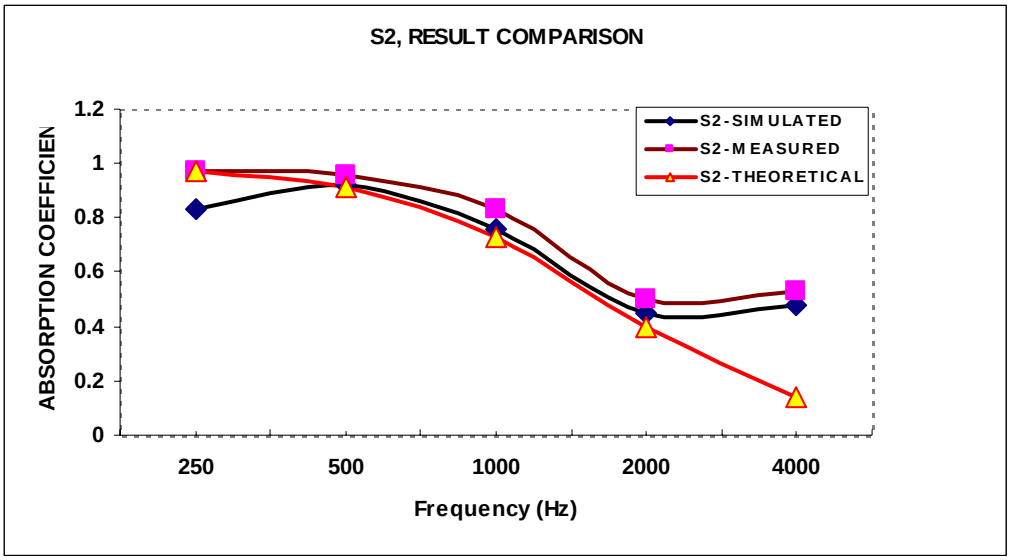

Figure 5.6 S2 α_n simulation result comparison

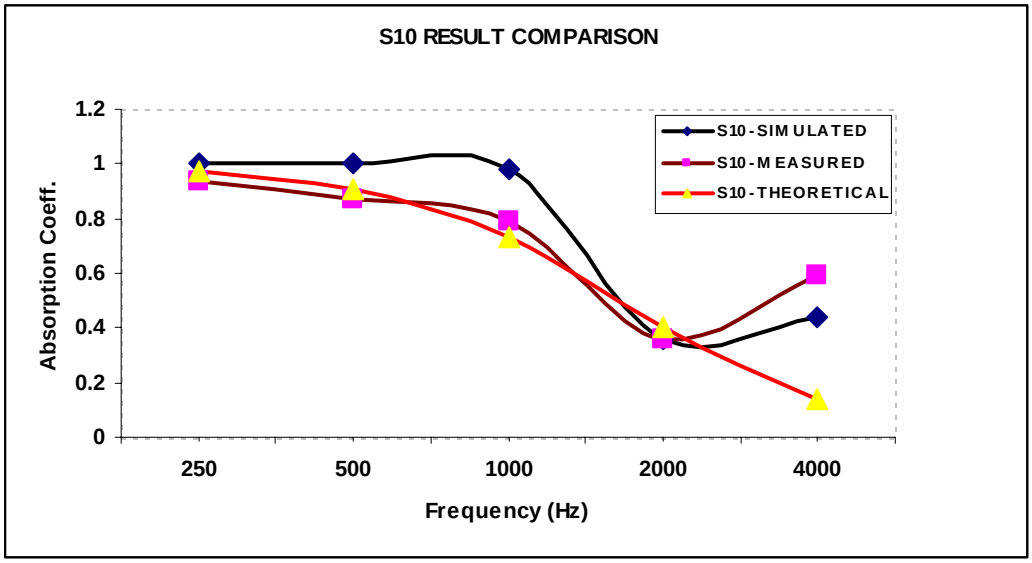

Figure 5.7 S10 α_n simulation result comparison

The α_n simulated compared with α_n measured which is derived from τ_n (Mohamad Ngasri Dimon, 2003b) and α_n calculated by theoretical prediction suggested that over all S2 simulated data has very close correlation with measured data and theoretical result. Simulated data is slightly lower than measured data and slightly higher than theoretical result. From 500 Hz to 4 kHz, S2 simulated has almost the same trend with measured data and calculated result, but from 2 kHz to 4 kHz, the simulated data and measured data are slightly increase while theoretical result show stepper decrease trend.

Over all S10 simulated data is higher than measured data and theoretical result. The trend differences are showed from 250 Hz to 1 kHz, simulated data is quite stable while measured and theoretical data is slightly decrease but the α_n values are still reasonably close together. For 1 kHz to 2 kHz simulated data and measured data have the same trend. For 2 kHz to 4 kHz, simulated data and measured data show the increasing trend while theoretical data show decay trend.

5.6 Simulation Result for WCPP with 40% Perforation Ratio

The samples characteristic of WCPP with 40 % perforation ratio is described in Table 5.7 below

Table 5.7: WCPP with 40 % perforation ratio

Ref. No.	r (mm)	d (mm)	% Perforation
S3	23	60	40
S6	20	52	40
S12	62	150	40

Table 5.8: α_n simulation result for 40% perforation ratio

Samples	Frequencies (Hz)				
	250	**500**	**1000**	**2000**	**4000**
S3	0.86	0.91	0.77	0.44	0.85
S6	0.83	0.92	0.97	0.58	0.70
S12	1.00	0.91	0.95	0.36	0.63

The simulated α_n showed in Table 5.8 and Figure 5.8 above show that α_n for S3 exhibit a small increment from 250 Hz to 500 Hz, then followed by steeper decay trend from 500 Hz to 2 kHz and a drastic increment from 2 kHz to 4 kHz. S6 exhibit a smooth increment from 250 Hz to 1 kHz, followed by drastic decay from 1 kHz to 2 kHz and an increment from 2 kHz to 4 kHz. S12 shows a small decay trend from 250 Hz to 500 Hz, followed by a small increment from 500 Hz to 1 kHz, and then followed by a drastic increment from 2 kHz to 4 kHz. It‘s observed that for WCPP with 40 % perforation ratio, α_n values are very high and shows that a small increment trend from 250 Hz to 1 kHz.

From 1 kHz to 2 kHz α_n would significantly reduce and followed by small increment trend from 2 kHz to 4 kHz.

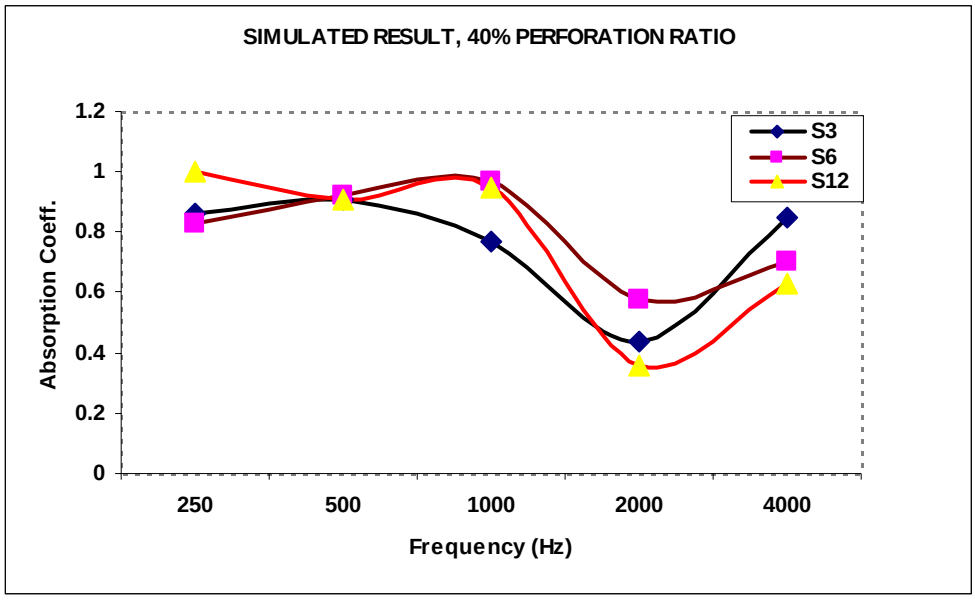

Figure 5.8 α_n simulated for WCPP 40% perforation ratio

5.7 Result Comparison for WCPP with 40% Perforation Ratio

The simulated result compared with measured data and theoretical result of WCPP with 40 % perforation ratio is described in Table 5.9 and Figure 5.9 5.10 and 5.11 below

Table 5.9: α_n comparison for 40% perforation ratio

		Frequencies (Hz)				
		250	500	1000	2000	4000
S3	**SIMULATED**	0.86	0.91	0.77	0.44	0.85
	MEASURED	0.99	1.00	0.86	0.65	0.64
S6	**SIMULATED**	0.83	0.92	0.97	0.58	0.70
	MEASURED	0.94	0.98	0.90	0.64	0.68
S12	**SIMULATED**	1.00	0.91	0.95	0.36	0.63
	MEASURED	0.98	0.94	0.92	0.54	0.62
	THEORY	0.99	0.95	0.82	0.54	0.23

The α_n simulated compared with α_n measured which is derived from τ_n (Mohamad Ngasri Dimon, 2003b) and α_n calculated by theoretical prediction are showed in Table 5.9 and Figure 5.9, 5.10 and 5.11. It's suggested that from 250 Hz to 2 kHz, S3 simulated has almost the same trend with measured data and calculated result but from 2 kHz to 4 kHz its trend is changing, the simulated data drastically increase to 0.85 while measured data is 0.64 and theoretical result decrease to 0.23.

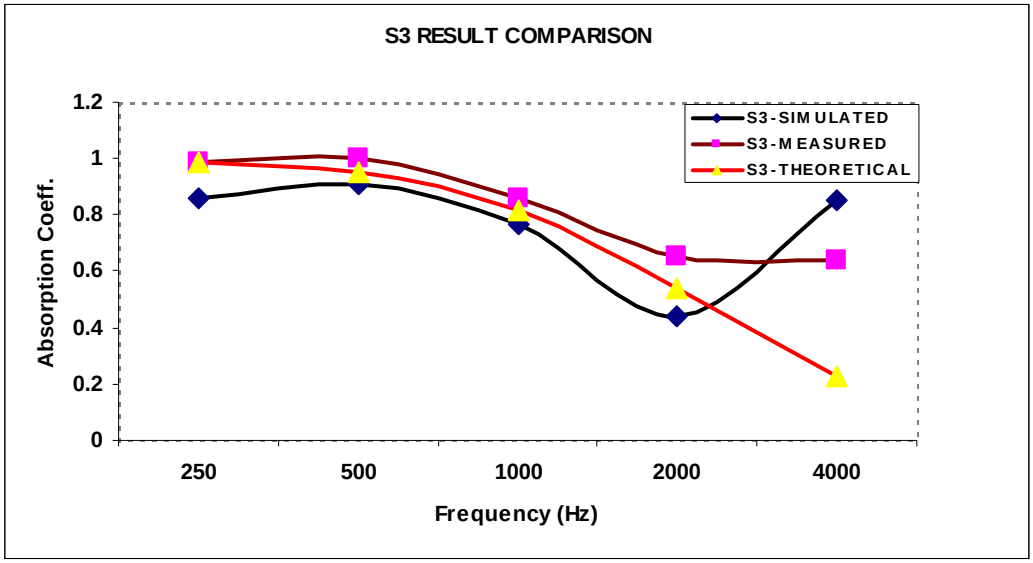

Figure 5.9 S3 α_n simulation result comparison

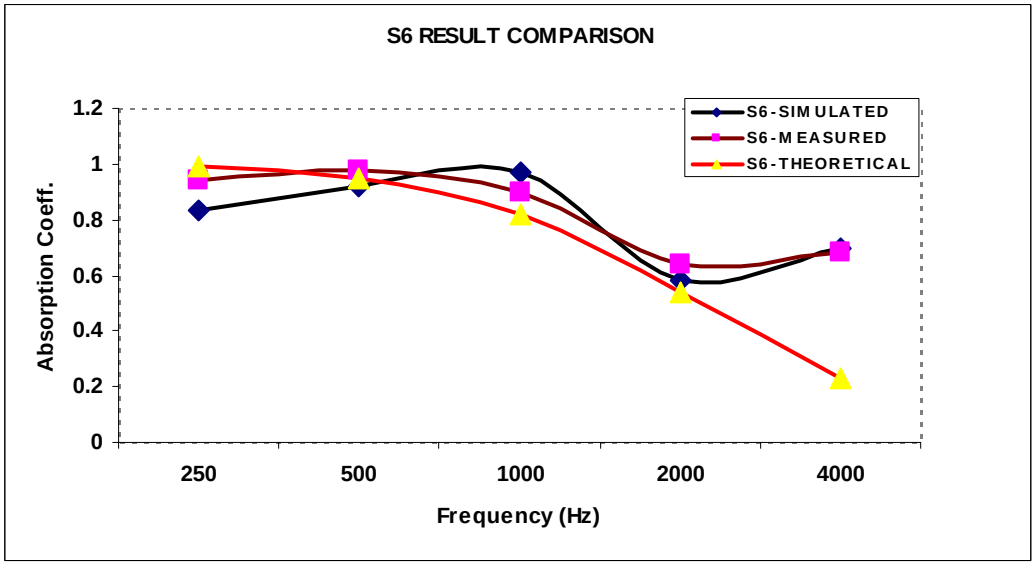

Figure 5.10 S6 α_n simulation result comparison

S6 simulated has a small trend differences from 250 Hz to 1 kHz, simulated data is slightly increase while measured and theoretical data is slightly decrease but the α_n values are still very close. For 1 kHz to 4 kHz simulated data have the same trend and

almost similar values but theoretical data, it's show quite drastic decay from 1 kHz to 2 kHz and followed by small increment from 2 kHz to 4 kHz, but theoretical data only show decay trend from 1 kHz to 4 kHz.

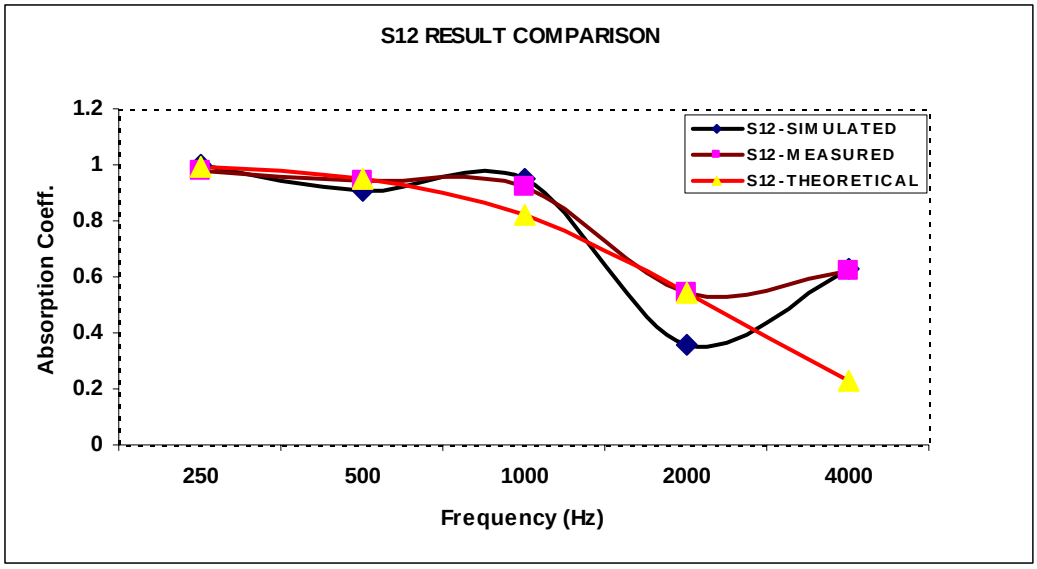

Figure 5.11 S12 α_n simulation result comparison

S12 simulated has the same trend and almost the same value with measured data from 250 Hz to 4 kHz. The result value difference occur only at 2 kHz, where simulated α_n is 0.36 and measured α_n is 0.54. While the α_n from theoretical prediction is very close with α_n simulated at low frequencies but its have different trend at high frequencies.

5.8 Result and Data Analysis

Generally, the simulation results show that α_n is very high for low frequencies (250 – 500 Hz), which are almost equal to 1. Then the trend shows decay for frequency from 500 Hz to 1 kHz follows by slight increment from frequency 2 kHz to 4 kHz. From over all simulation data generally suggest that the lowest α_n is at frequency 2 kHz. This dip is in correlation with measurement data trend from 250 Hz to 4 kHz. These increment phenomena at high frequencies shown by simulation results agree with the measurement results but rather opposite with theoretical prediction. The α_n increment is foreseen caused by resonance frequencies inside the air column in WCPP hole. The apertures of perforated panel can act as wave guide to generate the resonance. The resonance

frequency formulation for wave guide as shown in Figure 5.12 below is given by equation 2.74 (Fahy, 2001).

$$f_n = \frac{nc}{2d} \tag{2.74}$$

where,

f = Resonance frequency

n = Integer (1, 2, 3,. .)

d = hole diameter

c = speed of sound

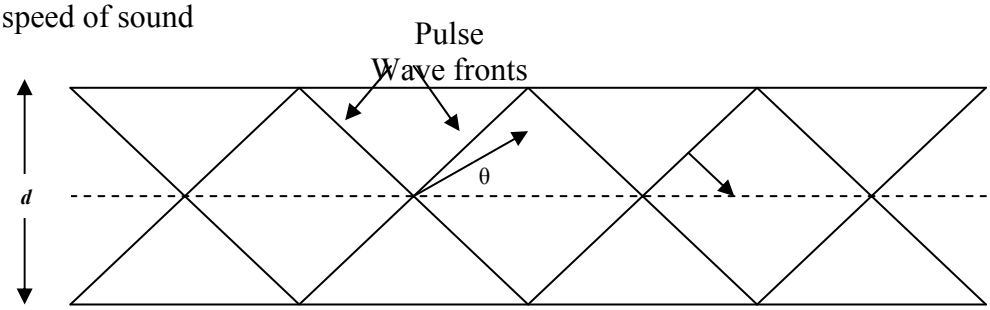

Figure 5.12 Periodically spaced plane pulses in a uniform wave guide

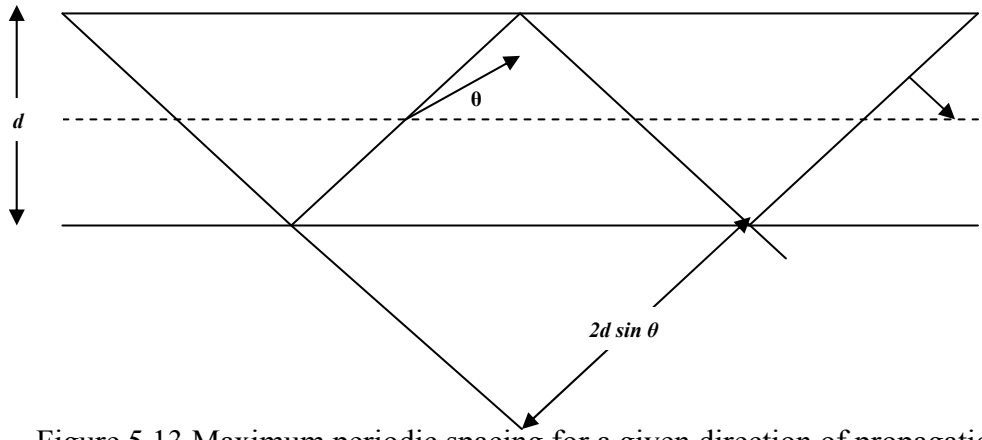

Figure 5.13 Maximum periodic spacing for a given direction of propagation

From the Equation 2.74, resonance frequency of WCPP is affected mainly by the diameter of apertures holes, where the larger the holes, the lower the resonance frequency.

The calculated resonance frequency using equation 2.74 for all simulation samples is described in Table 5.10 below.

Table 5.10: Calculated resonance frequencies for simulation samples

Sample No.	Perforation (%)	*D* (mm)	Resonance Frequency		
			f_1 (Hz)	f_2 (Hz)	f_3 (Hz)
S1	20	32	5312	10624	-
S4	20	40	4250	8500	-
S8	20	88	1932	3864	-
S2	30	40	4250	8500	-
S10	30	108	1574	3148	-
S3	40	46	3696	7392	-
S6	40	40	4250	8500	-
S12	40	124	1370	2741	5482

From simulated result suggest that α_n increment for high frequencies could be closely related with resonance frequency calculated using equation 5.1 in Table 5.10 above. WCPP with 20% perforation ratio, S1, S4 and S8 show α_n increment at higher frequency because its have resonance frequencies at 5312 Hz, 4250 Hz, and 3864 Hz respectively. WCPP with 30% perforation ratio, S2, and S10, show α_n increment at higher frequency because its have resonance frequencies at 4250 Hz and 3148 Hz respectively. WCPP with 40% perforation ratio, S3, S6 and S12, show α_n increment at higher frequency because its have resonance frequencies at 3696 Hz, 4250 Hz and 5482 Hz respectively.

5.9 Summary

The simulated result for WCPP with 20%, 30% and 40% perforation ratio generally showed that α_n is very high and almost constant for frequency 250 to 500 Hz, then it shows a decay trend for frequency 500 Hz to 2 kHz and followed by a small

increment from 2 kHz to 4 kHz. It is foreseen that an α_n increment trend from 2 kHz to 4 kHz could be caused by resonance frequencies effect. This requires further in depth study, beyond the scope of this work.

Result comparison show that simulated result generally has almost the same trend with measured data and theoretical prediction from 250 Hz to 1 kHz, but from 2 kHz to 4 kHz its trend is changing, the simulated result and measured data show the small increment trend and closely correlated to each other while theoretical prediction continue to decay.

The increment phenomena at high frequencies shown by simulation results agree with the measurement results but opposite with theoretical prediction. The α_n increment could cause by resonance frequency inside the air column in WCPP holes.

CHAPTER 6

STATISTICAL REGRESSION MODEL FOR SIMULATION DATA

6.1 Introduction

This chapter will cover topics in curve fitting regression and multiple regressions, as well as the supporting tasks that are important in preparing to analyze the simulation data described in Chapter 5 before. The basics of curve fitting and multiple regressions and demonstrate the importance of inspecting, checking and verifying the data before accepting the results of the analysis will be discussed. All statistical regression analysis applied in this thesis use Statistical Package for the Social Sciences (SPSS) software, one of the statistical software available.

α_n simulated from Figure 5.1, 5.5 and 5.8 show the non linear curve with increment trend from frequency 250 Hz to 500 Hz, then show stepper decay from frequency 500 Hz to 2000 Hz followed by increment for frequency 2000 Hz to 4000 Hz. These curves can be closely modeled by third order polynomial models using least square method. This method calculates the best-fitting line for the observed data by minimizing the sum of the squares of the vertical deviations from each data point to the line. The third order polynomial model is performed as follow (Schiff and Agostino, 1994a)

$$y = c + b_1 x \ + b_2 x^2 + b_3 x^2 + b_4 x^3 \qquad (6.1)$$

where *y* is the true dependent variable, the *b*'s are the regression coefficients for the corresponding independent variables *x*, and *c* is the constant or intercept.

Multiple regression to predict the overall α_n simulated model in SPSS is analyzed by using second order and third order polynomial equation 6.2 below (Schiff and Agostino, 1996b)

Second order, no interaction model,

$$y = c + b_1 x_1 + b_2 x_2 + b_3 x_1^2 + b_4 x_2^2 \tag{6.2}$$

Second order, interaction model

$$y = c + b_1 x_1 + b_2 x_2 + b_3 x_1 x_2 + b_4 x_1^2 + b_5 x_2^2 \tag{6.3}$$

Third order, no interaction model

$$y = c + b_1 x_1 + b_2 x_2 + b_3 x_1^2 + b_4 x_2^2 + b_5 x_1^3 + b_6 x_2^3 \tag{6.4}$$

Third order, interaction model

$$y = c + b_1 x_1 + b_2 x_2 + b_3 x_1^2 + b_4 x_2^2 + b_5 x_1^3 + b_6 x_2^3 + b_7 x_1 x_2 \tag{6.5}$$

where *y* is the true dependent variable, the *b*'s are the regression coefficients for the corresponding independent variables *x, c* is the constant or intercept. Equations as shown above, with no interaction effects are called main effects models.

The important parameters used in the development of α_n simulated regression model are as follows:

a. **Predicted values** which is also called fitted values, are the values obtained by using the regression equation for all cases in the analysis.

b. **Adjusted predicted values** are the values obtained by using the regression equation for all cases in the analysis except the given case.

c. **Residuals** are the difference between the real data values and those predicted by the regression equation.

d. **The regression coefficient, b,** is the unstandardized simple regression coefficient for the case of one independent variable. When there are two or more independent variables, the b coefficient is a partial regression coefficient.

e. **t-tests** are used to assess the significance of b coefficients, specifically for testing the null hypothesis that the regression coefficient is zero. A common rule of the test is to remove from the equation all variables not significant at the 0.05 level or better.

f. **Beta** is the regression coefficients (b) for standardized data. It is the average amount of the dependent variable increases when the independent variables increases one standard deviation and other independent variables are held constant. The ratio of the beta weights is the ratio of the estimated unique predictive importance of the independent variables

g. **Intercept** is the estimated *y* value when all the independents have a value of 0.

h. $\mathbf{R^2}$, coefficient of determination, is the percent of the variance in the dependent variable explained uniquely or jointly by the independent variables. It can also be interpreted as the proportionate reduction in error in estimating the dependent when knowing the independent variables. R^2 reflects the number of errors made when doing the regression model to predict the value of the dependent variable, in ratio to the total errors made when using only the dependent's mean for estimating all cases (Barnes, 1994)

$$R^2 = (1 - (SSE/SST)), \quad (6.6)$$

where

SSE = error sum of squares

$$SSE = SUM((Y - Y')^2), \quad (6.7)$$

where Y is the actual value of Y for the ith case and Y' is the regression prediction for the ith case.

SST = total sum of squares

$$SST = SUM((Yi - MeanY)^2). \quad (6.8)$$

The residual sum of squares output is SSE and reflects regression error. Thus R^2 is 1 minus regression error as a percent of total error and will be 0 when regression error is 1.

i. **F test** is used to test the significance of R, which is the same as testing the significance of the regression model as a whole. If prob (F) < .05, the independents variable is considered significantly influent the model estimation. F is calculated as follow,

$$F = (R^2/k)/((1 - R^2)/(n - k - 1)). \quad (6.9)$$

Where (n - k - 1) is degrees of freedom, k = number of terms in the equation not counting the constant.

j. **Stepwise method** is a way of computing the regression model in stages. In the first stage, the highest correlated independent variable with the dependent variable is included in the equation. Then, in the second stage, the remaining independent with the highest partial correlation with the dependent, controlling

for the first independent, is entered. This process is repeated until the addition of a remaining independent does not increase R^2 significantly.

k. **Residual plots** should show a random pattern, with no nonlinearity or heteroscedasticity to show that the model is adequate to represent the data. These are usually plots of standardized residuals against standardized the predicted dependent variable.

6.2 Regression Model of α_n Simulated for WCPP with 20% Perforation Ratio

α_n simulated data for 20% perforation ratio is fitted by applying polynomial equation using least square regression model with α_n as dependent variable and f as independent variable. Table 6.1 below shows the regression summary and parameter estimation for cubic (third order polynomial) model.

Table 6.1 Regression model summary for 20% perforation ratio

Equation	Model Summary					Parameter Estimates			
	R^2	F	df1	df2	Sig.	Constant	b1	b2	b3
Cubic	0.992	41.686	3	1	0.0113	0.823	0	-5.11E-007	9.70E-011

From parameter estimation in the Table 6.1 above, the regression equation for predicting α_n of WCPP with 20% perforation ratio can be written as follow

$$\alpha_n = 0.823 - 5.11x10^{-7} f^2 + 9.7x10^{-11} f^3 \qquad (6.10)$$

where,

f = Frequency (Hz)

From the model summary in Table 6.1, can be seen that coefficient of determination, R^2 is 0.99, meaning that approximately 99% of the variability of α_n is accounted by the variables in the model. It's also meaning that only 0,08 % error is made in regression model. The accuracy of the regression model to predict the α_n is

also showed by residual plot in Figure 6.1 below. It can be seen that the residual values versus predicted values plot shows a random pattern distribution, so that the regression model is adequate.

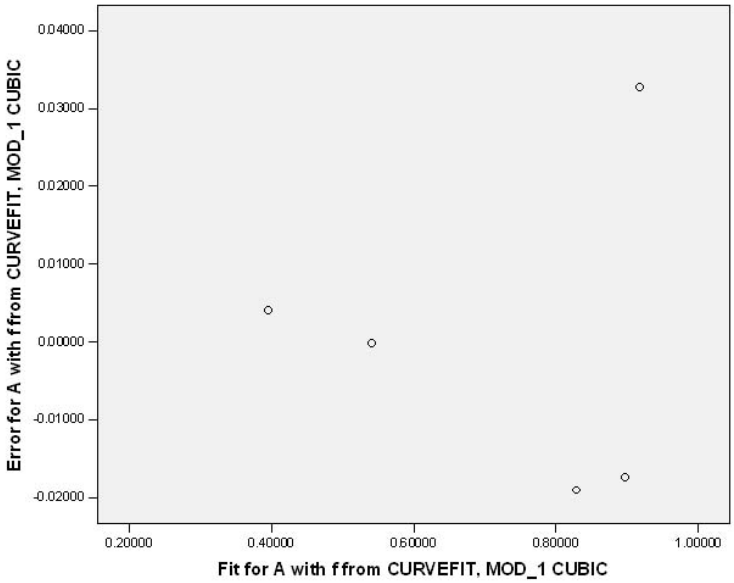

Figure 6.1 Residual analyses for 20% perforation ratio

The accuracy of the regression model is further examined by comparing simulated data with predicted value using regression model as shows in Table 6.2 below. It's clearly seen that the predicted values are very close to simulated data.

Table 6.2 α_n Simulated and predicted values comparison for 20% perforation ratio

Frequency (Hz)	**α_n simulated**	**α_n predicted**
250	0.88	0.89
500	0.95	0.92
1000	0.81	0.83
2000	0.40	0.40
4000	0.54	0.54

6.3 Regression Model of α_n Simulated for WCPP with 30% Perforation Ratio

α_n simulated data for 30% perforation ratio is fitted by applying polynomial equation using least square regression model with α_n as dependent variable and f as

independent variable. Table 6.3 below shows the regression summary and parameter estimation for cubic (third order polynomial) model.

Table 6.3 Regression model summary for 30% perforation ratio

Equation	Model Summary					Parameter Estimates			
	R^2	F	df1	df2	Sig.	Constant	b1	b2	b3
Cubic	1.000	1812.84	3	1	0.017	0.831	0.001	-5.66E-007	1.04E-010

From parameter estimation in the Table 6.3 above, the regression equation for predicting α_n of WCPP with 30% perforation ratio can be written as follow

$$\alpha_n = 0.831 + 0.001f - 5.66x10^{-7} f^2 + 1x10^{-10} f^3 \qquad (6.11)$$

where,

f = Frequency (Hz)

From the model summary in Table 6.3, can be seen that coefficient of determination, R^2 is 1, meaning that 100% of the variability of α_n is accounted by the variables in the model. It's also meaning that no error is made in regression model. The accuracy of the regression model to predict the α_n is also showed by residual plot in Figure 6.2 below. It can be seen that the residual values versus predicted values plot shows a random pattern distribution, so that the regression model is adequate.

The accuracy of the regression model is further examined by comparing simulated data with predicted value using regression model as shows in Table 6.4 below. It's clearly seen that the predicted values are very close to simulated data.

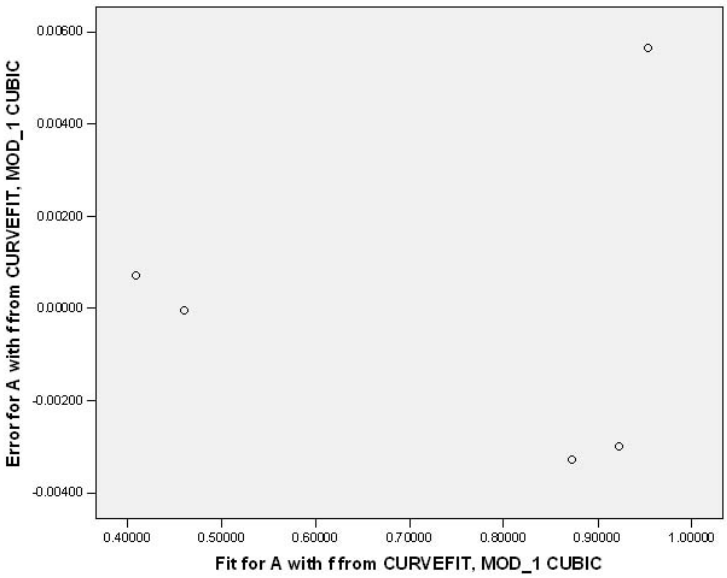

Figure 6.2 Residual analyses for 30% perforation ratio

Table 6.4 α_n simulated and predicted values comparison for 30% perforation ratio

Frequency (Hz)	α_n simulated	α_n predicted
250	0.92	0.92
500	0.96	0.95
1000	0.87	0.87
2000	0.41	0.41
4000	0.46	0.46

6.4 Regression Model of α_n Simulated for WCPP with 40% Perforation Ratio

α_n simulated data for 40% perforation ratio is fitted by applying polynomial equation using least square regression model with α_n as dependent variable and f as independent variable. Table 6.5 below shows the regression summary and parameter estimation for cubic (third order polynomial) model.

Table 6.5 Regression model summary for 40% perforation ratio

Equation	Model Summary					Parameter Estimates			
	R^2	F	df1	df2	Sig.	Constant	b1	b2	b3
Cubic	0.990	34.648	3	1	0.0124	0.785	0.001	-5.90E-007	1.11E-010

From parameter estimation in the Table 6.5 above, the regression equation for predicting α_n of WCPP with 40% perforation ratio can be written as follow

$$\alpha_n = 0.785 + 0.001f - 5.9x10^{-7} f^2 + 1.11x10^{-10} f^3 \qquad (6.12)$$

where,

f = Frequency (Hz)

From the model summary in Table 6.5, can be seen that coefficient of determination, R^2 is 0.99, meaning that almost 99% of the variability of α_n is accounted by the variables in the model. It's also meaning that only 0.001% error is made in regression model. The accuracy of the regression model to predict the α_n is also showed by residual plot in Figure 6.3 below. It can be seen that the residual values versus predicted values plot shows a random pattern distribution, so that the regression model is adequate.

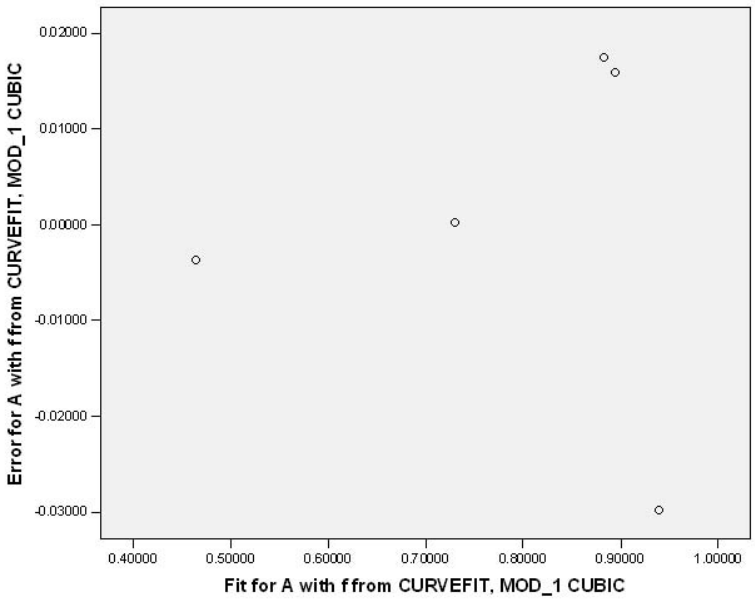

Figure 6.3 Residual analyses for 40% perforation ratio

The accuracy of the regression model is further examined by comparing simulated data with predicted value using regression model as shows in Table 6.6 below. It's clearly seen that the predicted values very close to simulated data.

Table 6.6 α_n simulated and predicted values comparison for 40% perforation ratio

Frequency (Hz)	α_n simulated	α_n predicted
250	0.91	0.90
500	0.91	0.94
1,000	0.90	0.89
2,000	0.46	0.46
4,000	0.73	0.73

6.5 Regression Model for Over All α_n Simulated Data

The statistical regression model to predict over all α_n from simulation data is fitted by applying multiple regression and stepwise method. By stepwise method the multiple regression model is created by computing the most correlated independent variables to the α_n prediction value then automatically remove the uncorrelated variables. The independent variable computed in the process are frequency (f), perforation ratio (σ), f^2, f^3, σ^2, and f x σ. Table 6.7 below shows the regression and stepwise summary, and parameter estimation for over all α_n model.

Table 6.7 Over all model summary

Model	R	R^2	Adjusted R^2	Std. Error of the Estimate
c, f	0.715(a)	0.511	0.473	0.15889
c, f, f^3	0.899(b)	0.808	0.776	0.10355
c, f, f^3, f^2	0.964(c)	0.930	0.911	0.06539
c, f, f^3, f^2, σ x f	0.981(d)	0.962	0.947	0.05053

Table 6.8 Over all parameters coefficients estimation

Model	variables	Unstandardized Coefficients		Standardized Coefficients		Sig.
		B	Std. error	Beta	t	
1	*c*	0.913	0.062		14.693	0.000
	f	0.000	0.000	-0.715	-3.685	0.003
2	*c*	1.078	0.056		19.328	0.000
	f	0.000	0.000	-2.244	-5.962	0.000
	f^3	1.38E-011	0.000	1.623	4.314	0.001
3	*c*	0.813	0.070		11.583	0.000
	f	0.001	0.000	3.226	2.532	0.028
	f^3	1.04E-010	0.000	12.213	5.015	0.000
	f^2	-5.55E-007	0.000	-15.853	-4.369	0.001
4	*c*	0.813	0.054		14.991	0.000
	f	0.000	0.000	2.792	2.803	0.019
	f^3	1.04E-010	0.000	12.213	6.490	0.000
	f^2	-5.55E-007	0.000	-15.853	-5.655	0.000
	σ x *f*	2.25E-006	0.000	0.470	2.902	0.016

From parameter estimation in the Table 6.8 above, the regression equation for over all α_n prediction of WCPP with 20% to 40% perforation ratio is shown by the latest step is model 4. The regression model can be written as follow

$$\alpha_n = 0.831 - 5.55^{-7} f^2 + 1.04x10^{-10} f^3 + 2.25x10^{-6} \sigma xf \qquad (6.13)$$

where,

f = Frequency (Hz)

σ = Perforation ratio

From the model summary in Table 6.7, can be seen that coefficient of determination, R^2 is 0.962 for f, f^2, f^3, and σ x f as independent variables, it mean

that 96.2 % of the variability of α_n is accounted by the variables in the model. It's also meaning that only 0.038 % error is made in regression model. The accuracy of the regression model to predict the α_n is also showed by residual plot in Figure 6.4 below. It can be seen that the residual values versus predicted values plot shows a random pattern distribution, so that the regression model is adequate.

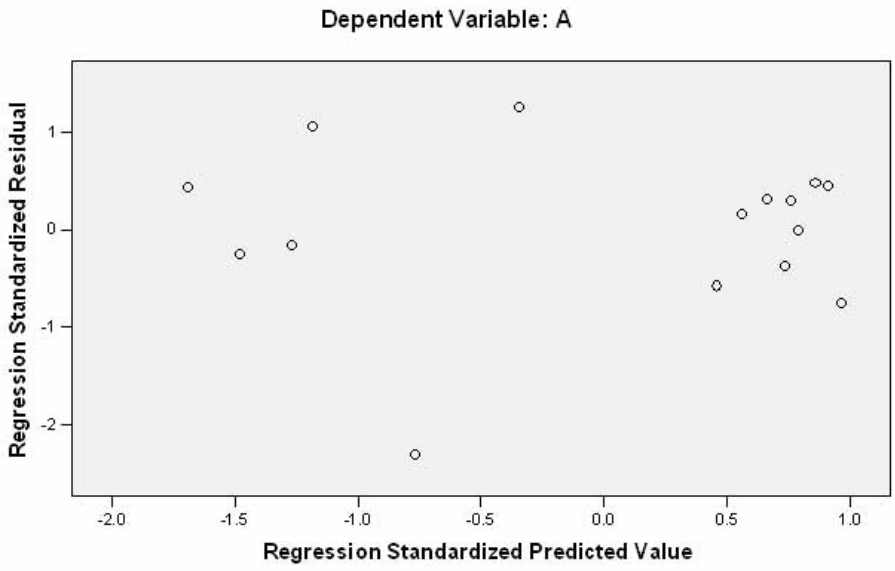

Figure 6.4 Residual analyses for over all α_n simulated data

The accuracy of the regression model is further examined by comparing simulated data with predicted value using regression model as shows in Table 6.9 below. It's clearly seen that the predicted values reasonably close to the simulated data.

Table 6.9 α_n simulated and predicted values comparison for over all simulated data

Frequency (Hz)	**α_n simulated**	**α_n predicted**	**% Perforation ratio**
250	0.88	0.90	20 %
500	0.95	0.93	20 %
1000	0.81	0.84	20 %
2000	0.40	0.38	20 %
4000	0.54	0.49	20 %
250	0.92	0.90	30 %
500	0.96	0.94	30 %

1000	0.87	0.86	30 %
2000	0.41	0.42	30 %
4000	0.46	0.58	30 %
250	0.91	0.91	40 %
500	0.91	0.94	40 %
1000	0.90	0.88	40 %
2000	0.46	0.47	40 %
4000	0.73	0.67	40 %

6.6 Summary

Regression prediction model for α_n simulated data with 20%, 30%, and 40% perforation ratio is fitted by least square method with *f* as independent variable. The third order polynomial equation is adequate to represent the data with very small error accounted in prediction data. The predicted data show very close correlation with simulation data.

Regression model for over all α_n simulated data is done by applying multiple regression with stepwise method. The independent variables computed in the process are f, f^2, f^3 , and σ x f. The predicted data show reasonably close correlation with simulation data.

CHAPTER 7

CONCLUSIONS AND RECOMENDATIONS

7.1 Conclusions

In this research work, normal incident sound absorption coefficient of WCPP with 20%, 30% and 40% perforation ratio have been successfully modeled using boundary element method. Based on the research work and simulation result analysis, the conclusions are as follows:

1. The simulated result for WCPP with 20%, 30% and 40% perforation ratio generally showed that α_n is very high and almost constant for frequency 250 Hz to 500 Hz, then it show a decay trend for frequency 500 Hz to 2 kHz and follow by a small increment from 2 kHz to 4 kHz.

2. Results comparison show that simulated result generally has almost the same trend with measured data and theoretical prediction from 250 Hz to 1 kHz, but from 2 kHz to 4 kHz its trend is changing, the simulated result and measured data show the small increment trend and closely correlated to each other while theoretical prediction continue to decay.

3. The increment phenomena at high frequencies shown by simulation results agree with the measurement results but rather opposite with theoretical

prediction. The α_n increment could cause by resonance frequency effect inside the air column in WCPP holes.

4. The α_n theoretical modeling based on mass of the air inside the hole per unit area has been adopted from the τ_n theoretical modeling developed in earlier research work.

5. Regression prediction model for α_n simulated data with 20%, 30%, and 40% perforation ratio is fitted by third order polynomial with f as independent variable. The statistical models are as follows

$$\alpha_{n(20\%)} = 0.823 - 5.11x10^{-7} f^2 + 9.7x10^{-11} f^3$$

$$\alpha_{n(30\%)} = 0.831 + 0.001f - 5.66x10^{-7} f^2 + 1x10^{-10} f^3$$

$$\alpha_{n(40\%)} = 0.785 + 0.001f - 5.9x10^{-7} f^2 + 1.11x10^{-10} f^3$$

where,

f : Frequency (Hz)

6. Regression model for over all α_n simulated data is done by applying multiple regression with stepwise method. The independent variables computed in the process are $f, f^2, f^3,$ and σ x f. The regression model for over all α_n simulated data is as follow

$$\alpha_n = 0.831 - 5.55^{-7} f^2 + 1.04x10^{-10} f^3 + 2.25x10^{-6} \sigma xf$$

where,

f: Frequency (Hz)

σ: Perforation ratio (20 – 40)%

7. The research work able to serve as a point of reference for future wood perforated panel α_n numerical modeling as the experimental results and simulation results for WCPP are closely correlated.

7.2 Proposed Future Research Works

The following suggestions able to complement and further improve the understanding of normal incident sound absorption coefficient of WCPP.

1. The increment phenomena at high frequencies shown by simulation results agree with the measurement results but opposite with theoretical prediction. . It is foresee that α_n increment trend from 2 kHz to 4 kHz could be cause by resonance frequencies effect. This requires further in depth research study to improve the accuracy of the existing theoretical prediction.

2. To further understand the characteristic of normal incident sound absorption of perforated panels, the investigation should be progressed to explore the effect of geometric patterns such triangle, square or combination of some simple patterns and floral patterns to absorption mechanism.

APPENDIX – A Data of Sound Intensity (simulated)

Table A.1: Sample 1 WCPP at 250 Hz

Point	x (meter)	y (meter)	z (meter)	Resultant sound intensity (W/m^2)
1	0.3600	0.1000	0.1000	0.1384
2	0.3600	0.4333	0.1000	0.1402
3	0.3600	0.7667	0.1000	0.1402
4	0.3600	1.1000	0.1000	0.1384
5	0.3600	0.1000	0.4300	0.1402
6	0.3600	0.4333	0.4300	0.1410
7	0.3600	0.7667	0.4300	0.1410
8	0.3600	1.1000	0.4300	0.1402
9	0.3600	0.1000	0.7600	0.1402
10	0.3600	0.4333	0.7600	0.1410
11	0.3600	0.7667	0.7600	0.1410
12	0.3600	1.1000	0.7600	0.1402
13	0.3600	0.1000	1.1000	0.1384
14	0.3600	0.4333	1.1000	0.1402
15	0.3600	0.7667	1.1000	0.1402
16	0.3600	1.1000	1.1000	0.1384

Table A.2: Sample 1 WCPP at 500 Hz

Point	x (meter)	y (meter)	z (meter)	Resultant sound intensity (W/m^2)
1	0.1900	0.1000	0.1000	0.5427
2	0.1900	0.4333	0.1000	0.5915
3	0.1900	0.7667	0.1000	0.5915
4	0.1900	1.1000	0.1000	0.5427
5	0.1900	0.1000	0.4300	0.5915
6	0.1900	0.4333	0.4300	0.6462
7	0.1900	0.7667	0.4300	0.6462
8	0.1900	1.1000	0.4300	0.5915
9	0.1900	0.1000	0.7600	0.5915
10	0.1900	0.4333	0.7600	0.6462
11	0.1900	0.7667	0.7600	0.6462
12	0.1900	1.1000	0.7600	0.5915
13	0.1900	0.1000	1.1000	0.5427
14	0.1900	0.4333	1.1000	0.5915
15	0.1900	0.7667	1.1000	0.5915
16	0.1900	1.1000	1.1000	0.5427

Table A.3: Sample 1 WCPP at 1000 Hz

Point	x (meter)	y (meter)	z (meter)	Resultant sound intensity (W/m^2)
1	0.1050	0.1000	0.1000	1.3900
2	0.1050	0.4333	0.1000	1.8900
3	0.1050	0.7667	0.1000	1.8900
4	0.1050	1.1000	0.1000	1.3900
5	0.1050	0.1000	0.4300	1.8900
6	0.1050	0.4333	0.4300	2.9930
7	0.1050	0.7667	0.4300	2.9930
8	0.1050	1.1000	0.4300	1.8900
9	0.1050	0.1000	0.7600	1.8900
10	0.1050	0.4333	0.7600	2.9930
11	0.1050	0.7667	0.7600	2.9930
12	0.1050	1.1000	0.7600	1.8890
13	0.1050	0.1000	1.1000	1.3900
14	0.1050	0.4333	1.1000	1.8900
15	0.1050	0.7667	1.1000	1.8900
16	0.1050	1.1000	1.1000	1.3900

Table A.4: Sample 1 WCPP at 2000 Hz

Point	x (meter)	y (meter)	z (meter)	Resultant sound intensity (W/m^2)
1	0.0625	-0.1800	-0.1800	4.4250
2	0.0625	-0.0600	-0.1800	0.2159
3	0.0625	0.0600	-0.1800	0.2171
4	0.0625	0.1800	-0.1800	4.2460
5	0.0625	-0.1800	-0.0600	0.2160
6	0.0625	-0.0600	-0.0600	1.9180
7	0.0625	0.0600	-0.0600	1.9140
8	0.0625	0.1800	-0.0600	0.2174
9	0.0625	-0.1800	0.0600	0.2175
10	0.0625	-0.0600	0.0600	1.9200
11	0.0625	0.0600	0.0600	1.9160
12	0.0625	0.1800	0.0600	0.2175
13	0.0625	-0.1800	0.1800	4.2460
14	0.0625	-0.0600	0.1800	0.2177
15	0.0625	0.0600	0.1800	0.2174
16	0.0625	0.1800	0.1800	4.4260

Table A.5: Sample 1 WCPP at 4000 Hz

Point	x (meter)	y (meter)	z (meter)	Resultant sound intensity (W/m^2)
1	0.0413	-0.1800	-0.1800	0.4209
2	0.0413	-0.0600	-0.1800	3.5220
3	0.0413	0.0600	-0.1800	3.5200
4	0.0413	0.1800	-0.1800	0.4202
5	0.0413	-0.1800	-0.0600	3.5220
6	0.0413	-0.0600	-0.0600	8.9880
7	0.0413	0.0600	-0.0600	3.9960
8	0.0413	0.1800	-0.0600	3.5220
9	0.0413	-0.1800	0.0600	3.5210
10	0.0413	-0.0600	0.0600	3.9940
11	0.0413	0.0600	0.0600	8.9870
12	0.0413	0.1800	0.0600	3.5210
13	0.0413	-0.1800	0.1800	0.4196
14	0.0413	-0.0600	0.1800	3.5200
15	0.0413	0.0600	0.1800	3.5200
16	0.0413	0.1800	0.1800	0.4202

Table A.6: Sample 2 WCPP at 250 Hz

Point	x (meter)	y (meter)	z (meter)	Resultant sound intensity (W/m^2)
1	0.3600	0.1000	0.1000	0.1384
2	0.3600	0.4333	0.1000	0.1401
3	0.3600	0.7667	0.1000	0.1401
4	0.3600	1.1000	0.1000	0.1384
5	0.3600	0.1000	0.4300	0.1401
6	0.3600	0.4333	0.4300	0.1410
7	0.3600	0.7667	0.4300	0.1410
8	0.3600	1.1000	0.4300	0.1401
9	0.3600	0.1000	0.7600	0.1401
10	0.3600	0.4333	0.7600	0.1410
11	0.3600	0.7667	0.7600	0.1410
12	0.3600	1.1000	0.7600	0.1401
13	0.3600	0.1000	1.1000	0.1384
14	0.3600	0.4333	1.1000	0.1401
15	0.3600	0.7667	1.1000	0.1401
16	0.3600	1.1000	1.1000	0.1384

Table A.7: Sample 2 WCPP at 500 Hz

Point	x (meter)	y (meter)	z (meter)	Resultant sound intensity (W/m^2)
1	0.1900	0.1000	0.1000	0.5430
2	0.1900	0.4333	0.1000	0.5918
3	0.1900	0.7667	0.1000	0.5918
4	0.1900	1.1000	0.1000	0.5430
5	0.1900	0.1000	0.4300	0.5918
6	0.1900	0.4333	0.4300	0.6466
7	0.1900	0.7667	0.4300	0.6466
8	0.1900	1.1000	0.4300	0.5918
9	0.1900	0.1000	0.7600	0.5918
10	0.1900	0.4333	0.7600	0.6466
11	0.1900	0.7667	0.7600	0.6466
12	0.1900	1.1000	0.7600	0.5918
13	0.1900	0.1000	1.1000	0.5430
14	0.1900	0.4333	1.1000	0.5918
15	0.1900	0.7667	1.1000	0.5918
16	0.1900	1.1000	1.1000	0.5430

Table A.8: Sample 2 WCPP at 1000 Hz

Point	x (meter)	y (meter)	z (meter)	Resultant sound intensity (W/m^2)
1	0.1050	0.1000	0.1000	1.4250
2	0.1050	0.4333	0.1000	1.9350
3	0.1050	0.7667	0.1000	1.9350
4	0.1050	1.1000	0.1000	1.4250
5	0.1050	0.1000	0.4300	1.9350
6	0.1050	0.4333	0.4300	3.0530
7	0.1050	0.7667	0.4300	3.0530
8	0.1050	1.1000	0.4300	1.9350
9	0.1050	0.1000	0.7600	1.9350
10	0.1050	0.4333	0.7600	3.0520
11	0.1050	0.7667	0.7600	3.0530
12	0.1050	1.1000	0.7600	1.9350
13	0.1050	0.1000	1.1000	1.4250
14	0.1050	0.4333	1.1000	1.9350
15	0.1050	0.7667	1.1000	1.9350
16	0.1050	1.1000	1.1000	1.4250

Table A.9: Sample 2 WCPP at 2000 Hz

Point	x (meter)	y (meter)	z (meter)	Resultant sound intensity (W/m^2)
1	0.0625	-0.1800	-0.1800	4.3710
2	0.0625	-0.0600	-0.1800	0.1536
3	0.0625	0.0600	-0.1800	0.1532
4	0.0625	0.1800	-0.1800	4.3720
5	0.0625	-0.1800	-0.0600	0.1539
6	0.0625	-0.0600	-0.0600	2.3640
7	0.0625	0.0600	-0.0600	2.3630
8	0.0625	0.1800	-0.0600	0.1546
9	0.0625	-0.1800	0.0600	0.1539
10	0.0625	-0.0600	0.0600	2.3600
11	0.0625	0.0600	0.0600	2.3620
12	0.0625	0.1800	0.0600	0.1546
13	0.0625	-0.1800	0.1800	4.3720
14	0.0625	-0.0600	0.1800	0.1541
15	0.0625	0.0600	0.1800	0.1548
16	0.0625	0.1800	0.1800	4.3720

Table A.10: Sample 2 WCPP at 4000 Hz

Point	x (meter)	y (meter)	z (meter)	Resultant sound intensity (W/m^2)
1	0.0413	-0.1800	-0.1800	0.3531
2	0.0413	-0.0600	-0.1800	2.9470
3	0.0413	0.0600	-0.1800	2.9560
4	0.0413	0.1800	-0.1800	0.3574
5	0.0413	-0.1800	-0.0600	2.9480
6	0.0413	-0.0600	-0.0600	8.6340
7	0.0413	0.0600	-0.0600	8.6460
8	0.0413	0.1800	-0.0600	2.9480
9	0.0413	-0.1800	0.0600	2.9510
10	0.0413	-0.0600	0.0600	8.6400
11	0.0413	0.0600	0.0600	8.6290
12	0.0413	0.1800	0.0600	2.9430
13	0.0413	-0.1800	0.1800	0.3574
14	0.0413	-0.0600	0.1800	2.9470
15	0.0413	0.0600	0.1800	2.9420
16	0.0413	0.1800	0.1800	0.3528

Table A.11: Sample 3 WCPP at 250 Hz

Point	x (meter)	y (meter)	z (meter)	Resultant sound intensity (W/m^2)
1	0.3600	0.1000	0.1000	0.1384
2	0.3600	0.4333	0.1000	0.1401
3	0.3600	0.7667	0.1000	0.1401
4	0.3600	1.1000	0.1000	0.1384
5	0.3600	0.1000	0.4300	0.1401
6	0.3600	0.4333	0.4300	0.1410
7	0.3600	0.7667	0.4300	0.1410
8	0.3600	1.1000	0.4300	0.1401
9	0.3600	0.1000	0.7600	0.1401
10	0.3600	0.4333	0.7600	0.1410
11	0.3600	0.7667	0.7600	0.1410
12	0.3600	1.1000	0.7600	0.1401
13	0.3600	0.1000	1.1000	0.1834
14	0.3600	0.4333	1.1000	0.1401
15	0.3600	0.7667	1.1000	0.1401
16	0.3600	1.1000	1.1000	0.1834

Table A.12: Sample 3 WCPP at 500 Hz

Point	x (meter)	y (meter)	z (meter)	Resultant sound intensity (W/m^2)
1	0.1900	0.1000	0.1000	0.5360
2	0.1900	0.4333	0.1000	0.5834
3	0.1900	0.7667	0.1000	0.5834
4	0.1900	1.1000	0.1000	0.5360
5	0.1900	0.1000	0.4300	0.5834
6	0.1900	0.4333	0.4300	0.6364
7	0.1900	0.7667	0.4300	0.6364
8	0.1900	1.1000	0.4300	0.5834
9	0.1900	0.1000	0.7600	0.5834
10	0.1900	0.4333	0.7600	0.6364
11	0.1900	0.7667	0.7600	0.6364
12	0.1900	1.1000	0.7600	0.5834
13	0.1900	0.1000	1.1000	0.5360
14	0.1900	0.4333	1.1000	0.5834
15	0.1900	0.7667	1.1000	0.5834
16	0.1900	1.1000	1.1000	0.5360

Table A.13: Sample 3 WCPP at 1000 Hz

Point	x (meter)	y (meter)	z (meter)	Resultant sound intensity (W/m^2)
1	0.1050	0.1000	0.1000	1.4460
2	0.1050	0.4333	0.1000	1.9520
3	0.1050	0.7667	0.1000	1.9510
4	0.1050	1.1000	0.1000	1.4460
5	0.1050	0.1000	0.4300	1.9520
6	0.1050	0.4333	0.4300	3.0580
7	0.1050	0.7667	0.4300	3.0580
8	0.1050	1.1000	0.4300	1.9520
9	0.1050	0.1000	0.7600	1.9510
10	0.1050	0.4333	0.7600	3.0580
11	0.1050	0.7667	0.7600	3.0580
12	0.1050	1.1000	0.7600	1.9520
13	0.1050	0.1000	1.1000	1.4460
14	0.1050	0.4333	1.1000	1.9510
15	0.1050	0.7667	1.1000	1.9520
16	0.1050	1.1000	1.1000	1.4460

Table A.14: Sample 3 WCPP at 2000 Hz

Point	x (meter)	y (meter)	z (meter)	Resultant sound intensity (W/m^2)
1	0.0625	-0.1800	-0.1800	4.2230
2	0.0625	-0.0600	-0.1800	0.4131
3	0.0625	0.0600	-0.1800	0.4135
4	0.0625	0.1800	-0.1800	4.2230
5	0.0625	-0.1800	-0.0600	0.4130
6	0.0625	-0.0600	-0.0600	1.4250
7	0.0625	0.0600	-0.0600	1.4250
8	0.0625	0.1800	-0.0600	1.4132
9	0.0625	-0.1800	0.0600	1.4133
10	0.0625	-0.0600	0.0600	1.4250
11	0.0625	0.0600	0.0600	1.4250
12	0.0625	0.1800	0.0600	0.4134
13	0.0625	-0.1800	0.1800	4.2230
14	0.0625	-0.0600	0.1800	0.4132
15	0.0625	0.0600	0.1800	0.4136
16	0.0625	0.1800	0.1800	4.2230

Table A.15: Sample 3 WCPP at 4000 Hz

Point	x (meter)	y (meter)	z (meter)	Resultant sound intensity (W/m^2)
1	0.0413	-0.1800	-0.1800	21.6500
2	0.0413	-0.0600	-0.1800	1.7440
3	0.0413	0.0600	-0.1800	1.7480
4	0.0413	0.1800	-0.1800	21.6400
5	0.0413	-0.1800	-0.0600	1.7420
6	0.0413	-0.0600	-0.0600	0.8109
7	0.0413	0.0600	-0.0600	0.8045
8	0.0413	0.1800	-0.0600	1.7450
9	0.0413	-0.1800	0.0600	1.7380
10	0.0413	-0.0600	0.0600	0.7960
11	0.0413	0.0600	0.0600	0.8138
12	0.0413	0.1800	0.0600	1.7440
13	0.0413	-0.1800	0.1800	21.6600
14	0.0413	-0.0600	0.1800	1.7390
15	0.0413	0.0600	0.1800	1.7490
16	0.0413	0.1800	0.1800	21.6800

Table A.16: Sample 4 WCPP at 250 Hz

Point	x (meter)	y (meter)	z (meter)	Resultant sound intensity (W/m^2)
1	0.3600	0.1000	0.1000	0.1385
2	0.3600	0.4333	0.1000	0.1402
3	0.3600	0.7667	0.1000	0.1402
4	0.3600	1.1000	0.1000	0.1385
5	0.3600	0.1000	0.4300	0.1402
6	0.3600	0.4333	0.4300	0.1411
7	0.3600	0.7667	0.4300	0.1411
8	0.3600	1.1000	0.4300	0.1402
9	0.3600	0.1000	0.7600	0.1402
10	0.3600	0.4333	0.7600	0.1411
11	0.3600	0.7667	0.7600	0.1411
12	0.3600	1.1000	0.7600	0.1402
13	0.3600	0.1000	1.1000	0.1385
14	0.3600	0.4333	1.1000	0.1402
15	0.3600	0.7667	1.1000	0.1402
16	0.3600	1.1000	1.1000	0.1385

Table A.17: Sample 4 WCPP at 500 Hz

Point	x (meter)	y (meter)	z (meter)	Resultant sound intensity (W/m^2)
1	0.1900	0.1000	0.1000	0.5412
2	0.1900	0.4333	0.1000	0.5898
3	0.1900	0.7667	0.1000	0.5898
4	0.1900	1.1000	0.1000	0.5412
5	0.1900	0.1000	0.4300	0.5898
6	0.1900	0.4333	0.4300	0.6444
7	0.1900	0.7667	0.4300	0.6444
8	0.1900	1.1000	0.4300	0.5898
9	0.1900	0.1000	0.7600	0.5898
10	0.1900	0.4333	0.7600	0.6444
11	0.1900	0.7667	0.7600	0.6444
12	0.1900	1.1000	0.7600	0.5898
13	0.1900	0.1000	1.1000	0.5412
14	0.1900	0.4333	1.1000	0.5898
15	0.1900	0.7667	1.1000	0.5898
16	0.1900	1.1000	1.1000	0.5412

Table A.18: Sample 4 WCPP at 1000 Hz

Point	x (meter)	y (meter)	z (meter)	Resultant sound intensity (W/m^2)
1	0.1050	0.1000	0.1000	1.3900
2	0.1050	0.4333	0.1000	1.8890
3	0.1050	0.7667	0.1000	1.8890
4	0.1050	1.1000	0.1000	1.3890
5	0.1050	0.1000	0.4300	1.8900
6	0.1050	0.4333	0.4300	2.9910
7	0.1050	0.7667	0.4300	2.9910
8	0.1050	1.1000	0.4300	1.8890
9	0.1050	0.1000	0.7600	1.8890
10	0.1050	0.4333	0.7600	2.9910
11	0.1050	0.7667	0.7600	2.9910
12	0.1050	1.1000	0.7600	1.8890
13	0.1050	0.1000	1.1000	1.3890
14	0.1050	0.4333	1.1000	1.8880

Table A.19: Sample 4 WCPP at 2000 Hz

Point	x (meter)	y (meter)	z (meter)	Resultant sound intensity (W/m^2)
1	0.0625	-0.1800	-0.1800	4.4290
2	0.0625	-0.0600	-0.1800	0.2246
3	0.0625	0.0600	-0.1800	0.2255
4	0.0625	0.1800	-0.1800	4.4310
5	0.0625	-0.1800	-0.0600	0.2233
6	0.0625	-0.0600	-0.0600	1.9240
7	0.0625	0.0600	-0.0600	1.9160
8	0.0625	0.1800	-0.0600	0.2240
9	0.0625	-0.1800	0.0600	0.2250
10	0.0625	-0.0600	0.0600	1.9180
11	0.0625	0.0600	0.0600	1.9180
12	0.0625	0.1800	0.0600	0.2249
13	0.0625	-0.1800	0.1800	4.4300
14	0.0625	-0.0600	0.1800	0.2251
15	0.0625	0.0600	0.1800	0.2250
16	0.0625	0.1800	0.1800	4.4300

Table A.20: Sample 4 WCPP at 4000 Hz

Point	x (meter)	y (meter)	z (meter)	Resultant sound intensity (W/m^2)
1	0.0413	-0.1800	-0.1800	0.5926
2	0.0413	-0.0600	-0.1800	4.0990
3	0.0413	0.0600	-0.1800	4.0890
4	0.0413	0.1800	-0.1800	0.5985
5	0.0413	-0.1800	-0.0600	4.0950
6	0.0413	-0.0600	-0.0600	9.9120
7	0.0413	0.0600	-0.0600	9.8950
8	0.0413	0.1800	-0.0600	4.0850
9	0.0413	-0.1800	0.0600	4.0860
10	0.0413	-0.0600	0.0600	9.9050
11	0.0413	0.0600	0.0600	9.9290
12	0.0413	0.1800	0.0600	4.1000
13	0.0413	-0.1800	0.1800	0.5977
14	0.0413	-0.0600	0.1800	4.0850
15	0.0413	0.0600	0.1800	4.1000
16	0.0413	0.1800	0.1800	0.5940

Table A.21: Sample 6 WCPP at 250 Hz

Point	x (meter)	y (meter)	z (meter)	Resultant sound intensity (W/m^2)
1	0.3600	0.1000	0.1000	0.1384
2	0.3600	0.4333	0.1000	0.1402
3	0.3600	0.7667	0.1000	0.1402
4	0.3600	1.1000	0.1000	0.1384
5	0.3600	0.1000	0.4300	0.1402
6	0.3600	0.4333	0.4300	0.1410
7	0.3600	0.7667	0.4300	0.1410
8	0.3600	1.1000	0.4300	0.1402
9	0.3600	0.1000	0.7600	0.1402
10	0.3600	0.4333	0.7600	0.1410
11	0.3600	0.7667	0.7600	0.1410
12	0.3600	1.1000	0.7600	0.1402
13	0.3600	0.1000	1.1000	0.1384
14	0.3600	0.4333	1.1000	0.1402
15	0.3600	0.7667	1.1000	0.1402
16	0.3600	1.1000	1.1000	0.1384

Table A.22: Sample 6 WCPP at 500 Hz

Point	x (meter)	y (meter)	z (meter)	Resultant sound intensity (W/m^2)
1	0.1900	0.1000	0.1000	0.5427
2	0.1900	0.4333	0.1000	0.5915
3	0.1900	0.7667	0.1000	0.5915
4	0.1900	1.1000	0.1000	0.5427
5	0.1900	0.1000	0.4300	0.5915
6	0.1900	0.4333	0.4300	0.6462
7	0.1900	0.7667	0.4300	0.6462
8	0.1900	1.1000	0.4300	0.5915
9	0.1900	0.1000	0.7600	0.5915
10	0.1900	0.4333	0.7600	0.6462
11	0.1900	0.7667	0.7600	0.6462
12	0.1900	1.1000	0.7600	0.5915
13	0.1900	0.1000	1.1000	0.5427
14	0.1900	0.4333	1.1000	0.5915
15	0.1900	0.7667	1.1000	0.5915
16	0.1900	1.1000	1.1000	0.5427

Table A.23: Sample 6 WCPP at 1000 Hz

Point	x (meter)	y (meter)	z (meter)	Resultant sound intensity (W/m^2)
1	0.1050	0.1000	0.1000	2.4000
2	0.1050	0.4333	0.1000	3.2150
3	0.1050	0.7667	0.1000	3.2150
4	0.1050	1.1000	0.1000	2.3990
5	0.1050	0.1000	0.4300	3.2150
6	0.1050	0.4333	0.4300	4.5010
7	0.1050	0.7667	0.4300	4.5000
8	0.1050	1.1000	0.4300	3.2150
9	0.1050	0.1000	0.7600	3.2160
10	0.1050	0.4333	0.7600	4.5010
11	0.1050	0.7667	0.7600	4.5000
12	0.1050	1.1000	0.7600	3.2150
13	0.1050	0.1000	1.1000	2.4020
14	0.1050	0.4333	1.1000	3.2160
15	0.1050	0.7667	1.1000	3.2150
16	0.1050	1.1000	1.1000	2.4000

Table A.24: Sample 6 WCPP at 2000 Hz

Point	x (meter)	y (meter)	z (meter)	Resultant sound intensity (W/m^2)
1	0.0625	-0.1800	-0.1800	2.0940
2	0.0625	-0.0600	-0.1800	0.4179
3	0.0625	0.0600	-0.1800	0.1795
4	0.0625	0.1800	-0.1800	0.2820
5	0.0625	-0.1800	-0.0600	1.8390
6	0.0625	-0.0600	-0.0600	1.4570
7	0.0625	0.0600	-0.0600	0.6638
8	0.0625	0.1800	-0.0600	0.1817
9	0.0625	-0.1800	0.0600	2.7950
10	0.0625	-0.0600	0.0600	2.4930
11	0.0625	0.0600	0.0600	1.4600
12	0.0625	0.1800	0.0600	0.4032
13	0.0625	-0.1800	0.1800	4.4790
14	0.0625	-0.0600	0.1800	2.7950
15	0.0625	0.0600	0.1800	1.8130
16	0.0625	0.1800	0.1800	2.0580

Table A.25: Sample 6 WCPP at 4000 Hz

Point	x (meter)	y (meter)	z (meter)	Resultant sound intensity (W/m^2)
1	0.0413	-0.1800	-0.1800	11.7100
2	0.0413	-0.0600	-0.1800	1.9030
3	0.0413	0.0600	-0.1800	5.2720
4	0.0413	0.1800	-0.1800	10.3900
5	0.0413	-0.1800	-0.0600	2.0650
6	0.0413	-0.0600	-0.0600	0.0390
7	0.0413	0.0600	-0.0600	2.1870
8	0.0413	0.1800	-0.0600	1.8130
9	0.0413	-0.1800	0.0600	6.0010
10	0.0413	-0.0600	0.0600	2.1410
11	0.0413	0.0600	0.0600	0.1240
12	0.0413	0.1800	0.0600	5.2860
13	0.0413	-0.1800	0.1800	12.5400
14	0.0413	-0.0600	0.1800	1.9800
15	0.0413	0.0600	0.1800	5.9510
16	0.0413	0.1800	0.1800	11.6100

Table A.26: Sample 8 WCPP at 250 Hz

Point	x (meter)	y (meter)	z (meter)	Resultant sound intensity (W/m^2)
1	0.3600	0.1000	0.1000	0.0422
2	0.3600	0.4333	0.1000	0.0474
3	0.3600	0.7667	0.1000	0.0474
4	0.3600	1.1000	0.1000	0.0422
5	0.3600	0.1000	0.4300	0.0474
6	0.3600	0.4333	0.4300	0.0594
7	0.3600	0.7667	0.4300	0.0594
8	0.3600	1.1000	0.4300	0.0474
9	0.3600	0.1000	0.7600	0.0474
10	0.3600	0.4333	0.7600	0.0596
11	0.3600	0.7667	0.7600	0.0596
12	0.3600	1.1000	0.7600	0.0474
13	0.3600	0.1000	1.1000	0.0422
14	0.3600	0.4333	1.1000	0.0474
15	0.3600	0.7667	1.1000	0.0474
16	0.3600	1.1000	1.1000	0.0422

Table A.27: Sample 8 WCPP at 500 Hz

Point	x (meter)	y (meter)	z (meter)	Resultant sound intensity (W/m^2)
1	0.1900	0.1000	0.1000	0.2306
2	0.1900	0.4333	0.1000	0.0720
3	0.1900	0.7667	0.1000	0.0720
4	0.1900	1.1000	0.1000	0.2306
5	0.1900	0.1000	0.4300	0.0732
6	0.1900	0.4333	0.4300	0.0954
7	0.1900	0.7667	0.4300	0.0954
8	0.1900	1.1000	0.4300	0.0732
9	0.1900	0.1000	0.7600	0.0697
10	0.1900	0.4333	0.7600	0.0975
11	0.1900	0.7667	0.7600	0.0975
12	0.1900	1.1000	0.7600	0.0697
13	0.1900	0.1000	1.1000	0.2306
14	0.1900	0.4333	1.1000	0.0720
15	0.1900	0.7667	1.1000	0.0720
16	0.1900	1.1000	1.1000	0.2306

Table A.28: Sample 8 WCPP at 1000 Hz

Point	x (meter)	y (meter)	z (meter)	Resultant sound intensity (W/m^2)
1	0.1050	0.1000	0.1000	0.3965
2	0.1050	0.4333	0.1000	0.1425
3	0.1050	0.7667	0.1000	0.1428
4	0.1050	1.1000	0.1000	0.3965
5	0.1050	0.1000	0.4300	0.1304
6	0.1050	0.4333	0.4300	0.0602
7	0.1050	0.7667	0.4300	0.0603
8	0.1050	1.1000	0.4300	0.1304
9	0.1050	0.1000	0.7600	0.1691
10	0.1050	0.4333	0.7600	0.0723
11	0.1050	0.7667	0.7600	0.0723
12	0.1050	1.1000	0.7600	0.1693
13	0.1050	0.1000	1.1000	0.3969
14	0.1050	0.4333	1.1000	0.1426
15	0.1050	0.7667	1.1000	0.1425
16	0.1050	1.1000	1.1000	0.3967

Table A.29: Sample 8 WCPP at 2000 Hz

Point	x (meter)	y (meter)	z (meter)	Resultant sound intensity (W/m^2)
1	0.0625	-0.1800	-0.1800	3.2180
2	0.0625	-0.0600	-0.1800	0.2553
3	0.0625	0.0600	-0.1800	0.2577
4	0.0625	0.1800	-0.1800	3.2220
5	0.0625	-0.1800	-0.0600	0.2563
6	0.0625	-0.0600	-0.0600	1.6940
7	0.0625	0.0600	-0.0600	1.6890
8	0.0625	0.1800	-0.0600	0.2566
9	0.0625	-0.1800	0.0600	0.2623
10	0.0625	-0.0600	0.0600	1.7030
11	0.0625	0.0600	0.0600	1.6920
12	0.0625	0.1800	0.0600	0.2578
13	0.0625	-0.1800	0.1800	3.2200
14	0.0625	-0.0600	0.1800	0.2599
15	0.0625	0.0600	0.1800	0.2578
16	0.0625	0.1800	0.1800	3.2220

Table A.30: Sample 8 WCPP at 4000 Hz

Point	x (meter)	y (meter)	z (meter)	Resultant sound intensity (W/m^2)
1	0.0413	-0.1800	-0.1800	5.4680
2	0.0413	-0.0600	-0.1800	3.4200
3	0.0413	0.0600	-0.1800	3.3920
4	0.0413	0.1800	-0.1800	5.4090
5	0.0413	-0.1800	-0.0600	3.4250
6	0.0413	-0.0600	-0.0600	4.8290
7	0.0413	0.0600	-0.0600	4.7450
8	0.0413	0.1800	-0.0600	3.4260
9	0.0413	-0.1800	0.0600	3.4330
10	0.0413	-0.0600	0.0600	4.7810
11	0.0413	0.0600	0.0600	4.7600
12	0.0413	0.1800	0.0600	3.4220
13	0.0413	-0.1800	0.1800	5.4990
14	0.0413	-0.0600	0.1800	3.3990
15	0.0413	0.0600	0.1800	3.4150
16	0.0413	0.1800	0.1800	5.4860

Table A.31: Sample 10 WCPP at 250 Hz

Point	x (meter)	y (meter)	z (meter)	Resultant sound intensity (W/m^2)
1	0.3600	0.1000	0.1000	0.0423
2	0.3600	0.4333	0.1000	0.0477
3	0.3600	0.7667	0.1000	0.0477
4	0.3600	1.1000	0.1000	0.0423
5	0.3600	0.1000	0.4300	0.0477
6	0.3600	0.4333	0.4300	0.0602
7	0.3600	0.7667	0.4300	0.0602
8	0.3600	1.1000	0.4300	0.0477
9	0.3600	0.1000	0.7600	0.0477
10	0.3600	0.4333	0.7600	0.0603
11	0.3600	0.7667	0.7600	0.0603
12	0.3600	1.1000	0.7600	0.0477
13	0.3600	0.1000	1.1000	0.0423
14	0.3600	0.4333	1.1000	0.0477
15	0.3600	0.7667	1.1000	0.0477
16	0.3600	1.1000	1.1000	0.0423

Table A.32: Sample 10 WCPP at 500 Hz

Point	x (meter)	y (meter)	z (meter)	Resultant sound intensity (W/m^2)
1	0.1900	0.1000	0.1000	0.1160
2	0.1900	0.4333	0.1000	0.0375
3	0.1900	0.7667	0.1000	0.0375
4	0.1900	1.1000	0.1000	0.1160
5	0.1900	0.1000	0.4300	0.0381
6	0.1900	0.4333	0.4300	0.0464
7	0.1900	0.7667	0.4300	0.0464
8	0.1900	1.1000	0.4300	0.0381
9	0.1900	0.1000	0.7600	0.0363
10	0.1900	0.4333	0.7600	0.0474
11	0.1900	0.7667	0.7600	0.0474
12	0.1900	1.1000	0.7600	0.0363
13	0.1900	0.1000	1.1000	0.1160
14	0.1900	0.4333	1.1000	0.0375
15	0.1900	0.7667	1.1000	0.0375
16	0.1900	1.1000	1.1000	0.1160

Table A.33: Sample 10 WCPP at 1000 Hz

Point	x (meter)	y (meter)	z (meter)	Resultant sound intensity (W/m^2)
1	0.1050	0.1000	0.1000	0.4248
2	0.1050	0.4333	0.1000	0.1641
3	0.1050	0.7667	0.1000	0.1641
4	0.1050	1.1000	0.1000	0.4248
5	0.1050	0.1000	0.4300	0.1505
6	0.1050	0.4333	0.4300	0.0594
7	0.1050	0.7667	0.4300	0.0594
8	0.1050	1.1000	0.4300	0.1505
9	0.1050	0.1000	0.7600	0.1924
10	0.1050	0.4333	0.7600	0.0613
11	0.1050	0.7667	0.7600	0.0613
12	0.1050	1.1000	0.7600	0.1924
13	0.1050	0.1000	1.1000	0.4247
14	0.1050	0.4333	1.1000	0.1641
15	0.1050	0.7667	1.1000	0.1641
16	0.1050	1.1000	1.1000	0.4247

Table A.34: Sample 10 WCPP at 2000 Hz

Point	x (meter)	y (meter)	z (meter)	Resultant sound intensity (W/m^2)
1	0.0625	-0.1800	-0.1800	2.9800
2	0.0625	-0.0600	-0.1800	0.2950
3	0.0625	0.0600	-0.1800	0.2945
4	0.0625	0.1800	-0.1800	2.9790
5	0.0625	-0.1800	-0.0600	0.2948
6	0.0625	-0.0600	-0.0600	2.0380
7	0.0625	0.0600	-0.0600	2.0380
8	0.0625	0.1800	-0.0600	0.2951
9	0.0625	-0.1800	0.0600	0.2953
10	0.0625	-0.0600	0.0600	2.0400
11	0.0625	0.0600	0.0600	2.0380
12	0.0625	0.1800	0.0600	0.2952
13	0.0625	-0.1800	0.1800	2.9800
14	0.0625	-0.0600	0.1800	0.2954
15	0.0625	0.0600	0.1800	0.2954
16	0.0625	0.1800	0.1800	2.9800

Table A.35: Sample 10 WCPP at 4000 Hz

Point	x (meter)	y (meter)	z (meter)	Resultant sound intensity (W/m^2)
1	0.0413	-0.1800	-0.1800	5.3540
2	0.0413	-0.0600	-0.1800	3.5850
3	0.0413	0.0600	-0.1800	3.5600
4	0.0413	0.1800	-0.1800	5.3820
5	0.0413	-0.1800	-0.0600	3.5600
6	0.0413	-0.0600	-0.0600	0.6852
7	0.0413	0.0600	-0.0600	0.6829
8	0.0413	0.1800	-0.0600	3.5590
9	0.0413	-0.1800	0.0600	3.5670
10	0.0413	-0.0600	0.0600	0.8441
11	0.0413	0.0600	0.0600	0.7573
12	0.0413	0.1800	0.0600	3.5730
13	0.0413	-0.1800	0.1800	5.3760
14	0.0413	-0.0600	0.1800	3.5160
15	0.0413	0.0600	0.1800	3.5830
16	0.0413	0.1800	0.1800	5.4420

Table A.36: Sample 12 WCPP at 250 Hz

Point	x (meter)	y (meter)	z (meter)	Resultant sound intensity (W/m^2)
1	0.3600	0.1000	0.1000	0.0427
2	0.3600	0.4333	0.1000	0.0477
3	0.3600	0.7667	0.1000	0.0477
4	0.3600	1.1000	0.1000	0.0427
5	0.3600	0.1000	0.4300	0.0477
6	0.3600	0.4333	0.4300	0.0596
7	0.3600	0.7667	0.4300	0.0596
8	0.3600	1.1000	0.4300	0.0477
9	0.3600	0.1000	0.7600	0.0478
10	0.3600	0.4333	0.7600	0.0597
11	0.3600	0.7667	0.7600	0.0597
12	0.3600	1.1000	0.7600	0.0478
13	0.3600	0.1000	1.1000	0.0427
14	0.3600	0.4333	1.1000	0.0477
15	0.3600	0.7667	1.1000	0.0477
16	0.3600	1.1000	1.1000	0.0427

Table A.37: Sample 12 WCPP at 500 Hz

Point	x (meter)	y (meter)	z (meter)	Resultant sound intensity (W/m^2)
1	0.1900	0.1000	0.1000	0.1833
2	0.1900	0.4333	0.1000	0.0346
3	0.1900	0.7667	0.1000	0.0346
4	0.1900	1.1000	0.1000	0.1833
5	0.1900	0.1000	0.4300	0.0354
6	0.1900	0.4333	0.4300	0.1705
7	0.1900	0.7667	0.4300	0.1705
8	0.1900	1.1000	0.4300	0.0354
9	0.1900	0.1000	0.7600	0.0330
10	0.1900	0.4333	0.7600	0.1835
11	0.1900	0.7667	0.7600	0.1835
12	0.1900	1.1000	0.7600	0.0330
13	0.1900	0.1000	1.1000	0.1833
14	0.1900	0.4333	1.1000	0.0346
15	0.1900	0.7667	1.1000	0.0346
16	0.1900	1.1000	1.1000	0.1833

Table A.38: Sample 12 WCPP at 1000 Hz

Point	x (meter)	y (meter)	z (meter)	Resultant sound intensity (W/m^2)
1	0.1050	0.1000	0.1000	0.4258
2	0.1050	0.4333	0.1000	0.1498
3	0.1050	0.7667	0.1000	0.1498
4	0.1050	1.1000	0.1000	0.4258
5	0.1050	0.1000	0.4300	0.1371
6	0.1050	0.4333	0.4300	0.0574
7	0.1050	0.7667	0.4300	0.0574
8	0.1050	1.1000	0.4300	0.1371
9	0.1050	0.1000	0.7600	0.1763
10	0.1050	0.4333	0.7600	0.0670
11	0.1050	0.7667	0.7600	0.0670
12	0.1050	1.1000	0.7600	0.1763
13	0.1050	0.1000	1.1000	0.4258
14	0.1050	0.4333	1.1000	0.1499
15	0.1050	0.7667	1.1000	0.1499
16	0.1050	1.1000	1.1000	0.4258

Table A.39: Sample 12 WCPP at 2000 Hz

Point	x (meter)	y (meter)	z (meter)	Resultant sound intensity (W/m^2)
1	0.0625	-0.1800	-0.1800	3.7300
2	0.0625	-0.0600	-0.1800	0.1176
3	0.0625	0.0600	-0.1800	0.1175
4	0.0625	0.1800	-0.1800	3.7300
5	0.0625	-0.1800	-0.0600	0.1710
6	0.0625	-0.0600	-0.0600	1.7410
7	0.0625	0.0600	-0.0600	1.7430
8	0.0625	0.1800	-0.0600	0.1176
9	0.0625	-0.1800	0.0600	0.1176
10	0.0625	-0.0600	0.0600	1.7410
11	0.0625	0.0600	0.0600	1.7410
12	0.0625	0.1800	0.0600	0.1760
13	0.0625	-0.1800	0.1800	3.7300
14	0.0625	-0.0600	0.1800	0.1175
15	0.0625	0.0600	0.1800	0.1175
16	0.0625	0.1800	0.1800	3.7300

Table A.40: Sample 12 WCPP at 4000 Hz

Point	x (meter)	y (meter)	z (meter)	Resultant sound intensity (W/m^2)
1	0.0413	-0.1800	-0.1800	9.4660
2	0.0413	-0.0600	-0.1800	2.8530
3	0.0413	0.0600	-0.1800	2.8370
4	0.0413	0.1800	-0.1800	9.5100
5	0.0413	-0.1800	-0.0600	2.8440
6	0.0413	-0.0600	-0.0600	4.1220
7	0.0413	0.0600	-0.0600	4.1200
8	0.0413	0.1800	-0.0600	2.8370
9	0.0413	-0.1800	0.0600	2.8460
10	0.0413	-0.0600	0.0600	4.1340
11	0.0413	0.0600	0.0600	4.1330
12	0.0413	0.1800	0.0600	2.8410
13	0.0413	-0.1800	0.1800	9.5020
14	0.0413	-0.0600	0.1800	2.8410
15	0.0413	0.0600	0.1800	2.8510
16	0.0413	0.1800	0.1800	9.4660

Table A.41: Anechoic Room at 250 Hz

Point	X (meter)	Y (meter)	Z (meter)	Resultant sound intensity (W/m^2)
1	0.3600	0.1000	0.1000	0.1669
2	0.3600	0.4333	0.1000	0.1690
3	0.3600	0.7667	0.1000	0.1690
4	0.3600	1.1000	0.1000	0.1669
5	0.3600	0.1000	0.4300	0.1690
6	0.3600	0.4333	0.4300	0.1701
7	0.3600	0.7667	0.4300	0.1701
8	0.3600	1.1000	0.4300	0.1690
9	0.3600	0.1000	0.7600	0.1690
10	0.3600	0.4333	0.7600	0.1701
11	0.3600	0.7667	0.7600	0.1701
12	0.3600	1.1000	0.7600	0.1690
13	0.3600	0.1000	1.1000	0.1669
14	0.3600	0.4333	1.1000	0.1690
15	0.3600	0.7667	1.1000	0.1690
16	0.3600	1.1000	1.1000	0.1669

Table A.42: Anechoic Room at 500 Hz

Point	X (meter)	Y (meter)	Z (meter)	Resultant sound intensity (W/m^2)
1	0.1900	0.1000	0.1000	0.5917
2	0.1900	0.4333	0.1000	0.6433
3	0.1900	0.7667	0.1000	0.6433
4	0.1900	1.1000	0.1000	0.5917
5	0.1900	0.1000	0.4300	0.6433
6	0.1900	0.4333	0.4300	0.7010
7	0.1900	0.7667	0.4300	0.7010
8	0.1900	1.1000	0.4300	0.6433
9	0.1900	0.1000	0.7600	0.6433
10	0.1900	0.4333	0.7600	0.7010
11	0.1900	0.7667	0.7600	0.7010
12	0.1900	1.1000	0.7600	0.6433
13	0.1900	0.1000	1.1000	0.5917
14	0.1900	0.4333	1.1000	0.6433
15	0.1900	0.7667	1.1000	0.6433
16	0.1900	1.1000	1.1000	0.5917

Table A.43: Anechoic Room at 1000 Hz

Point	X (meter)	Y (meter)	Z (meter)	Resultant sound intensity (W/m^2)
1	0.1050	0.1000	0.1000	1.8410
2	0.1050	0.4333	0.1000	2.5390
3	0.1050	0.7667	0.1000	2.5390
4	0.1050	1.1000	0.1000	1.8410
5	0.1050	0.1000	0.4300	2.5390
6	0.1050	0.4333	0.4300	4.0060
7	0.1050	0.7667	0.4300	4.0060
8	0.1050	1.1000	0.4300	2.5390
9	0.1050	0.1000	0.7600	2.5390
10	0.1050	0.4333	0.7600	4.0060
11	0.1050	0.7667	0.7600	4.0060
12	0.1050	1.1000	0.7600	2.5390
13	0.1050	0.1000	1.1000	1.8410
14	0.1050	0.4333	1.1000	2.5390
15	0.1050	0.7667	1.1000	2.5390
16	0.1050	1.1000	1.1000	1.8410

Table A.44: Anechoic Room at 2000 Hz

Point	X (meter)	Y (meter)	Z (meter)	Resultant sound intensity (W/m^2)
1	0.0625	-0.1800	-0.1800	8.9780
2	0.0625	-0.0600	-0.1800	0.8228
3	0.0625	0.0600	-0.1800	0.8228
4	0.0625	0.1800	-0.1800	8.9770
5	0.0625	-0.1800	-0.0600	0.8228
6	0.0625	-0.0600	-0.0600	5.0690
7	0.0625	0.0600	-0.0600	5.0690
8	0.0625	0.1800	-0.0600	0.8228
9	0.0625	-0.1800	0.0600	0.8228
10	0.0625	-0.0600	0.0600	5.0690
11	0.0625	0.0600	0.0600	5.0690
12	0.0625	0.1800	0.0600	0.8228
13	0.0625	-0.1800	0.1800	8.9780
14	0.0625	-0.0600	0.1800	0.8228
15	0.0625	0.0600	0.1800	0.8228
16	0.0625	0.1800	0.1800	8.9770

Table A.45: Anechoic Room at 4000 Hz

Point	X (meter)	Y (meter)	Z (meter)	Resultant sound intensity (W/m^2)
1	0.0413	-0.1800	-0.1800	14.6700
2	0.0413	-0.0600	-0.1800	2.7420
3	0.0413	0.0600	-0.1800	2.7420
4	0.0413	0.1800	-0.1800	14.6700
5	0.0413	-0.1800	-0.0600	2.7420
6	0.0413	-0.0600	-0.0600	10.2600
7	0.0413	0.0600	-0.0600	10.2600
8	0.0413	0.1800	-0.0600	2.7420
9	0.0413	-0.1800	0.0600	2.7420
10	0.0413	-0.0600	0.0600	10.2600
11	0.0413	0.0600	0.0600	10.2600
12	0.0413	0.1800	0.0600	2.7420
13	0.0413	-0.1800	0.1800	14.6700
14	0.0413	-0.0600	0.1800	2.7420
15	0.0413	0.0600	0.1800	2.7420
16	0.0413	0.1800	0.1800	14.6700

APPENDIX B: SPSS Regression Syntaxes

B.1 SPSS Regression Syntax for WCPP with 20% Perforation Ratio

```
Fri June 09 17:46:43 2006 :journaling started
SET Small 0.000100 OLang English .
SET Small 0.000100 OLang English .

GET DATA /TYPE=XLS
 /FILE='C:\Documents and Settings\ula\My Documents\DATA excel\20%.xls'
 /SHEET=name 'Sheet1'
 /CELLRANGE=full
 /READNAMES=on
 /ASSUMEDSTRWIDTH=32767.


SAVE OUTFILE='C:\Documents and Settings\ula\My Documents\DATA excel\20%.sav'
 /COMPRESSED.

* Curve Estimation.

CURVEFIT /VARIABLES=A  WITH f
 /CONSTANT
 /MODEL=QUADRATIC CUBIC
 /PLOT FIT
 /CIN=95
 /SAVE=PRED RESID CIN.


GRAPH
 /SCATTERPLOT(BIVAR)=FIT_2 WITH ERR_2
 /MISSING=LISTWISE .


SAVE TRANSLATE OUTFILE='C:\Documents and Settings\ula\My Documents\DATA
excel\result 20.xls'
 /TYPE=XLS /VERSION=8 /MAP /REPLACE /FIELDNAMES
 /CELLS=VALUES .
```

B.2 SPSS Regression Syntax for WCPP with 30% Perforation Ratio

```
Fri June 09 17:01:18 2006 :journaling started
SET Small 0.000100 OLang English .
SET Small 0.000100 OLang English .

GET DATA /TYPE=XLS
 /FILE='C:\Documents and Settings\ula\My Documents\DATA excel\30%.xls'
 /SHEET=name 'Sheet1'
 /CELLRANGE=full
 /READNAMES=on
 /ASSUMEDSTRWIDTH=32767.

* Curve Estimation.

CURVEFIT /VARIABLES=A  WITH f
 /CONSTANT
 /MODEL=QUADRATIC CUBIC
 /PLOT FIT
 /SAVE=PRED RESID .

GRAPH
 /SCATTERPLOT(BIVAR)=FIT_2 WITH ERR_2
 /MISSING=LISTWISE .

SAVE TRANSLATE OUTFILE='C:\Documents and Settings\ula\My Documents\DATA
excel\result 30.xls'
 /TYPE=XLS /VERSION=8 /MAP /REPLACE /FIELDNAMES
 /CELLS=VALUES .
```

B.3 SPSS Regression Syntax for WCPP with 40% Perforation Ratio

```
Fri June 09 17:15:39 2006 :journaling started
SET Small 0.000100 OLang English .
SET Small 0.000100 OLang English .

GET DATA /TYPE=XLS
 /FILE='C:\Documents and Settings\ula\My Documents\DATA excel\40%.xls'
 /SHEET=name 'Sheet1'
 /CELLRANGE=full
 /READNAMES=on
 /ASSUMEDSTRWIDTH=32767.

* Curve Estimation.

CURVEFIT /VARIABLES=A  WITH f
 /CONSTANT
 /MODEL=QUADRATIC CUBIC EXPONENTIAL
 /PLOT FIT
 /CIN=95
 /SAVE=PRED RESID CIN.


GRAPH
 /SCATTERPLOT(BIVAR)=FIT_2 WITH ERR_2
 /MISSING=LISTWISE .

SAVE TRANSLATE OUTFILE='C:\Documents and Settings\ula\My Documents\DATA
excel\result 40.xls'
 /TYPE=XLS /VERSION=8 /MAP /REPLACE /FIELDNAMES
 /CELLS=VALUES .
```

B.4 SPSS Regression Syntax for Over All simulated Result

```
Fri June 09 22:59:57 2006: journaling started
GET DATA /TYPE=XLS
 /FILE='C:\Documents and Settings\ula\My Documents\DATA excel\all.xls'
 /SHEET=name 'Sheet1'
 /CELLRANGE=full
 /READNAMES=on
 /ASSUMEDSTRWIDTH=32767.


REGRESSION
 /MISSING LISTWISE
 /STATISTICS COEFF OUTS R ANOVA
 /CRITERIA=PIN(.05) POUT(.10)
 /NOORIGIN
 /DEPENDENT A
 /METHOD=ENTER p f fxf pxp pxf fxfxf
 /SCATTERPLOT=(*ZRESID ,*ZPRED )
 /RESIDUALS DURBIN
 /SAVE PRED RESID .

REGRESSION
 /MISSING LISTWISE
 /STATISTICS COEFF OUTS R ANOVA
 /CRITERIA=PIN(.05) POUT(.10)
 /NOORIGIN
 /DEPENDENT A
 /METHOD=STEPWISE p f fxf pxp pxf fxfxf
 /SCATTERPLOT=(*ZRESID ,*ZPRED )
 /RESIDUALS DURBIN
 /SAVE PRED RESID .


SAVE TRANSLATE OUTFILE='C:\Documents and Settings\ula\My Documents\DATA
excel\result all.xls'
 /TYPE=XLS /VERSION=8 /MAP /REPLACE /FIELDNAMES
 /CELLS=VALUES .
```

REFERENCES

Barnes, J.W. (1994). *Statistical Analysis for Engineers and Scientists.* McGRAW-HILL. Inc. New York. pp 250-252.

Blackstock, D.T. (2000). *Fundamentals of Physic Acoustics*. John Wiley and Sons Inc. New York. USA. pp 163-168

Brebbia, C. A. and Dominquez, J. (1992). *Boundary Element Introductory Course.* McGraw-Hill. New York. pp. 119.

Cowan, J. (2000a). *Architectural Acoustics – Design Guide.* Mc Graw Hill. New York. pp. 25.

Cowan, J. (2000b). *Architectural Acoustics – Design Guide.* Mc Graw Hill. New York. pp. 23-25.

Cox, T.J. and D'Antonio, P. (2004a). *Acoustic Absorbers and Diffusers*. SPON Press. Taylor& Francis Group. pp 129-131.

Cox, T.J. and D'Antonio, P. (2004b). *Acoustic Absorbers and Diffusers.* SPON Press. Taylor& Francis Group. pp 58-67.

Cox, T.J. and D'Antonio, P. (2004c). *Acoustic Absorbers and Diffusers.* SPON Press. Taylor& Francis Group. pp 6-22

Cox, T.J. and D'Antonio, P. (2004d). *Acoustic Absorbers and Diffusers.* SPON Press. Taylor& Francis Group. pp 12-21

Cremer, L and Muller, H.A. (1982a). *Principles and Application of Room Acoustics.* Vol. 1. Applied Science Publishers London. pp 139-141.

Cremer, L and Muller, H.A. (1982b). *Principles and Application of Room Acoustics.* Vol. 1. Applied Science Publishers London. pp .181-183.

Everest, F.A. (1994a). *The Master Handbook of Acoustics*. 3rd edition. TAB Books. New York. pp. 152.

Everest, F.A. (1994b). *The Master Handbook of Acoustics*. 3rd edition. TAB Books. New York. pp. 158-163.

Everest, F.A. (1994c). *The Master Handbook of Acoustics*. 3rd edition. TAB Books. New York. pp. 189.

Fahy, F.J.. (2001). *Foundation of Engineering Acoustics*. Academic Press. London. pp. 211-218

Hall, D.E.. (1987). *Basic Acoustics.* John Wiley and Sons. New York. pp 232-235

Kirkup, S. (1998a). *The Boundary Element Method in Acoustic*. Integrated Sound Software. West Yorkshire. England. pp 12.

Kirkup, S. (1998b). *The Boundary Element Method in Acoustic*. Integrated Sound Software. West Yorkshire. England. pp 14-15

Kutruff, H. (1979). *Room Acoustics 2nd Edition*. Applied Science Publishers Ltd. London. pp. 138-141.

Lai, J.C.S and Burgess, M. (1991). *Application of Sound Intensity Technique to Measure of Field Sound Transmission Loss.* Applied Acoustic. Vol34. pp77-87

Lawrence, A. (1970a). *Architectural Acoustics*. Applied Science Publishers. London. pp 170-172

Lawrence, A. (1970b). *Architectural Acoustics*. Applied Science Publishers. London. pp 172-174

Leonard, R. W. Delsasso, L. P. and Knudsen, V. O. (1964). *Diffraction of Sound by an Array of Rectangular Reflective Panels*. Journal Acoustic Society of America. Vol. 36. pp 2328-2333.

Lim Jee Yuan. (1987) *The Malay House Rediscovering Malaysian's Indigenous Shelter System*. Institut Masyarakat. Pulau Pinang. Pp 68-69.

Maekawa, Z and Lord. P (1994a). *Environmental and Architectural Acoustics*. E & FN SPON. London. pp 11-12.

Maekawa, Z and Lord. P (1994b). *Environmental and Architectural Acoustics*. E & FN SPON. London. pp 14

Maekawa, Z and Lord. P (1994c). *Environmental and Architectural Acoustics*. E & FN SPON. London. pp 119.

Maekawa, Z and Lord. P (1994d). *Environmental and Architectural Acoustics*. E & FN SPON. London. pp 126-130.

Maekawa, Z and Lord. P (1994e). *Environmental and Architectural Acoustics*. E & FN SPON. London. pp 135-137.

Maekawa, Z and Lord. P (1994f). *Environmental and Architectural Acoustics*. E & FN SPON. London. pp 122-124

Marsh, A. UWA. (1999). *Membrane Absorber*. The School of Architecture and Fine Arts. The University of Western Australia: Lecturer note.

Mohamad Ngasri Dimon. (2003a). *Normal Incidence Sound Transmission Coefficient Prediction Using Sound Intensity Technique.* Universiti Teknologi Malaysia: Ph.D Thesis. pp 52-96

Mohamad Ngasri Dimon. (2003b). *Normal Incidence Sound Transmission Coefficient Prediction Using Sound Intensity Technique.* Universiti Teknologi Malaysia: Ph.D Thesis. pp 114-120

Mohamad Ngasri Dimon. (2003c). *Normal Incidence Sound Transmission Coefficient Prediction Using Sound Intensity Technique.* Universiti Teknologi Malaysia: Ph.D Thesis. pp 99

Mohamad Ngasri Dimon. (2003d). *Normal Incidence Sound Transmission Coefficient Prediction Using Sound Intensity Technique.* Universiti Teknologi Malaysia: Ph.D Thesis. pp 103-109. 121-122

Niku, M.R.A. and Adey. T.R. Bridges. *Application of BEASY to Industrial and Environmental Acoustics*. Beasy Publications. Southampton.

Rizzo, F.J. (1967). *An Integral Equation Approach to Boundary Value Problems of Classical Elastostatics*. Q Appl Math . Vol 25. pp. 83-95.

Schiff, D and D'Agostino. R. (1996a). *Practical Engineering Statistics.* John Wiley & Sons. Inc. Toronto. pp 229-231

Schiff, D and D'Agostino. R (1996b). *Practical Engineering Statistics.* John Wiley & Sons. Inc. Toronto. pp 234-243

Seybert, A.F et al. (1985). *An Advanced Computational Method for Radiation and Scattering of Acoustic Waves in Three Dimensions*. J. Acoust. Soc. Am.. pp 364

Seybert, A.F. and Wu, T. W. (1997a). *Encyclopaedia of Acoustics*. . John Wiley and Sons.Inc. pp.173.

Seybert, A.F. and Wu, T. W. (1997b). *Encyclopaedia of Acoustics*. . John Wiley and Sons.Inc. pp.178.

Silva, J. J. Do Rego. (1994). *Acoustic and Elastic Wave Scattering Using Boundary Element*. Computational Mechanics Publications. Southampton. pp. 9.

Wrobel, L.C. (2002a). *The Boundary Element Method.* Volume 1. John Wiley and Sons. LTD. West Sussex. pp 14-25.

Wrobel, L.C. (2002b). *The Boundary Element Method* Volume 1. John Wiley and Sons. LTD. West Sussex. pp 32-33

Wu, T. W. (2000). *Boundary Element Acoustics: Fundamental and Computer Codes.* WIT Press. pp. 20-22.

Yerges, L.F. (1978). *Sound. Noise and Vibration Control*. 2nd Edition. Van Nostrand Rainhold Campany. New York. 1978.